DYNAMIC SIMULATION OF LOW ALTITUDE

AERIAL TOW SYSTEMS

By

JOHNNY EARL QUISENBERRY JR.

Bachelor of Science

Oklahoma State University

Stillwater, Oklahoma

2002

Submitted to the Faculty
of the Graduate College of
Oklahoma State University
in partial fulfillment of
the requirements for
the Degree of
MASTER OF SCIENCE
July, 2005

DYNAMIC SIMULATION OF LOW ALTITUDE

AERIAL TOW SYSTEMS

Thesis Approved:

_____

Thesis Advisor

_____

_____

_____

Dean of the Graduate College

ACKNOWLEDGEMENTS

This research was conducted in cooperation with the engineers at Zivko Inc. Specifically; I would like to thank Todd C. Morse for his assistance. In addition I would like to thank the NASA Oklahoma Space Grant Consortium for their financial support for the duration of the project.

I would like to express my deepest appreciation to my major advisor, Dr. Andrew S. Arena, for his guidance and support in this research. I would also like to thank the other members of my committee, Dr. R. D. Delahoussaye and Dr. P. R. Pagilla for their time and efforts.

I could not have made the accomplishments I have here at OSU without the love and support of my family; mother, Susan Quisenberry, father, John Quisenberry, sister, Kiesha Quisenberry, and brother Clint Quisenberry.

TABLE OF CONTENTS

LIST OF TABLES

LIST OF FIGURES

NOMENCLATURE

A_0 $\Rightarrow$ general amplitude of oscillation

A,B,C $\Rightarrow$ augmented equation of motion matrix

$\underline{C}$ $\Rightarrow$ coordinate transformation from segment to host frame

$C_{ß},S_{ß},$ $\Rightarrow$ shorthand notation for cosine and sine of generic angle $ß$

c_f $\Rightarrow$ cable friction coefficient

c_p $\Rightarrow$ cable pressure coefficient

d $\Rightarrow$ cable diameter

F_x,F_y,F_z $\Rightarrow$ X,Y,Z component of the aerodynamic force, in the cable segment frame

f $\Rightarrow$ generic function

h $\Rightarrow$ wave height in host vehicle frame

h_n $\Rightarrow$ sea level in host vehicle frame

I $\Rightarrow$ ATV inertia matrix, in ATV frame

I' $\Rightarrow$ ATV inertia matrix, in ATV segment frame

I_X,I_Y,I_Z $\Rightarrow$ ATV X,Y,Z inertia components, in ATV frame

k_d $\Rightarrow$ derivative gain

k_p $\Rightarrow$ proportional gain

l $\Rightarrow$ segment length

L,M,N $\Rightarrow$ aerodynamic moments about X,Y,Z, in ATV frame

M_X,M_Y,M_Z $\Rightarrow$ moment about X,Y,Z, in segment frame

$M_{\dot{f}}$ $\Rightarrow$ moment matrix about the Euler rates $\dot{f}$

$M_{\dot{q}}$ $\Rightarrow$ moment matrix about the Euler rates $\dot{q}$

$M_{\dot{y}}$ $\Rightarrow$ moment matrix about the Euler rates $\dot{y}$

m $\Rightarrow$ mass

n $\Rightarrow$ number of cable segments

p,q,r $\Rightarrow$ angular rates about X,Y,Z, in ATV aircraft frame

Q_i $\Rightarrow$ generalized force for the i^{th} generalized coordinate

q $\Rightarrow$ generalized coordinate

t $\Rightarrow$ time

T $\Rightarrow$ kinetic energy

T_{rot} $\Rightarrow$ rotational kinetic energy

U_0,V_0,W_0 $\Rightarrow$ freestream flow, in inertial frame

u,v,w $\Rightarrow$ perturbation velocities, in ATV aircraft frame

V $\Rightarrow$ velocity

V_x, V_y, V_z $\Rightarrow$ velocity in the X,Y,Z direction, in segment frame

$X_u,\ldots N_p$ $\Rightarrow$ ATV stability derivatives

X,Y,Z $\Rightarrow$ Cartesian coordinate directions, in host frame

x,y,z $\Rightarrow$ Cartesian coordinate directions, in segment frame

$\underline{z}$ $\Rightarrow$ vertical host aircraft displacement, inertial frame

l $\Rightarrow$ wavelength

p $\Rightarrow$ circular constant

r $\Rightarrow$ air density

f,q,y $\Rightarrow$ Euler angles

? $\Rightarrow$ Angle between the ATV segment frame and ATV aircraft frame

w $\Rightarrow$ vector of Cartesian angular rates

w_0 $\Rightarrow$ general frequency

Dh $\Rightarrow$ difference in ATV and wave altitude, in host frame

Di_w $\Rightarrow$ wing angle correction

CHAPTER 1

INTRODUCTION

1.1 Background

The aerial tow system is a relatively common flight configuration. It is a necessity for gliding aircraft to achieve altitude; it is common to have targets towed by aircraft for weapons testing and target practice; it is even being proposed by NASA as a platform for reusable launch space-vehicles. The configuration has been proven to be well suited for these uses, though they are primarily a means of transportation of the towed vehicle.

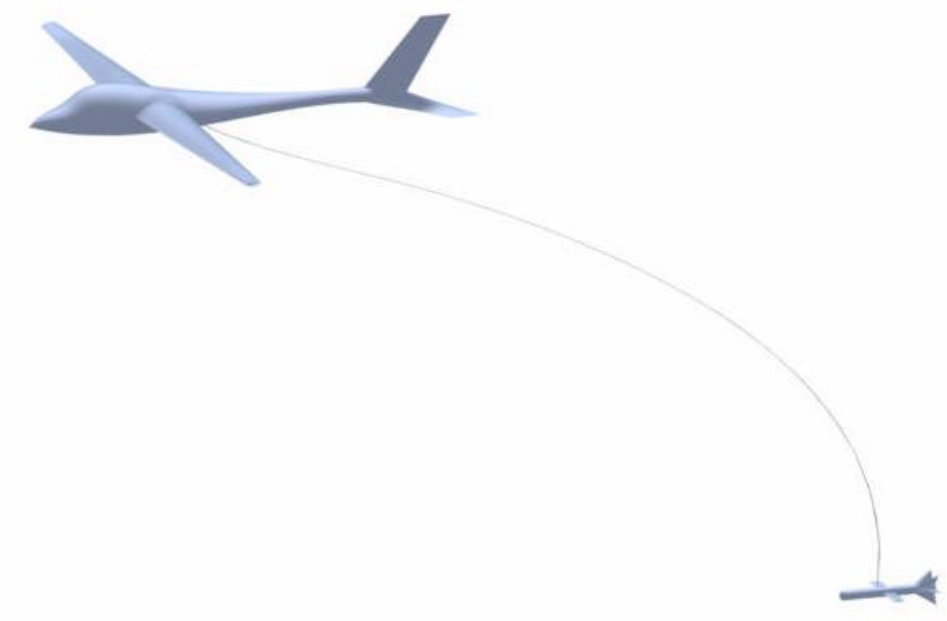

Figure 1.1 The aerial tow system

The aerial tow system is composed of three major components (1) host vehicle, (2) aerial tow vehicle (ATV), and (3) connecting cable, figure 1.1. In general, the host vehicle is larger than that of the tow vehicle and provides the thrust for both aircrafts. The cable is connected to both the host vehicle and the ATV in such a way that both aircraft can safely maintain flight. It is not uncommon in this configuration for the connecting cable to be hundreds or thousands of feet in length. As a result, the cable orientation is subject to change due to variations in the freestream conditions, cable dynamics, and the dynamics of the two aircrafts. The thrust produced by the host aircraft's engines is directly applied to the host aircraft and indirectly applied to the ATV thru the tension in the connecting cable. The tension in the cable produces a force on the ATV that may differ from the host vehicle thrust in magnitude and direction depending on the cable orientation. The variable cable force on the ATV causes a dynamic response resulting in further deformation of the connecting cable. Clearly, the conditions effecting these variations are coupled. Historical research suggests that, in general, the system is stable, and given sufficient time the disturbances in the system will damp out. However the degree to which the atmospheric and dynamic alterations affect the system depends principally on the system components and is, of yet, not well known.

Recently the aerial tow system has been chosen as a means to carry out the measurement of atmospheric conditions in close proximity to the ocean surface. The proposed system calls for a general aviation aircraft to tow the measurement instrumentation equipped ATV near (or approximately 30 feet) above the ocean surface. The emphasis of this system is the controlled altitude of the ATV. This is a deviation of

the aerial tow system from its roots as a means of transportation. Using the aerial tow system simply for transportation places no strict requirement on the motion of the ATV.

The aerial tow system is proposed as a safer, more robust alternative for recording oceanic atmospheric conditions. The traditional method necessitates an aircraft fitted with the appropriate sensory equipment fly immediately above the ocean surface. The aircraft's autopilot cannot be relied upon to safely maintain such altitude in this environment. Variable terrain and unknown atmospheric conditions could, indeed, result in disaster for the aircraft. As a result, the mission puts forth a tremendous workload upon the pilot. Due to the intense flight regime and pilot stress, the testing is usually limited to short duration and is confined to calm conditions.

The implementation of the aerial tow system as a method to take oceanic atmospheric measurements would allow the piloted host aircraft to fly at a safe height above sea level (such as 250 to 2000 feet) under the control of the aircraft autopilot while towing an unmanned sensory aircraft a matter of feet above the ocean. This would allow for longer tests runs, eliminate pilot stress, expand the mission envelope, as well as reduce the worst-case scenario to the mere loss of the unmanned aircraft, assuming this flight configuration is suitable for the task at hand.

Given the possibility of difficult ocean and atmospheric conditions, such as swales and wind gusts, the controllability of the tow system is in question. The system component interactions are complex, and neither the system configurations for the most advantageous performance nor the circumstances at which the system fails to adequately

perform are obvious. As a result, a system simulation preceding construction and testing is desirable.

Each component of the aerial tow system must be mathematically modeled in order to build a numerical system simulation. Simultaneous derivation of the component equations of motion will produce the governing equations for the aerial towed system from which a response to initial and applied conditions can be simulated.

The utilization of a system simulation would allow for prediction of the system's ability to perform under various conditions such as, wind gust, wave shape, and host aircraft oscillation. Previous aerial tow systems do not place such heavy emphasis on the maintenance of the altitude of the ATV. The unique mission of near ocean atmospheric measurement has driven the design of a mathematical simulation of the low altitude aerial tow system.

1.2 Design Goals

The objectives of this study is to create a dynamic simulation of the aerial tow system with the main focus surrounding the derivation of the system and component equations of motion in both two and three-dimensions. The study includes mathematical models for each of the system components as well as the methodology for the derivation of the equations of motion for each of the component models mentioned. The system will be adequately designed such that the effect of the following conditions on the tracking ability of the ATV may be simulated:

- Variable surface oscillations (ocean swales)

- Variable host vehicle altitudes
- Lateral gusts
- Host vehicle oscillation

The decisions upon the design of the system will be made with the versatility of the simulation in mind, in the hopes that this research will assist with a wide range of future studies of aerially towed systems, underwater towed systems, or cable dynamics.

1.3 Literature Review

The study of the tow system and its components has been well documented. The interest of cable dynamics, alone has produced analysis on the topics of cable oscillation and damping due to uniform flow, three-dimensional cable shaping, cable drag model validity, and numerical simulations of cable dynamics. Refs 1-4. However, the integrated effect of the ATV is necessary to simulate the aerial tow system.

As various tow systems come into existence study of the systems have flourished. Papers on tow vehicle controllability, stability augmentation, and release and retrieval dynamics build upon the dynamics of the cable in a flow, Refs 5 and 6. The investigation of tethered aerostat dynamics and underwater towing illustrates the range of the application and research of the tow system, Refs 7-9. Each of these references provides greater understanding of the tow system and its components.

1.3.1 Cable Dynamics

The cable has found its way into many applications involving fluid flow through out the years. As a result, countless papers have been written for discussion on various cable related topics. In general, the research was initiated for reasons supplementary to the cable's effect on aerial tow systems; however, each gives insight into the overall behavior of the cable in fluid flow. The past studies give a foothold for future system analysis containing cable components. Of particular interest are the studies on the physical and aerodynamic models of the cable.

1.3.1.1 Cable Models

A prediction of the dynamic response of a cable to given conditions requires a mathematical model of the cable from which the equations of motion can be derived. Choo and Casarella[10] produced a survey of various methods for modeling cables. The motivation behind this article was to acknowledge various methods that could be used for a basis of cable system simulations and analyzing the merits and demerits of each technique.

Among the methods discussed is the finite element method. This method breaks the continuous cable into an arbitrary number of segments which themselves can be modeled in a number of ways, such as the ideal pendulum, a mass on a spring, a cylinder, or curved segment model. In any case, each segment is free to rotate about its neighboring segments. Discretizing the cable allows for the derivation of the equations of motion of the interacting cable segments. The shortcoming to this technique is that the quality of the simulation is directly dependant upon the number of segments used to model the cable; a

finer discretization produces a superior simulation. However, as Walton and Polachek[18] discuss, when the segment length decreases a smaller step size is necessary for numerical convergence during simulation, which translates to more computation time. The benefit of using the finite element technique is that it can be used to study several types of unsteady motion in a cable or cable-body system. It is for this primary reason the Choo and Casarella[10] labeled this method as the most versatile.

Also discussed in the survey are the method of characteristics, the linearization method, and the equivalent lumped mass method. The method of characteristics employs constitutive laws such as Hooke's law, to convert the partial differential equations of motion into ordinary differential equations of motion. This technique allows the study of any sort of unsteady cable motion as long as the constitutive laws are satisfied, as an example; this method cannot be used on inextensible and viscoelastic cables as there are fewer ordinary differential equations than are original partial differential equations. In addition, the method of characteristics requires a large amount of computation.

The linearization method, as it suggests, linearizes the cable equations of motion. This linearization limits the technique to perturbation, small deviations from equilibrium, studies, such as stability and frequency response of the system. This technique is not applicable in cases where a limit cycle persists and additionally is not useful in the analysis of unsteady cable motion.

The equivalent lumped mass technique is useful when the most important aspect of the cable-body system is the body. In this method, the dynamics of the cable are completely ignored and the equations of motion of the system are largely due to the rigid-body

equations of motion of the body with added terms representing the cable dynamic effects. Since the equations of motion of the cable are omitted the system is greatly simplified. The simplicity, unfortunately, comes at the cost of the robustness of the model.

Each of these methods has a configuration or condition in which it gains advantage over the rest. However, the only one of the techniques with no system-type limitations is the finite element technique. An additional detailed description of the finite element method will be given in the following chapters.

1.3.1.2 Cable Drag Model

The work of Hoerner[13] is directed at analyzing and modeling fluid drag about various bodies. The cable is among the bodies researched. Hoerner[13] produced the cross-flow method for calculating the drag forces on a cable within a fluid. This technique analyzes the friction and pressure forces on the cable. The method is limited to straight cables of circular cross-section and fluid conditions that produce subcritical Reynolds numbers with respect to the cable diameter.

Despite the straight cable limitation of the cross-flow principle it can predict the drag force on a flexible cable (even though the cable is rarely completely straight). A curved cable can be approximated by a series of connected straight segment. Given the orientation of the straight segment relative to the fluid flow, the drag on each segment can be predicted using the cross-flow principle. Thus, the resultant fluid force on a curved cable is the accumulation of the individual segment's drag forces. As the number of cable segments increase so to does the accuracy of the overall drag prediction on the curved cable (to an extent).

The cross-flow principle works well with the finite element model of a cable (as it necessitates breaking the cable into straight cable segments). The applied drag forces on each of the cable segments can easily be applied to the dynamic equations of motion for each segment. The exact equation for the cross-flow principle in its original two-dimensional form and modified three-dimensional form are presented in chapters two and three.

1.3.2 Lagrange's Equations

Newtonian mechanics states that the motion of a particle can be determined provided that there is a complete knowledge of the external forces acting on the particle and that the initial conditions of the particle are known; the same is true for groups of interacting particles. This is a fundamental step in producing the equations of motion necessary to create a simulation of a system in response to inertial and external forces. The development of the equations of motion of a system can be trivial or quite complex depending on the composition of the system and its environment.

The direct application of Newton's laws becomes difficult as the number of groups of particles needed to represent the system increase. The motion of the system components and internal and external forces acting on the system exist as vectors, with magnitude and direction. Thus, keeping track of the external forces, internal forces, and motion of the system components in vector form is often difficult. A less complex method of deriving system equations of motion is attained by implementing Lagrange's equations, Greenwood[11].

The Lagrange method has two main advantages over the direct application of Newton's Laws in attaining the system equations of motion. The first is that the Lagrange approach is energy based rather than spatially based, thus it deals with scalar values which circumvents the vector bookkeeping involved with Newton's method. The other benefit of using the Lagrange equations is that, unlike the application of Newton's laws, it specifies an exact process to develop the equations of motion for any well defined system. After defining the system and its constraints, all one needs to do to develop the system equations of motion is to carryout the manipulation of Lagrange's equations.

An important concept in the application of Lagrange's equations is degree of freedom of the system. The number of degrees of freedom of a system is equal to the number of coordinates necessary to define the configuration of the system minus the number equations that constrain the position of the system. For example, assume the system is that of a simple two-dimensional ideal pendulum.

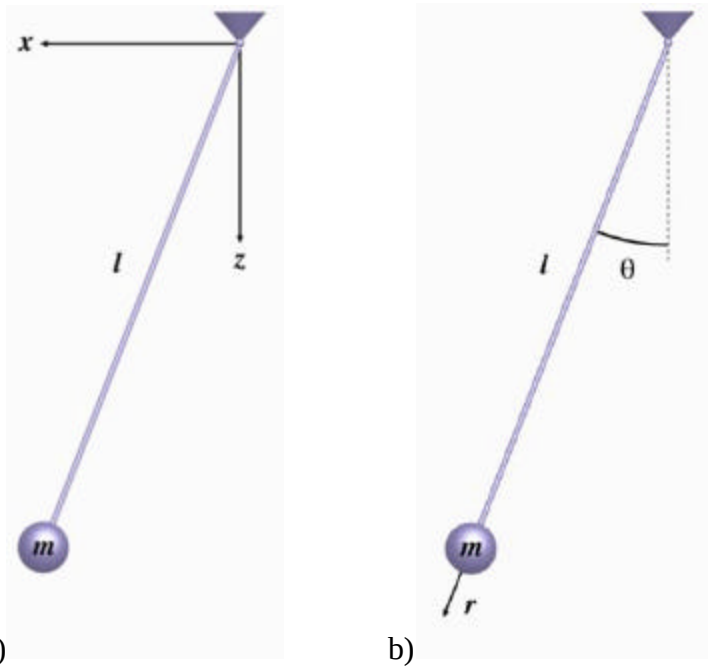

a) b)

Figure 1.2 Simple pendulum shown in two-dimensional a) Cartesian coordinates, and b) cylindrical coordinates

In two-dimensional Cartesian coordinates the location of the pendulum mass is determined by its *x* and *z* positions. However, the *x* and *z* positions are constrained to a circular path around the pendulum hinge with a radius equal to the length of the pendulum (we are assuming the length of the pendulum is rigid). The constraint equation would be the sum of the square of the *x* and *z* position is equal to the square of the length of the pendulum. Thus, if the *x* position is known then the application of the constraint equation will produce the *z* position of the pendulum mass. With two coordinates utilized to specify the orientation of the pendulum and the existence of one constraint equation the degree of freedom of the system is one.

Imagine the same example in cylindrical coordinates. The position of mass of the pendulum is determined simply by the angle *q* of the pendulum relative to the coordinate

frame. There is then one coordinate necessary to define the pendulum orientation and no constraint equation resulting in one degree of freedom for the pendulum.

As the pendulum example shows, the degree of freedom of the system is independent of the coordinates chosen to represent the system. The coordinates needed to represent the orientation of the system are deemed generalized coordinates. The generalized coordinates of the simple pendulum in the two-dimensional Cartesian coordinate system are the x and z position of the pendulum mass. The generalized coordinate of the same pendulum in cylindrical coordinates is simply the angle q. Therefore, since there are infinite possibilities of coordinate systems that could be used to analyze the pendulum there are infinite possibilities for generalized coordinates. However, in many cases there is a set of generalized coordinates in which the number of coordinates is equal to the degree of freedom of the system. This set is referred to as the independent generalized coordinates. The independent generalized coordinates require no constraint equations; as a result it is often simpler, mathematically, to analyze the system using the set of independent generalized coordinates. In the pendulum example the angle q is the independent generalized coordinate.

In a dynamic system the generalized coordinates, independent or not, vary with time and are algebraic variables in Lagrange's equations. As stated previously, Lagrange's equations are energy based. Prior to manipulation of Lagrange's equations the energy of the system must be represented in terms of the generalized coordinates. The manipulation of Lagrange's equations requires derivation of the system energies with respect to time and the generalized coordinates. The exact form of Lagrange's equations

as well as the execution of Lagrange's equations will be undertaken in detail in the next two chapters.

1.3.3 Aircraft Dynamics

There has been much effort spent by researchers and scientists in the study of aerodynamics as it relates to aircraft. This work ranges from simple analysis of fluid flow over a two-dimensional airfoil-shape to the development of nonlinear equations of motion for high speed maneuverable aircraft. The extensive work accomplished for a wide variety of aircraft and flight conditions has produced reliable models for the prediction of aircraft response to fluid forces.

The method used to represent the dynamics of the aircraft in this system is small-disturbance theory, Nelson[14]. Small-disturbance theory assumes that the motion of an aircraft consists of steady-state motion and small perturbations about its steady-state. Small-disturbance theory linearizes the rigid body equations of motion. This is accomplished by substituting reference values plus a perturbation for the all variables in the rigid body equations of motion. Many reference values (e.g. pitch, roll, etc.,) can be set to zero by assuming a symmetric reference flight condition. Simplification of the equations of motion after substitution produces products of perturbation. These nonlinearities are ignored in the assumption that higher order small disturbances will produce negligible overall effects.

Further simplifications of the equations of motion produce aerodynamic stability derivatives. The stability derivatives represent the change in forces or moments of a body due to some change in the flight conditions, such as forward velocity or angle of attack.

The stability derivatives are approximated based upon the size, shape, and mass distribution of an aircraft and its components. Methods for approximation of aircraft stability derivatives are presented in Nelson[14] and Raymer[16].

The equations of motion for aircraft are written in terms of normalized stability derivatives. As a result, these general equations apply to a wide variety of general aviation aircraft over most flight conditions. However, since the equations were linearized using small disturbances, the theory breaks down and thus does not produce accurate predictions when the motion of the system involves large amplitude motions such as aircraft stall or spinning. Given the simple shape of the ATV and its proposed flight conditions the small-disturbance theory will be adequate in modeling dynamics of the aircraft.

1.3.4 Cable Towed Systems

A cable tow system in its most simple form consists of a body constrained by cable in a fluid. There are a wide range of system configurations that meet the requirements of a cable tow system, such as kites, tethered aerostats, mooring lines, towed buoys (above and below the ocean surface), gliders, and towed aircraft targets. Research on many of these systems has been accomplished in the past. Each system has its own nuances that separate one author's work from another, and although not all are directly applicable to the aerial towed system they help to illustrate the diversity of the system. A few of the papers that do apply to the aerial tow system are discussed below.

Huffman and Genin[1] research the stability of a simple aerial towed system. Their research suggests that there is no direct instability in the dynamics of the towed cable

system. In each case tested the disturbances of the system were damped out in time. They concluded that a likelihood of instability is present, however, when the dynamic frequency of the towed body matches the natural frequency of the cable. The result would be a limit cycle oscillation. Huffman and Genin[1] also show that the natural frequency of cable can vary based upon parameters such as cable length and flight speed. As a result, the limit cycle behavior could be present in tow system at particular flight conditions. However, this depends largely on many variables in the system. As a result, there was no generalized parametric study.

Cochran et al.[6] investigate the effect of controlling an aerial towed vehicle. The authors designed a control system that would augment the stability of the towed vehicle. Simulations were run in conditions that produced unstable dynamic motion in the uncontrolled towed vehicle (perturbed retrieval of the towed aircraft). When the control system was activated the authors showed that the system damped out quickly. This paper addresses the difficulties of designing a controlled aerially towed system and the results suggest that improved stability can be achieved during maneuvers that could otherwise result in instability.

Nakagawa and Obata[15] studied the longitudinal dynamic modes of the aerial tow system. They analyzed the modes of three flight configurations, a straight cable connected to a sphere, a straight cable connected to an aircraft, and a curved cable connected to an aircraft. The results of the study helped to classify the types of motion of the aerial tow system. In all of the configurations the main dynamic modes were the pitching mode, pendulum mode, and first vibration mode. The pitching mode is simply

the pitching of the towed body; this has little effect on the cable dynamics or the translation of the towed body. The pendulum mode oscillates the towed body about its static configuration. The motion causes slight bending in the cable and little if any towed body pitching. In both of the straight cable configurations the first vibration mode has little effect on the position or the orientation of the towed body, and simply causes oscillations in the cable. However, in the curved cable configuration the first vibration mode causes the towed aircraft to surge fore and aft in an elliptical pattern. The authors labeled this as the bowing mode.

The authors complete a parametric study of the aircraft longitudinal stability derivatives and found that two of them, Z_w and M_w as well as the cable-towed body hitch point played an important roll in the stability of the system. The results showed a strong relationship between the stability derivatives and the bowing mode. As the absolute values of Z_w and M_w increase and decrease, respectively, the bowing mode becomes less stable, and eventually an unstable phenomenon known as pitching or bowing flutter occurs. Nakagawa and Obata[15] noticed a similar behavior as the cable hitch point on the towed aircraft was moved more and more fore of its center of gravity.

The system dynamic oscillations are of the utmost importance when attempting to fly the towed body very near the ocean surface. The research completed by Nakagawa and Obata[15] suggest care should be taken when designing the ATV as its stability derivatives have a direct effect on unwanted system oscillations. Lawhon and Arena[19] investigated the effects of aircraft size and shape as well as cable parameters to develop the optimum

system configuration for aerially towed systems tracking very near the ocean surface. The ATV used in this paper was a result of the work done by Lawhon and Arena[19].

CHAPTER 2

TWO-DIMENSIONAL DYNAMICS

2.1 Introduction

It is the focus of this paper to derive and produce the mathematical equations that accurately describe the three-dimensional motion of the aerially towed system. Followed by, implementing the equations of motion to produce a dynamic simulation of the aerially towed system. The simulation will then be used to draw general conclusions about the system and its ability to perform the maneuvers desired to obtain atmospheric measurements near the oceans surface.

The individual dynamic behavior of the system components and the interactions between them will result in quite complex set of equations of motion. As a result of this complexity, it is easy to get bogged down by the shear volume of the equations and lose sight of the steps taken to derive the final set of equations. This is especially true in reference to the three-dimensional system. Therefore, the two-dimensional equations of motion will be laid out in this chapter. The two-dimensional equations of motion will also act to verify that the more complex three-dimensional equations of motion are derived without error. It is important to note that the same principles will be held for the derivation of both the two and three-dimensional systems although they may differ in clarity.

The basis of any simulation is the modeling of the system components. The quality of the models directly affects the value of the simulation. The derivation of the equations that dictate the dynamics of a component is possible upon the completion of its mathematical model. To accurately model the system, the individual component dynamics are important however, the modeling of the system necessitates the equations of motion represent the dynamic interaction between the components as well. Thus, in general, the derivation of the equations of motion of a system component must be accomplished simultaneously with the dynamic equations of the remaining objects. The result will be a set of equations that represent the dynamics of the entire system, i.e. if the host vehicle oscillates the system equations of motion will reflect the oscillations effect on the dynamics of the cable and the ATV.

The following sections discuss the modeling of the system components and the development of the individual dynamic equations of each component. As stated previously, the individual component dynamics are not enough to model the system; however, they may be of academic interest, and will lead to a clear understanding of the derivation of the system equations of motion.

2.2 Cable Dynamics

As discussed in the literature review there has been extensive study on cable dynamics and cable modeling for a wide range of applications. Due its versatility the finite element technique will be used to model the connecting cable. The main drawback of the finite element technique is its computational expense. The great strides in computer speed over the years helps to soften this blow. There may also be situations when the operator is not

interested in a completely rigorous simulation but rather just a feel of the system's behavior, this can be accomplish quickly by using fewer segments.

As mentioned previously, the finite element technique requires that the cable be broken into an arbitrary number of segments which are free to rotate about their neighboring segments. The types of segments used to model the cable can vary. Notable models include the simple pendulum, spring mass, thin rod, and curved structure model.

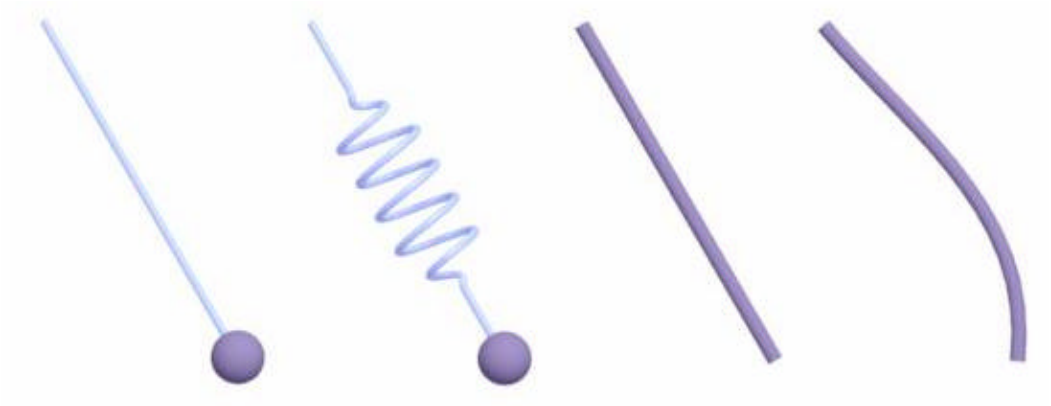

Figure 2.1 Finite element cable segment models

In the simple pendulum model, the segment is straight and inextensible. The mass of the segment is lumped to a single point at the tip of the segment, resulting in a model that resembles that of a simple pendulum. Being that the segment is straight the cross-flow method can be used to predict the drag force on the segment. The applied force on the segment is exerted at the point mass or node. The inextensible constraint lends this model to a system in which the strain on the cable is minimal. The benefit of this technique is its simplicity. The draw back is that placing the inertial and applied forces at the tip of the segment only becomes a good approximation when the number of segments used is large.

The spring mass segment also lumps the mass at tip of the segment, however the segment length acts as a spring. This allows for strain effects to be incorporated into the equations of motion of the cable. The change in length of each segment adds an additional degree of freedom to the system, which increases the complexity of the equations of motion and increase computational intensity. If the strain on the cable can be neglected the spring mass segment model expends much unneeded effort and time.

The thin rod model is similar to the lumped mass model. It too is straight and inextensible. However, the model places the inertial forces and applied forces at the center of mass of the segment. The additional complexity of this model is that the mass of the rod is not lumped to a point; therefore, it has inertia that impedes segment rotation and must be taken into account the derivation of the equations of motion. The benefit of the better physical model is it will take fewer segments to accurately represent the motion of the continuous cable than the lumped mass model.

The last model represents the cable segment as a curved structure. This technique models the segments as polynomials or splines which require slope continuity at the segment connections. Due to the fact that most cable configurations are curved this method reduces the number of segment needed to attain an accurate simulation. However, the evaluation of the drag on a curved cable is not well known. The more complex drag model and polynomial or spline calculations make derivation of the cable equations of motion difficult.

Neglecting the strain in the cable is acceptable as we are dealing with a fairly light ATV and a high tensile steel connecting cable, thus the spring mass model unnecessary;

and given that there is a historically accepted method to model the drag on a straight cable the complexities of the curved structure will be avoided. The equations of motion of the cable will be derived using the simplest segment model, the pendulum model, shown in figure 2.1. However, a discussion about the changes to the cable equations of motion as a result of modeling the cable segments as thin rods will take place at the end of this chapter.

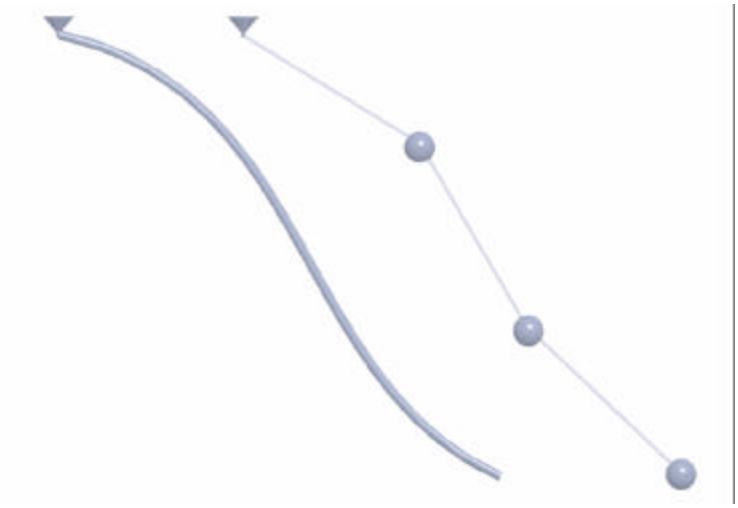

Figure 2.2 Lumped mass finite element cable model

2.2.1 Coordinate Systems

In this section the primary concern is the development of the two-dimensional equations of motion for a flexible cable. As a result, the host aircraft and the ATV will be neglected for now. The cable is broken into *n* arbitrary segments in accordance with the finite element cable model. Therefore, one end of the cable is fix to a point in space and is free to rotate while the other is end is constrained only by its preceding segments.

The coordinate system at the cable attach point is the inertial coordinate system. This coordinate system is orthogonal. The *X* axis is locally parallel to the 'ground' and the *Z*

axis is pointing toward and is normal to the 'ground'. The derivation of the equations of motion of the flexible cable will be carried out in the inertial frame. As a result, it is necessary to be able to describe the orientation of the cable in this coordinate system. The location of the i^{th} cable node in the inertial frame can be resolved using the length, l_i, and angle of orientation, q_i, of the segment and each preceding segment, as shown below.

$$\begin{aligned} X_i &= \sum_{j=1}^{i} l_j S_{q_j} \\ Z_i &= \sum_{j=1}^{i} l_j C_{q_j} \end{aligned} \qquad (i = 1,2 \ldots n) \tag{2.1}$$

where, l_j is the length of the j^{th} segment and X_i and Z_i are the position of the i^{th} segment in the inertial frame. Also note C and S are short notation for cosine and sine, this notation will be used throughout the remainder of this paper.

Aside from the inertial frame, each cable segment has its own coordinate system. The cable segment coordinate system is orthogonal and is configured such that the node of that segment is located in the positive z-direction a distance equal to that of the cable segment. For example, the origin of the coordinate axis for the first cable segment is located at the exact same point as that of the origin of the inertial frame. The two frames differ only by the angle rotation of the segment, q_1. When the angle is equal to zero the two frames are identical. In a similar manner, the origin of the second cable segment is located at the node of the first cable segment, and the first and second frame differ rotationally by the difference of q_2 and q_1. This is evident from Figure 2.2.

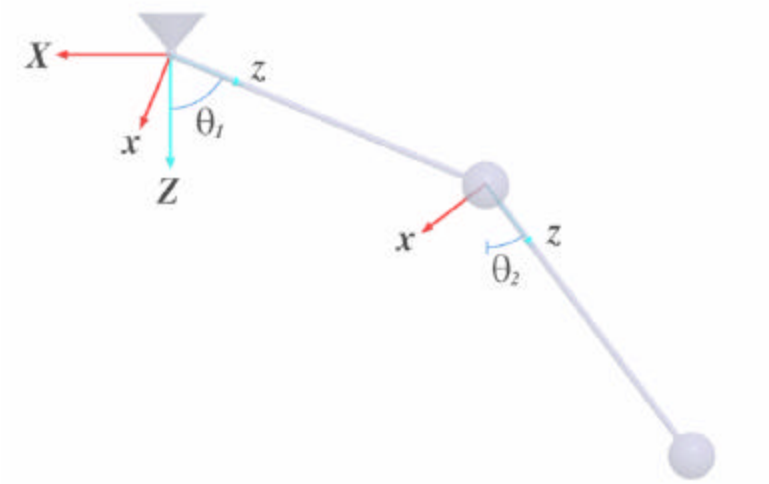

Figure 2.3 Two-dimensional inertial and cable segment coordinate systems

Throughout the analysis of the system it will be necessary to convert from the inertial frame to the segment frame. This is accomplished by utilizing a rotational coordinate transformation. The rotational coordinate transformation from the i^{th} cable segment frame to the inertial frame is represented by the directional cosine matrix as follows,

$$\underline{\underline{C}}_{q_i} = \begin{bmatrix} C_{q_i} & S_{q_i} \\ -S_{q_i} & C_{q_i} \end{bmatrix} \tag{2.2}$$

The inverse of the directional cosine matrix produces a rotational coordinate transformation from the inertial frame to the i^{th} cable segment frame.

Calculating the inertial position of the node of the i^{th} cable segment is a common implementation of the rotational transformation. Recall that in the cable segment frame the node is located at a distance equal to the length of the segment in the z-direction. Using the directional cosine matrix the position of the i^{th} cable segment node in the inertial coordinate system is as follows,

$$\begin{bmatrix} X_i \\ Z_i \end{bmatrix} = \sum_{j=1}^{i} \left[\underline{\underline{C_{q_j}}} \right] \begin{bmatrix} 0 \\ l_j \end{bmatrix} \quad (i = 1,2,\ldots,n) \tag{2.3}$$

Note that equation 2.3 and 2.1 are equivalent.

2.2.2 Lagrange Equations

As discussed earlier, the connecting cable is broken into *n* arbitrary number of segments, and each segment has its own coordinate system. Deriving the equations of motion for the cable using the direct application of Newton's laws of motion becomes increasingly difficult as the number of segments used to model the cable increases. This is primarily due to the fact the Newton's laws of motion are vector based and as the system increases the number of coordinate systems increase resulting in labor-intensive derivation. Another difficulty when using the Newtonian approach is that there is no general method to derive the equations of motion. As discussed in the previous chapter, an alternative to using Newton's laws of motion is the utilization of Lagrange's equations, which is energy based. Consequently, it circumvents many of the complexities of vector-based derivation, as well as, gives a standard process for developing the system equations of motion.

To recap, the derivation of Lagrange's equations depends on the degree of freedom of the system, and the degree of freedom of the system is the number of coordinates needed to define the system minus the number of constraint equations of the system. In the Cartesian coordinates of the inertial frame for a cable broken into *n* segments there are 2*n* coordinates needed to define the location of the node of each segment. However, each segment has a constraint equation of the form,

$$l_i^2 = \left(X_i - \sum_{j=1}^{i-1} X_j \right)^2 + \left(Z_i - \sum_{j=1}^{i-1} Z_j \right)^2 \quad (i = 1,2,\ldots,n) \tag{2.4}$$

As a result, 2*n* coordinates and *n* constraint equations produce *n* degrees of freedom. In other words, the two-dimensional finite element cable has a degree of freedom equal to the number of segments used to model the cable.

The coordinates used to define the system are the generalized coordinates. The generalized coordinates are general due to the fact that there are an infinite number of coordinate systems that could be used to define the system all with varying number of constraint equations (although every system has *n* degrees of freedom). Consequently, there are no specific coordinates that need to be used to define the system. The implementation of Lagrange's equations will be simplified if the independent generalized coordinates are used (recall, the independent generalized coordinates are the set of coordinates that define the system yet have no constraint equations).

For the flexible cable system the independent generalized coordinates are the orientation or attitude angles of each of the segments, q_i (i = 1, 2… n). For the duration of the chapter the attitude angles of the cable segments will be used and referred to as the generalized coordinates of the system. The generalized coordinates will be generically referred to by the variable *q*.

As stated previously, Lagrange's equations are energy based. The Lagrangian function, *L*, represents the energies of the system and is equivalent to the kinetic energy minus the potential energy of the system,

$$L = T - U \tag{2.5}$$

where, T and U are kinetic and potential energy functions, respectively.

Lagrange's equations are as follows,

$$\frac{d}{dt}\left(\frac{\partial L}{\partial \dot{q}_i}\right) - \frac{\partial L}{\partial q_i} = Q_i' \quad (i = 1,2,\ldots,n) \tag{2.6}$$

where, Q_i' represents the applied, or generalized, forces that are not derivable from a potential function, such forces include friction forces and forcing functions. However, since the potential function for this system is not velocity dependant Lagrange's equations can be reduced to the following,

$$\frac{d}{dt}\left(\frac{\partial T}{\partial \dot{q}_i}\right) - \frac{\partial T}{\partial q_i} = Q_i' - \frac{\partial U}{\partial q_i} = Q_i \quad (i = 1,2,\ldots,n) \tag{2.7}$$

where, Q_i are the generalized forces that include applied forces and the inertial forces derived from the potential function. Note that Equations 2.6 and 2.7 is actually a set of n equations, one equation for each generalized coordinate of the system. Thus, in the case of the two-dimensional finite element modeled cable there is one equation for each attitude angle of the n cable segments. Therefore, Lagrange's equations can be rewritten as,

$$\frac{d}{dt}\left(\frac{\partial T}{\partial \dot{q}_i}\right) - \frac{\partial T}{\partial q_i} = Q_i \quad (i = 1,2,\ldots,n) \tag{2.8}$$

In order to implement Lagrange's equations it is necessary to get the energies of the systems in terms of the generalized coordinate. Only then can the proper derivation of the equations of motion take place. The kinetic energy of the system at any given time is due to the summation of the rotational and translational motion of the inertial components of the system. For the finite element cable the inertial components are simply the segment nodes. Thus, the kinetic energy of the cable is the summation of the nodal rotational and translational kinetic energy. However, since the mass of a segment is localized to a point it has no rotational inertial and consequently has no rotational kinetic energy. As a result, the kinetic energy of the system is solely a function of the translational velocity of each node.

$$T = \frac{1}{2}\sum_{j=1}^{n} m_j V_j^2 \tag{2.9}$$

The velocity components of a node can be found by simply taking the time derivative of its position.

$$\begin{aligned} \dot{X}_i &= \sum_{j=1}^{i} \dot{q}_j l_j C_{q_j} \\ \dot{Z}_i &= \sum_{j=1}^{i} -\dot{q}_j l_j S_{q_j} \end{aligned} \qquad (i = 1,2,\ldots,n) \tag{2.10}$$

Equation 2.10 shows that the translational velocity of a node results from the rate of rotation of its segment and each preceding segment. At this moment, the velocity of each node is in vector form. However, squaring the velocity for the kinetic energy releases

any further vector bookkeeping. The square of velocity, *V*, for the k^{th} segment is can be written in series form as follows,

$$V_k^2 = \left(\dot{X}_k^2 + \dot{Z}_k^2\right) = \sum_{j=1}^{k}\sum_{i=1}^{k} l_i l_j \dot{q}_i \dot{q}_j \left(C_{q_i} C_{q_j} + S_{q_i} S_{q_j}\right) = \sum_{j=1}^{k}\sum_{i=1}^{k} l_i l_j \dot{q}_i \dot{q}_j C_{(q_i - q_j)} \qquad (2.11)$$

Similarly, the total kinetic energy for *n* cable segments is written in summation form as,

$$T = \frac{1}{2}\sum_{k=1}^{n} m_k V_k^2 = \frac{1}{2}\sum_{k=1}^{n}\sum_{j=1}^{k}\sum_{i=1}^{k} m_k l_i l_j \dot{q}_i \dot{q}_j C_{(q_i - q_j)} \qquad (2.12)$$

Being that the kinetic energy has been derived in terms of the generalized coordinates the implementation of Lagrange's equations can commence. The derivative of kinetic energy with respect to the i^{th} generalized coordinate and the time rate of change of the i^{th} generalized coordinate yields the following,

$$\frac{\partial T}{\partial q_i} = \sum_{k=1}^{n}\sum_{j=1}^{k} m_k l_i l_j \dot{q}_i \dot{q}_j S_{(q_j - q_i)} \qquad (2.13)$$

$$\frac{\partial T}{\partial \dot{q}_i} = \sum_{k=1}^{n}\sum_{j=1}^{k} m_k l_i l_j \dot{q}_j C_{(q_j - q_i)} \qquad (2.14)$$

Finally evaluating the time rate of change of equation 2.14 produces,

$$\frac{d}{dt}\left(\frac{\partial T}{\partial \dot{q}_i}\right) = \sum_{k=1}^{n}\sum_{j=1}^{k} m_k l_i l_j \left[\ddot{q}_j C_{(q_j - q_i)} - \dot{q}_j S_{(q_j - q_i)}\left(\dot{q}_j - \dot{q}_i\right)\right] \qquad (2.15)$$

Combining equations 2.13 and 2.15 results in the series representation of the left hand side of the Lagrange's equations for the two-dimensional finite element modeled cable,

$$\frac{d}{dt}\left(\frac{\partial T}{\partial \dot{q}_i}\right) - \frac{\partial T}{\partial q_i} = \sum_{k=1}^{n}\sum_{j=1}^{k} m_k l_i l_j \left(\ddot{q}_j C_{(q_j - q_i)} - \dot{q}_j^{\,2} S_{(q_j - q_i)}\right) \quad (i = 1,2,\ldots,n) \qquad (2.16)$$

The right hand side of equation 2.8 represents the generalized forces of the system. Note that due to the fact that the generalized coordinates of the system are angles the general forces are actually moments. These moments are about the pivot point of each segment and result from the inertial and applied forces on the node of the segment as well as any applied moments.

The generalized force equation is derived from the concept of virtual work. Suppose forces $F_1, F_2, \ldots, F_k$ are applied at position $x_1, x_2, \ldots, x_k$ and moments $M_1, M_2, \ldots, M_k$ are applied at angles $f_1, f_2, \ldots, f_k$. Now let us assume that the system undergoes arbitrary small displacements $dx_1, dx_2, \ldots, dx_k$ and $df_1, df_2, \ldots, df_k$. The work done by these applied forces and moments is known as virtual work and the small displacements are known as virtual displacements,

$$dW = \sum_{j=1}^{k} F_j dx_j + M_j d\,j_j \qquad (2.17)$$

The virtual displacements can be rewritten in terms of the virtual displacement of the generalized coordinates,

$$dx_j = \sum_{i=1}^{n} \frac{\partial x_j}{\partial q_i} dq_i \qquad (2.18)$$

$$d\,j_j = \sum_{i=1}^{n} \frac{\partial j_j}{\partial q_i} dq_i \qquad (2.19)$$

The relationship between the generalized forces and the virtual work of the system due to the virtual displacement of the generalized coordinates is as follows,

$$dW = \sum_{j=1}^{k}\sum_{i=1}^{n} F_j \frac{\partial x_j}{\partial q_i} dq_i + M_j \frac{\partial j_j}{\partial q_i} dq_i = \sum_{i}^{n} Q_i dq_i \tag{2.20}$$

Simplification of equation 2.20 produces the generalized force equation for the applied forces and moments in terms of the generic variables x and f.

$$Q_i' = \sum_{i=1}^{n} F_j \frac{\partial x_j}{\partial q_i} dq_i + M_j \frac{\partial j_j}{\partial q_i} dq_i \tag{2.21}$$

In the case of the two-dimensional cable segment system the position variables are X and Z while the angles are q. Incidentally, the generalized coordinate for this system is also q. The equation for the generalized forces not produced by the potential function is as follows,

$$Q_i' = \sum_{j=1}^{n} F_{X\,j} \frac{\partial X_j}{\partial q_i} + F_{Z\,j} \frac{\partial Z_j}{\partial q_i} + M_{q_i} \frac{\partial q_j}{\partial q_i} \quad (i = 1, 2, \ldots, n) \tag{2.22}$$

The total generalized force equation is made up of the external forces and moments as well as the inertial forces,

$$Q_i = -\frac{\partial U}{\partial q_i} + \sum_{j=1}^{n} F_{X\,j} \frac{\partial X_j}{\partial q_i} + F_{Z\,j} \frac{\partial Z_j}{\partial q_i} + M_{q\,j} \frac{\partial q_j}{\partial q_i} \quad (i = 1, 2, \ldots, n) \tag{2.23}$$

where, $F_{X\,j}$ and $F_{Z\,j}$ are applied forces and $M_{q\,j}$ is the applied moment of the j^{th} segment in the inertial coordinate frame.

In the expansion of equations 2.23 let us look first at the term that is the derivative of potential energy with respect to the i^{th} generalized coordinate. The potential energy of the cable is the summation of the potential energy of each segment node.

$$U = \sum_{k=1}^{n} \sum_{i=1}^{k} m_k g(Z_i - D) \tag{2.24}$$

where, D is the datum line from which potential energy is measured. Note that since potential energy is being differentiated the location of the datum line is inconsequential. Taking the derivative of equation 2.24 with respect to the i^{th} generalized coordinate produces,

$$\frac{\partial U}{\partial q_i} = \sum_{j=1}^{n} m_j g \frac{\partial Z_j}{\partial q_i} \tag{2.25}$$

The resulting equation allows the inertial force to be included with the z-direction applied force. Simplify the generalized force equation to that shown below,

$$Q_i = \sum_{j=1}^{n} F_{X_j} \frac{\partial X_j}{\partial q_i} + \left(F_{Z_j} + m_j g\right) \frac{\partial Z_j}{\partial q_i} + M_{q_j} \frac{\partial q_j}{\partial q_i} \quad (i = 1, 2, \ldots, n) \tag{2.26}$$

The derivative of position and angle with respect to the i^{th} generalized coordinate is as follows,

$$\frac{\partial X_j}{\partial q_i} = l_i C_{q_i} \qquad (j \geq i)$$
$$\frac{\partial Z_j}{\partial q_i} = -l_i S_{q_i} \qquad (j \geq i) \tag{2.27}$$
$$\frac{\partial q_j}{\partial q_i} = 1 \qquad (j = i)$$

Note that the position of the node of a segment is dependant upon that segments attitude angle and the attitude angle of each preceding segment. Due to the nature of the dependence of position on the generalized coordinate, the evaluation of the derivative of the position of the j^{th} segment with respect to the i^{th} generalized coordinate results in zero when i is greater than j. The derivative of angle with respect to the i^{th} generalized coordinate is equal to one when i is equal to j and zero otherwise. Thus,

$$Q_i = M_{q\,i} + \sum_{j=i}^{n} F_{X\,j} l_i C_{q_i} - \left(F_{Z\,j} + m_j g\right) l_i S_{q_i} \qquad (i = 1, 2, \ldots, n) \tag{2.28}$$

The complete derivation of Lagrange's equations for the two-dimensional finite element modeled cable is attained by combining equations 2.16 and 2.28. The resulting set of n equations of motion is presented as follows in summation form.

$$\sum_{k=1}^{n}\sum_{j=1}^{k} m_k l_i l_j \left(\ddot{q}_j C_{(q_j - q_i)} - \dot{q}_j^{\,2} S_{(q_j - q_i)}\right) =$$
$$M_{q\,i} + \sum_{j=i}^{n} F_{X\,j} l_i C_{q_i} - \left(F_{Z\,j} + m_j g\right) l_i S_{q_i} \tag{2.29}$$
$$(i = 1, 2, \ldots, n)$$

The set of equations of motion can be more clearly presented in matrix form, yielding,

$$[A][\ddot{q}]+[B][\dot{q}^2]=[Q] \tag{2.30}$$

where, A and B are coefficient matrices and are size *n* by *n*. The remaining three matrices are column matrices of size *n* by 1. The values of the coefficient matrices are as follows,

$$A_{i,j} = l_i l_j C_{(q_j - q_i)} \underline{m}_{i,j} \tag{2.31}$$

$$B_{i,j} = -l_i l_j S_{(q_j - q_i)} \underline{m}_{i,j} \tag{2.32}$$

where, the subscripts *i* and *j* represent the row and column of the appropriate matrix, and $\underline{m}_{i,j}$ represents the mass distribution for row *i* and column *j*. For the lumped mass model of the *n* segments the mass distribution is simply a sum of segment masses.

$$\underline{m}_{i,j} = \sum_{k=\max(i,j)}^{n} m_k \tag{2.33}$$

For example, the equations of motion for a cable modeled using two cable segments without fluid drag would be as follows,

$$\begin{bmatrix} (m_1+m_2)l_1^2 & m_2 l_1 l_2 C_{(q_2-q_1)} \\ m_2 l_1 l_2 C_{(q_1-q_2)} & m_2 l_2^2 \end{bmatrix} \begin{bmatrix} \ddot{q}_1 \\ \ddot{q}_2 \end{bmatrix} + \begin{bmatrix} 0 & -m_2 l_1 l_2 S_{(q_2-q_1)} \\ -m_2 l_1 l_2 S_{(q_1-q_2)} & 0 \end{bmatrix} \begin{bmatrix} \dot{q}_1^2 \\ \dot{q}_2^2 \end{bmatrix} = \begin{bmatrix} -(m_1+m_2) g l_1 S_{q_1} \\ -m_2 g l_2 S_{q_2} \end{bmatrix} \tag{2.34}$$

These two equations are analogous to the equations of motion of a two-dimensional ideal double pendulum.

The resulting fully nonlinear two-dimensional equations of motion describe the dynamics of the system due to inertial and applied loads, as well as, the dynamic interaction between all segments; and the set of equations place no limitations on the number of segments of the system (while the equations hold true independent of the number of segments the effects on simulation computation varies, this will be discussed in chapter 5). The angular acceleration of each segment can be calculated given appropriate initial conditions, such as segment attitude angle and angular velocity of the system. The implementation of a numerical integration routine on the set of ordinary differential equations allows the prediction of cable motion for various initial conditions, and with the addition of a drag model to predict the applied friction forces on the segments the simulation can be extended to that of a cable in fluid flow.

2.2.3 Aerodynamic Forces

The generalized force matrix in the equation 2.30 is composed of the inertial forces and applied forces of each of the cable segment. These applied forces are the friction forces produced by the fluid interaction with the cable. Thus to fully derive the equations of motion for a cable in a fluid a drag model is necessary. As stated previously, the study of cable drag has a history that dates back to the early aircraft and thus has been well documented.

The cable crossflow-principle, Hoerner[13], is a drag model that was presented in the sixties and has since been used as a basis for numerous research papers involving fluid immersed cables. Its limitations require the cable cross-section be circular, the cable be straight, and fluid be at a subcritical Reynolds number. In general, aircraft tow cables are

circular in cross-section; due to our relatively low airspeeds the Reynolds number is subcritical; and our finite element model for the cable requires that the cable be broken into straight segments. Therefore, the Hoerner crossflow-principle applies very nicely to our model of the cable system.

The crossflow-principle calculates the tangential and normal forces on a straight cable segment produced by tangential and normal velocities about the cable, as shown below,

$$\begin{aligned} F_{x_j} &= -\frac{1}{2} r dl_j V_{x_j} \left(p c_f \sqrt{V_{x_j}^2 + V_{z_j}^2} + c_p |V_x| \right) \\ F_{z_j} &= -\frac{1}{2} r dl_j V_{z_j} \left(p c_f \sqrt{V_{x_j}^2 + V_{z_j}^2} \right) \end{aligned} \tag{2.35}$$

where, r, d, c_f, and c_p are air density, cable diameter, frictional coefficient, and pressure coefficient, respectively, and F_x, F_z, V_x, and V_z are the aerodynamic forces and the flow field velocity in the cable segment coordinate system, respectively.

The cable velocity in the cable segment frame can be attained simply by using the rotational coordinate transformation of the relative velocity of the segment node in the inertial frame, as shown below,

$$\begin{bmatrix} V_{x\,j} \\ V_{z\,j} \end{bmatrix} = \left[\underline{\underline{C_{q_j}}} \right]^T \begin{bmatrix} U_0 + \dot{X}_j \\ W_0 + \dot{Z}_j \end{bmatrix} \tag{2.36}$$

Presumably the freestream velocities, U_0 and W_0, are known and the equations for calculating the velocity of a segment node in the inertial frame were derived in equation 2.10.

Note that the drag forces produced by the drag model are in the cable frame yet the forces in the generalized coordinate equation are in the inertial frame. As a result, the calculated normal and tangential drag forces must go through a rotational coordinate transformation before application can be made.

$$\begin{bmatrix} F_{X_j} \\ F_{Z_j} \end{bmatrix} = \begin{bmatrix} \underline{\underline{C_{q_j}}} \end{bmatrix} \begin{bmatrix} F_{x_j} \\ F_{z_j} \end{bmatrix} \tag{2.37}$$

The implementation of the Hoerner drag model produces the mathematical model of the applied loads on a cable segment. The generalized forces for each segment can be calculated based on cable motion and numerous freestream conditions and thus allows for the dynamic simulation of a cable in a fluid.

2.3 ATV Dynamics

The ATV alone is an aircraft, and a very simple one at that. As a result, its rigid body dynamics could be easily modeled due to the extensive research and documentation done in the area aircraft flight dynamics. However, in the aerial towed system the dynamics of the cable and the dynamics of the ATV are intertwined, consisting of individual dynamics and the interaction of the two components. As a result, a system of equations containing both the equations of motion of the cable and that of the ATV must be derived and solved simultaneously. This is most easily accomplished by reproducing the ATV as an additional segment, one which is attached to n^{th} cable segment. Thus the equations of motion for both the cable and ATV can be derived using Lagrange's equations. Since the equations of motion of the cable were derived to be independent of the number of segments this does not change the form of the equations previously derived. The

variation in the set of equations arises because the ATV segment model differs from the cable segment model. The set of equations for the cable and ATV and there variations from the previous cable dynamic set will be laid out in the subsequent sections.

2.3.1 Coordinate system

Modeling the ATV as an additional segment adds an extra coordinate system just as adding an extra cable segment to the cable model. This system is analogous to the cable coordinate system described previously, the origin is the cable-ATV hitch point and its z-axis passes through the center of mass of the ATV. However, there is another coordinate system necessary to fully describe the orientation of the ATV. This coordinate system corresponds to the standard aircraft body fixed coordinate system.

The aircraft body fixed coordinate system has it origin at the center of gravity of the aircraft, and for the two-dimensional case the aircraft body fixed *x*-direction is pointing out of the nose of the aircraft and its *z*-axis is pointing out of the bottom of the aircraft (presumably towards the ground). The two additional axes are present in figure 2.3.

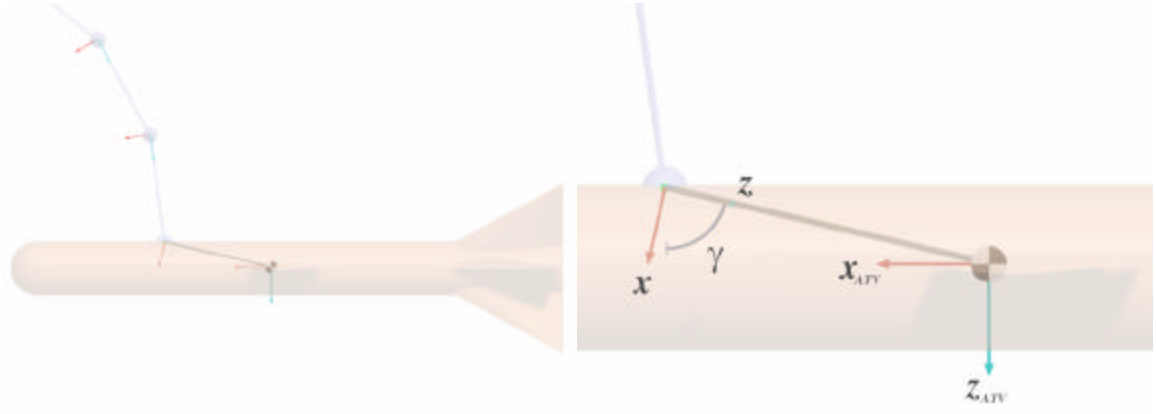

Figure 2.4 Two-dimensional ATV coordinate system

Thus, the ATV segment coordinate system and the ATV aircraft coordinate system differ directionally by a fixed rotation angle, γ. This angle is geometrically defined by the shape of the ATV as well as the location of the cable-ATV hitch point, figure 2.3. The ATV aircraft coordinate system is necessary to calculate the aerodynamic forces and moments of the ATV using small disturbance theory. The ATV orientation, as seen by the inertial frame, is determined by the ATV segment angle and ATV geometric attitude angle. Thus two rotational coordinate transformations are needed to describe the ATV attitude in the inertial frame. The rotational transformation from the ATV aircraft coordinate system to the ATV segment coordinate system is as follows,

$$\begin{bmatrix} x \\ z \end{bmatrix} = \begin{bmatrix} \underline{\underline{C_g}} \end{bmatrix} \begin{bmatrix} x' \\ z' \end{bmatrix} \tag{2.38}$$

where, x' and z' are the x and z-directions in the aircraft fixed frame.

The rotational transformation from the ATV segment coordinate system to the inertial coordinate system is as follows,

$$\begin{bmatrix} X \\ Z \end{bmatrix} = \begin{bmatrix} \underline{\underline{C_{q_{n+1}}}} \end{bmatrix} \begin{bmatrix} x \\ z \end{bmatrix} \tag{2.39}$$

As a result, the equation for rotational transformation from aircraft fixed coordinate system to the inertial coordinate system is found by combining equations 2.38 and 2.39.

$$\begin{bmatrix} X \\ Z \end{bmatrix} = \begin{bmatrix} \underline{\underline{C_{q_{n+1}}}} \end{bmatrix} \begin{bmatrix} \underline{\underline{C_g}} \end{bmatrix} \begin{bmatrix} x' \\ z' \end{bmatrix} \tag{2.40}$$

This transformation is necessary in converting the aerodynamic loads to the generalized forces of the ATV segment (due to the fact that our generalized force equations require the applied loads be in the inertial system).

2.3.2 Lagrange equations

The parameters of the additional segment, which will be henceforth deemed the ATV segment, is dictated by the size and shape of the ATV. The length of the segment is actually the distance between the cable-ATV hitch point and the center of gravity of the ATV. The mass of the ATV segment is simply the mass of the aircraft itself. Therefore, the equations of motion for the translation of the ATV segment require no additional derivation from that accomplished in the cable dynamics section. As a result, the complex dynamic interaction between each cable segment and the ATV are inherently represented by the equations of motion. However, the equations of motion for the ATV segment are not complete. Recall that the nodes used to model the cable are point masses, thus they have no inertia to resist rotation. The same cannot be said for the ATV. To complete the equations of motion for the cable-ATV system the Lagrange equation must be derived for the rotational kinetic energy of the ATV segment

The complete representation of Lagrange's equations for the cable and ATV system is as follows,

$$\begin{aligned} &\frac{d}{dt}\left[\frac{\partial(T+T_{rot})}{\partial \dot{q}_i}\right]-\frac{\partial(T+T_{rot})}{\partial q_i}=Q_i \\ &\frac{d}{dt}\left(\frac{\partial T}{\partial \dot{q}_i}\right)-\frac{\partial T}{\partial q_i}+\frac{d}{dt}\left(\frac{\partial T_{rot}}{\partial \dot{q}_i}\right)-\frac{\partial T_{rot}}{\partial q_i}=Q_i \end{aligned} \qquad (i=1,2,\ldots,n+1) \qquad (2.41)$$

Due to the fact that the total kinetic energy of the system is composed of the summation of translational and rotational kinetic energy the resulting equations of motion due to the rotational kinetic energy can simply be superimposed upon the previously derived equations of motion (i.e. the derivation of the components of the equation 2.41 that represent the translational kinetic energy need not be carried out as they will yield the same results). The analysis of the rotation kinetic energy will focus on the following portion of equation 2.41,

$$\frac{d}{dt}\left(\frac{\partial T_{rot}}{\partial \dot{q}_i}\right) - \frac{\partial (T_{rot})}{\partial q_i} \qquad (i = 1,2,\ldots,n+1) \tag{2.42}$$

The equation for rotational kinetic energy of a rigid body is as follows,

$$T_{rot} = \frac{1}{2}\{w\}^T [I]\{w\} \tag{2.43}$$

where, I is the inertial matrix and w is the angular velocity vector of the rigid body. For the two-dimensional case the segment rotational equation of motion can be simplified since the only allowable rotation is about the *y*-axis. The rotational kinetic energy of the system is the sum of the rotational kinetic energy of each segment. The rotational kinetic energy of the two-dimensional system is as follows,

$$T_{rot} = \sum_{i=1}^{n+1} \frac{1}{2} \dot{q}_i^{\,2} I_{y_i} \qquad (i = 1,2,\ldots,n+1) \tag{2.44}$$

where, I_y is the rotational inertial of the node about its *y*-axis.

The derivation of Lagrange's equations for rotational kinetic energy term is quite straightforward, producing,

$$\frac{\partial T_{rot}}{\partial q_i} = 0 \tag{2.45}$$

$$\frac{\partial T}{\partial \dot{q}_i} = \dot{q}_i I_{y_i} \tag{2.46}$$

Finally evaluating the time rate of change of equation 2.46 produces,

$$\frac{d}{dt}\left(\frac{\partial T}{\partial \dot{q}_i}\right) = \ddot{q}_i I_{y_i} \tag{2.47}$$

Combining equations 2.45 and 2.47 produces the supplementary left hand side of Lagrange's equations due to the rotation of the each segment for the two-dimensional finite element modeled cable,

$$\frac{d}{dt}\left(\frac{\partial T}{\partial \dot{q}_i}\right) - \frac{\partial T}{\partial q_i} = \ddot{q}_i I_{y_i} \qquad (i = 1,2,\ldots,n+1) \tag{2.48}$$

The combination of the rotational and translational components of the equations of motion and the addition of the ATV segment result in a set of equations of the form shown in equation 2.30. The inclusion of the ATV segment into the system adds an extra degree of freedom and thus an extra equation to the set of the equations of motion of the system, resulting in the coefficient matrices increasing to size n+1 by n+1 and the column matrices to size n+1 by 1. The additional column in the coefficient matrices represents the effect of the motion of the ATV segment on the dynamics of the cable segments. The

additional row of the coefficient matrices represents the equation of motion of the ATV segment, which contains the effects of the dynamics of each cable segment.

The changes to the set of equations derived for the translation of the nodes of the segments are in the terms of the *A* coefficient matrix. The corrected terms of the *A* matrix are as follows,

$$A_{i,j} = I_{y_i} d_{i,j} + l_i l_j C_{(q_j - q_i)} \underline{m}_{i,j} \tag{2.49}$$

where, the kronecker delta, $d_{i,j}$, is zero at all time except when *i* equals *j* at which time its value is unity. Thus the inertia term only appears on the diagonal of the *A* matrix, and since the segment nodes, in accordance with the chosen segment model, have a zero value for inertia the only change in *A* is at *n*+1, *n*+1.

2.3.3 Generalized Forces

The generalized force equation derived in equation 2.28 applies to all segments including the newly added ATV segment. However, the crossflow method does not apply to aircraft. As a result, a method for modeling the aerodynamic forces and moments on the aircraft are necessary. As stated in chapter 1, there is no shortage of research on the aerodynamics of general aircraft. The technique to be used in this paper is the linearized small-disturbance theory, Nelson[14].

In short, linearized small-disturbance theory simplifies the motion of the aircraft to perturbations of the aircraft about some fixed reference flight condition, such as typical cruising conditions. Dealing with perturbations allows for the elimination of higher order terms in the aircraft equations of motion, thus linearizing them. The aerodynamics of the

aircraft in the equations of motion are represented by stability derivatives. Stability derivatives approximate the change in aerodynamic forces or moments due to the deviations from the reference flight condition. These stability derivatives are based upon the size, shape, and mass distribution of the aircraft, and apply to a wide range of aircraft. The method does breakdown when the aircraft enters a flight regime in which the nonlinearities are important, such as stalling and spinning.

The two-dimensional equations for the aerodynamic forces, F_X' and F_Z', and moment, *M*, in the aircraft fixed frame are as follows,

$$\begin{aligned} F_X' &= X_0 + m\left(X_u u + X_w w\right) \\ F_Z' &= Z_0 + m\left(Z_u u + Z_w w + Z_{\dot{w}}\dot{w} + Z_q q\right) \\ M &= M_0 + I_Y\left(M_u u + M_w w + M_{\dot{w}}\dot{w} + M_q q\right) \end{aligned} \tag{2.50}$$

where, *m* and I_Y are aircraft mass and longitudinal rotational inertia. Also, *u* and *w* are the *x*-direction and *z*-direction perturbation velocities and *q* is the pitch rate in the ATV fixed frame. X_u, X_w,…, M_q are the stability derivatives. (Note that notation in equation 2.50 is commonly used when discussing aircraft dynamics. The pitch rate *q* is not to be confused with the generalized coordinate *q* which is itself commonly used in the notation of Lagrange's equations.)

In the aerial tow system the reference flight condition for the ATV is that of the host aircraft, and the host aircraft reference flight conditions can simply be viewed as the freestream conditions, U_o and W_o. As a result, the perturbation of the ATV about the reference conditions is simply a result of the attitude of the ATV and the motion due to segment rotation. As we have already derived the velocity of a node due to rotation in

the inertial frame, a coordinate transformation from the inertial frame to the ATV aircraft frame can be utilized to develop the equation for perturbation velocity,

$$\begin{bmatrix} u \\ w \end{bmatrix} = \left[\underline{\underline{C_g}}\right]^T \left[\underline{\underline{C_{q_{n+1}}}}\right]^T \begin{bmatrix} U_o + \dot{X}_{n+1} \\ W_o + \dot{Z}_{n+1} \end{bmatrix} - \begin{bmatrix} U_o \\ W_0 \end{bmatrix} \tag{2.51}$$

With the perturbation parameters in the ATV aircraft frame the aerodynamic forces and moments on the aircraft can easily be attained. To calculate the generalized forces produced by the aerodynamics of the ATV the forces must be in the inertial frame. This requires the following rotational coordinate transformation,

$$\begin{bmatrix} F_X \\ F_Z \end{bmatrix} = \left[\underline{\underline{C_{q_{n+1}}}}\right] \left[\underline{\underline{C_g}}\right] \begin{bmatrix} F'_X \\ F'_Z \end{bmatrix} \tag{2.52}$$

No rotational transformation is necessary for the two-dimensional applied moment. Thus, the aerodynamic moment, M, is directly translated to the ATV segment moment M_q. The forces and moments are applied to the generalized force equation, equation 2.28, following the translation.

The dynamics as well as the applied aerodynamic forces and moments of the cable-ATV system have been modeled. As a result, it is possible to simulate the effect of the cable and ATV system due to various initial conditions. However, to fully analyze the aerial towed system one last component is necessary, the host aircraft.

2.4 Host Vehicle

Up to this point, the model of the system has the cable, immersed in a flowing fluid, connected to a fixed point in space. In reality, the cable will be connected to the host

aircraft, and while the ideal case has the host vehicle flying at a constant speed and altitude it is likely that, for one reason or another, the position of the host vehicle will be disturbed. The host vehicle is an airplane, and as a result its dynamics are dictated by the aerodynamic equations presented in equation 2.50, and as it is the towing vehicle it is affected by the motion of the cable and ATV segments. On the other hand, the motion of the cable and ATV will also be affected by the host vehicle motion.

In general, the host vehicle is much larger than the ATV and as a result its aerodynamic loads will overpower the loads produced by the motion of the cable and ATV. Thus, a simplifying assumption can be made that the host vehicle is unaffected by the dynamics of the cable and ATV, yet the cable and ATV are affected by the motion of the host vehicle. This assumption allows the host vehicle to be modeled as a simple point. The motion of the host aircraft is independent of the cable and the ATV dynamics and consequently the movement of this point can be chosen arbitrarily. For instance, the equations of motion for longitudinal oscillation in the *z*-direction of the host aircraft frame can be written simply as

$$\begin{aligned} \underline{z} &= A_o \sin(w_o t) \\ \dot{\underline{z}} &= A_o w_o \cos(w_o t) \\ \ddot{\underline{z}} &= -A_o w_o^2 \sin(w_o t) \end{aligned} \tag{2.53}$$

where, $\underline{z}$ is the host vehicle vertical displacement, t is time, A_o is amplitude, and w_o is frequency. The amplitude and frequency can be chosen to represent the longitudinal dynamics of a wide range of host aircraft. The effect of host aircraft oscillation on the vertical position of the ATV is of critical importance when the ATV is very near the

ground; however the aircraft is not limited to simply vertical motion. The equations of motion can be derived for horizontal motion, vertical motion, or any combination of the two.

The technique for modeling the cable and ATV dynamics with the introduction of the varying host vehicle position remains more or less the same. In the previous models the cable connecting point always coincided with the origin of the inertial coordinate system. However, with the introduction of the movable host vehicle this is not so. Any movement of the host aircraft results in the translation of the cable connection point. The derivation of Lagrange's equations for the cable and ATV hinges on the location and velocity of the segment nodes. Thus, to account for host vehicle movement the inertial position equation must be altered to represent the translation of the cable connection point. The resulting equation is as follows,

$$\begin{bmatrix} X_i \\ Z_i \end{bmatrix} = \begin{bmatrix} \underline{x} \\ \underline{z} \end{bmatrix} + \sum_{j=1}^{i} \begin{bmatrix} \underline{\underline{C}}_{q_j} \end{bmatrix} \begin{bmatrix} 0 \\ l_j \end{bmatrix} \tag{2.54}$$

where, $\underline{x}$ is the difference in the x-direction of the host aircraft in the inertial frame.

Due to the fact that the position of the host aircraft is a function of time the derivation of Lagrange's equations will produce a different outcome from that derived previously, the difference being the effect of the host vehicle oscillation. The derivation of Lagrange's equations begins by taking the time rate of change of position,

$$\dot{X}_j = \underline{\dot{x}} + \sum_{i=1}^{j} \dot{q}_i l_i C_{q_i}$$
$$\dot{Z}_j = \underline{\dot{z}} + \sum_{i=1}^{j} -\dot{q}_i l_i S_{q_i} \tag{2.55}$$

The square of velocity with the incorporation of a moving host vehicle is as follows,

$$V_k^2 = \left(\dot{X}_k^2 + \dot{Z}_k^2\right) = \underline{\dot{z}}^2 + \underline{\dot{x}}^2 + \sum_{i=1}^{k}\left(\underline{\dot{x}}\dot{q}_i l_i C_{q_i} - \underline{\dot{z}}\dot{q}_i l_i S_{q_i}\right) + \sum_{j=1}^{k}\sum_{i=1}^{k} l_i l_j \dot{q}_i \dot{q}_j C_{(q_i - q_j)} \tag{2.56}$$

Thus, the total kinetic energy for the aerial tow system is as follows,

$$T = \frac{1}{2}\sum_{k=1}^{n+1} m_k V_k^2 = \frac{1}{2}\sum_{k=1}^{n+1} m_k \left(\underline{\dot{z}}^2 + \underline{\dot{x}}^2 + \sum_{i=1}^{k}\left(\underline{\dot{x}}\dot{q}_i l_i C_{q_i} - \underline{\dot{z}}\dot{q}_i l_i S_{q_i}\right) + \sum_{j=1}^{k}\sum_{i=1}^{k} l_i l_j \dot{q}_i \dot{q}_j C_{(q_i - q_j)} \right) \tag{2.57}$$

Note that the last term in equation 2.57 is the same as that derived in the cable dynamics section, equation 2.12. Thus, the derivation of Lagrange equations for the last term will yield the same results. As a result, we can focus on the host vehicle oscillation terms when deriving the Lagrange equations and simply superimpose the results onto the equations of motion for the cable and ATV. The kinetic energy due to the host vehicle oscillation, T_{host}, is as follows,

$$T_{osc} = \frac{1}{2}\sum_{k=1}^{n+1} m_k \left(\underline{\dot{z}}^2 + \underline{\dot{x}}^2 + \sum_{i=1}^{k}\left(2\underline{\dot{x}}\dot{q}_i l_i C_{q_i} - 2\underline{\dot{z}}\dot{q}_i l_i S_{q_i}\right) \right) \tag{2.58}$$

Note that the first two terms in the equation 2.58 are only a function of time. Therefore, they will disappear during the differentiation of the kinetic energy with respect to the generalized coordinates.

The derivative of kinetic energy with respect to the i^{th} generalized coordinate and the time rate of change of the i^{th} generalized coordinate yields the following,

$$\frac{\partial T_{osc}}{\partial q_i} = \sum_{k=i}^{n+1} - m_k \left(\underline{\dot{x}} \dot{q}_i l_i S_{q_i} + \underline{\dot{z}} \dot{q}_i l_i C_{q_i} \right) \tag{2.59}$$

$$\frac{\partial T_{osc}}{\partial \dot{q}_i} = \sum_{k=i}^{n+1} m_k \left(\underline{\dot{x}} l_i C_{q_i} - \underline{\dot{z}} l_i S_{q_i} \right) \tag{2.60}$$

Finally, the time rate of change of equation 2.60 produces,

$$\frac{d}{dt}\left(\frac{\partial T_{osc}}{\partial \dot{q}_i} \right) = \sum_{k=i}^{n+1} m_k \left(\underline{\ddot{x}} l_i C_{q_i} - \underline{\ddot{z}} l_i S_{q_i} - \underline{\dot{x}} \dot{q}_i l_i S_{q_i} - \underline{\dot{z}} \dot{q}_i l_i C_{q_i} \right) \tag{2.61}$$

Combining equations 2.59 and 2.61, in accordance with Lagrange's equations, results in the following,

$$\frac{d}{dt}\left(\frac{\partial T_{osc}}{\partial \dot{q}_i} \right) - \frac{\partial T_{osc}}{\partial q_i} = \sum_{k=i}^{n+1} m_k \left(\underline{\ddot{x}} l_i C_{q_i} - \underline{\ddot{z}} l_i S_{q_i} \right) \quad (i = 1,2,\ldots,n+1) \tag{2.62}$$

Note that equation 2.62 has units of force times distance just as the generalized forces. As a result, the equation 2.62 can be thought of as generalized forces due to host vehicle acceleration, as shown below,

$$Q_{osci} = \sum_{k=i}^{n+1} m_k \left(\ddot{\underline{x}} l_i C_{q_i} - \ddot{\underline{z}} l_i S_{q_i} \right) \quad (i = 1,2,\ldots,n+1) \tag{2.63}$$

The superposition of equation 2.63 into the generalized force equation 2.28 yields,

$$Q_i = M_{q\,i} + \sum_{j=i}^{n+1} \left(F_{X\,j} - m_j \ddot{\underline{x}} \right) l_i C_{q_i} - \left(F_{Z\,j} + m_j \left(g - \ddot{\underline{z}} \right) \right) l_i S_{q_i} \tag{2.64}$$
$$(i = 1,2,\ldots,n+1)$$

Thus in the matrix form of the set of equations of motion, the host vehicle oscillation has no affect on the *A* or *B* coefficient matrix. The results of the derivation show that the moving host frame produces applied loads on each segment node proportional to the host vehicle acceleration. Note that the derivation due to the host vehicle motion is independent of the functions used to model it, allowing for any harmonic model of the host aircraft dynamics.

2.5 System Equations of Motion of an Alternate Segment Model

At this point, the equations of motion for the two-dimensional aerial tow system are complete, and given a proper numerical integration routines and a set of valid initial conditions a simulation of the two-dimensional aerial tow system can be accomplished. However, the lumped mass model used for the finite element segments is quite simplistic. As discussed earlier, this model places the mass of a segment at the node at the base of the segment and all applied forces on the segment are located at the node. This simplification is particularly poor when there are few segments that make up the model of the cable.

Imagine the cable is modeled as one lumped mass segment. The segment is in the presence of moving fluid, as a result there is a distributed friction load on the segment. According to the lumped mass assumption the inertial force of the segment and the accumulated drag force are applied at the base of the segment. The lumped mass segment equation of motion is as follows,

$$\ddot{q} = \frac{F_X C_q - (F_Z + mg) S_q}{ml} \tag{2.65}$$

It would seem a much better model would have the mass and applied force applied at the midpoint of the segment. The resulting angular acceleration is twice that of the lumped mass model.

$$\ddot{q} = 2\frac{F_X C_q - (F_Z + mg) S_q}{ml} \tag{2.66}$$

An even better model would have the segment modeled as a thin rod or cylinder. This would have the inertial and applied loads at the center of mass of the rod as in the previous model. However, it also has its rotational inertia that resists rotation (the rotational inertia about the center of gravity of a thin rod is $I_y = (ml^2)/12$). The resulting angular acceleration is an average of the two previous equations.

$$\ddot{q} = \frac{3}{2}\frac{F_X C_q - (F_Z + mg) S_q}{ml} \tag{2.67}$$

The one segment example illustrates the weakness of the lumped mass model. Presumably as the number of segment increase the difference in the dynamics of the

lumped mass and the thin rod models will decrease (this will be shown in chapter five). However, the as the number of segments increase so too does the computational workload.

The question remains how do the equations of motion derived throughout this chapter for the lumped mass model change for a system modeled by thin rod segments. The answer can be found by rederiving Lagrange's equations with a new position equation that represents the center of mass of each segment. Upon completion one will realized that equation 2.30 remains true, recall,

$$[A][\ddot{q}]+[B][\dot{q}^2]=[Q]$$

The only changes in the equations of motion for the thin rod modeled segments are in the mass distribution in the A and B coefficient matrices and the lever arm of the generalized force equations.

The mass distribution of the coefficient matrices in the lumped mass model is given in equation 2.33. The mass distribution of the coefficient matrices in the thin rod modeled system for n+1 segments is as follows,

$$\underline{m}_{i,j} = -m_{\max(i,j)}\left(\frac{1}{2}+\frac{d_{i,j}}{4}\right)+\sum_{k=\max(i,j)}^{n+1} m_k \qquad (2.68)$$

The generalized force equation remains much the same however since the forces on the i^{th} segment are applied at the center of mass and not at the base of the segment the lever arm is halved when i is equal to j,

$$Q_i = M + \sum_{j=i}^{n+1} \left[\left(F_{X\,j} - m_j \underline{\ddot{x}} \right) l_i C_{q_i} - \left(F_{Z\,j} + m_j \left(g - \underline{\ddot{z}} \right) \right) l_i S_{q_i} \left(1 - \frac{d_{i,j}}{2} \right) \right] \qquad (2.69)$$
$$(i = 1,2,\ldots,n+1)$$

Note the for equation 2.69 to be accurate for the ATV segment the ATV center of mass must coincide with the center of mass of the segment model. In other words, the length of the ATV segment will be twice the distance between the cable-ATV hitch point and the ATV center of mass.

The set of equations of motion for the aerial towed system with segments modeled as thin rods is attained with the implementation of equations 2.32, 2.49, 2.68 and 2.69 on equation 2.30. Given a proper numerical integration routines and a set of valid initial conditions a simulation of the two-dimensional aerial tow system can be accomplished. The difference in the results of the lumped mass and thin rod segment modeled system simulations with the same initial conditions will be analyzed in chapter five. It is only then a conclusion can be drawn about the pros and cons of the two methods.

CHAPTER 3

THREE-DIMENSIONAL DYNAMICS

3.1 Introduction

Modeling the aerial tow system for the two-dimensional case is more-or-less straight forward. The equations of motion have been thoroughly derived, include nonlinearities, and make few assumptions. As a result, we can expect that the simulation of the system will be thorough as well; the system could be used to complete a wide variety of case studies, such as, ATV position due to wind gust or host vehicle motion, as well as ATV tracking ability under various conditions. However, it is still limited the phenomena that occur only in the two-dimensional plane. For a more robust simulation it is necessary to derive the equations of motion in three dimensions. Being that the actual system exists in three dimensions, this will more accurately represent the real world dynamic occurrences. The addition of the third dimension will drastically increase the complexity of the mathematical models. The methodology for the derivation of the three-dimensional equations of motion is the same as that used for the two-dimensional case (chapter 2) although a few new concepts are necessary to carryout that methodology.

3.2 Cable Dynamics

The three-dimensional model of the cable is attained via the application of the finite element technique. As in the two-dimensional case, the continuous cable is broken into an arbitrary number of segments. The lumped mass model of the cable segments will be

used in the initial analysis of the cable. Each segment is free to rotate about its neighbors, giving the series of rigid connections flexibility as a whole. The added dimension allows the segments two additional rotations, the rotation about the x-axis and the ability for each segment to spin (rotation about the z-direction). The equations of motion for the segment motion will include the new dynamic freedom, and as a result, the equations will increase in complexity.

To focus on the dynamics of the cable we will assume that the cable is attached to the origin of the inertial frame. In other words, assume that the host vehicle is steady. Thus, the focus of the dynamics will be on the three-dimensional motion of the cable. The effects of the motion of the cable connection point will be addressed in a later section.

3.2.1 Coordinate Systems

The addition of the third dimension does not have an effect on the number of coordinate systems needed, although it does affect the type and complexity of the orientation of the coordinate systems. The inertial frame is orthogonal and fixed. Each cable segment has an orthogonal coordinate system which has its origin such that the location of the node of that segment is the length of the segment in the positive z-direction. For instance, imagine there is one cable segment that rotates about the inertial frame. The origin of the cable segment frame is at the point of rotation of the segment. Thus, the location of the origin of the first cable segment frame and the origin of the inertial frame are the same; the difference is in the orientation of the frames, figure 3.1.

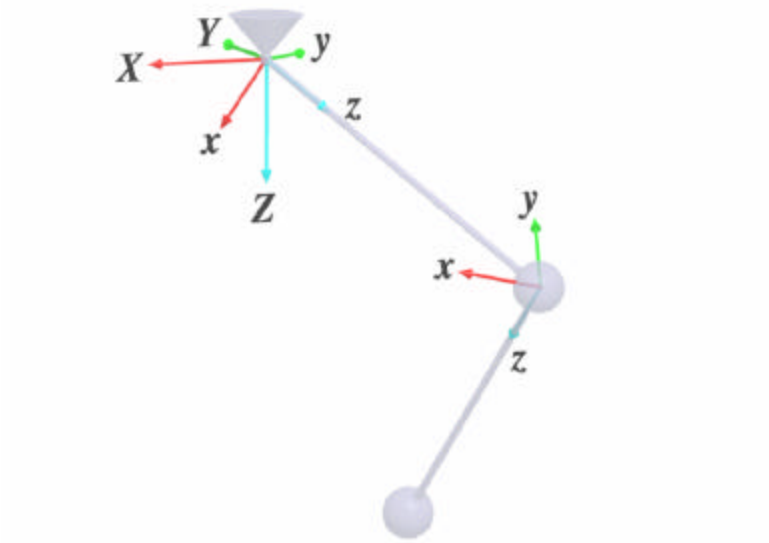

Figure 3.1 Three-dimensional inertial and cable segment coordinate systems

The orientation of the cable segment relative to the inertial frame is due to the angle of rotation of the cable frame. The cable frame can rotate about three separate axes (*x*, *y*, and *z*-axes) unlike the two-dimensional case in which it can rotate about only one (the *y*-axis). The common method for describing the three-dimensional rotation requires the use of Euler angles. These Euler angles are the heading angle y, the attitude angle q, and the bank angle f. Any orientation of the cable frame relative to the inertial frame can be described by using these three angles. However, it is important to note that the order of rotation is important.

Imagine that a cable segment frame is parallel to the inertial frame and their origins are coincident, figure 3.2. Allow the cable frame to rotate about its z-axis by an angle y. The resulting coordinate system is the double primed system. Thus, the coordinate transformation from the double-primed system to the fixed inertial frame is as follows,

$$\begin{bmatrix} X \\ Y \\ Z \end{bmatrix} = \begin{bmatrix} x' \\ y' \\ z' \end{bmatrix} = \begin{bmatrix} C_y & S_y & 0 \\ -S_y & C_y & 0 \\ 0 & 0 & 1 \end{bmatrix} \begin{bmatrix} x'' \\ y'' \\ z'' \end{bmatrix} = \left[\underline{\underline{C_y}}\right] \begin{bmatrix} x'' \\ y'' \\ z'' \end{bmatrix} \tag{3.1}$$

Next, allow the double-primed system to rotate about the y''-axis by an angle q. The resulting coordinate system is the triple-primed system. The coordinate transformation from the triple-primed system to the double primed system is as follows,

$$\begin{bmatrix} x'' \\ y'' \\ z'' \end{bmatrix} = \begin{bmatrix} C_q & 0 & S_q \\ 0 & 1 & 0 \\ -S_q & 0 & C_q \end{bmatrix} \begin{bmatrix} x''' \\ y''' \\ z''' \end{bmatrix} = \left[\underline{\underline{C_q}}\right] \begin{bmatrix} x''' \\ y''' \\ z''' \end{bmatrix} \tag{3.2}$$

Finally, allow the triple-primed system to rotate about the x'''-axis by an angle f. The resulting coordinate system is the unprimed cable segment frame. The coordinate transformation from the cable segment frame to the triple-primed system is as follows,

$$\begin{bmatrix} x''' \\ y''' \\ z''' \end{bmatrix} = \begin{bmatrix} 1 & 0 & 0 \\ 0 & C_f & S_f \\ 0 & -S_f & C_f \end{bmatrix} \begin{bmatrix} x \\ y \\ z \end{bmatrix} = \left[\underline{\underline{C_f}}\right] \begin{bmatrix} x \\ y \\ z \end{bmatrix} \tag{3.3}$$

The rotational coordinate transformation from the cable segment frame to the inertial frame is attained by combining equations 3.1, 3.2, and 3.3,

$$\begin{bmatrix} X \\ Y \\ Z \end{bmatrix} = \left[\underline{\underline{C_y}}\right]\left[\underline{\underline{C_q}}\right]\left[\underline{\underline{C_f}}\right] \begin{bmatrix} x \\ y \\ z \end{bmatrix} = \begin{bmatrix} C_y C_q & -S_y C_f + C_y S_q S_f & S_y S_f + C_y S_q C_f \\ S_y C_q & C_y C_f + S_y S_q S_f & -C_y S_f + S_y S_q C_f \\ -S_q & C_q S_f & C_q C_f \end{bmatrix} \begin{bmatrix} x \\ y \\ z \end{bmatrix} \tag{3.4}$$

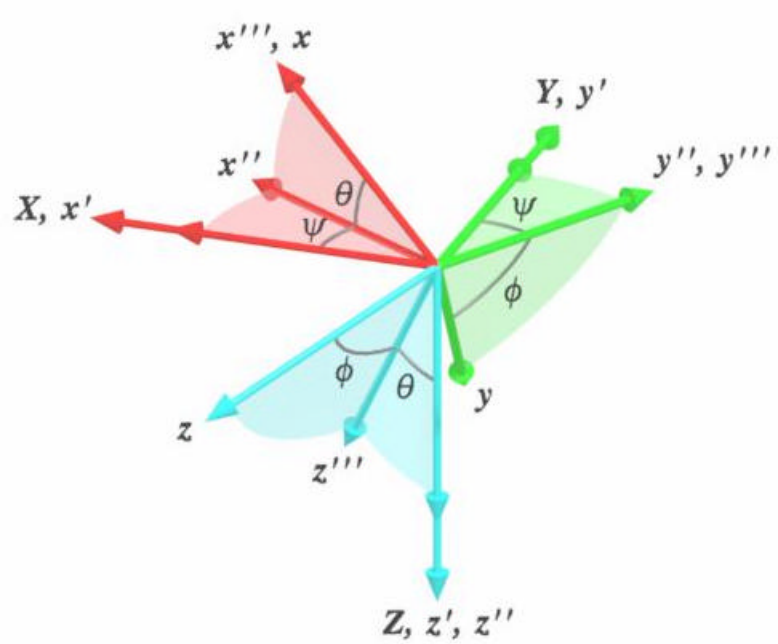

Figure 3.2 Euler angle rotations

The series of three rotations of the cable frame are sufficient to attain any orientation. The same is true independent of the order of rotation. However, the order of rotation does have an effect on the final position of the cable frame. The order used throughout this paper is y, q, and f for every three-dimensional segment rotation. Let us assume that the Euler angles are limited to the following rotations,

$$0 \le y < 2p, \qquad -\frac{p}{2} \le q \le \frac{p}{2}, \qquad 0 \le f < 2p \tag{3.5}$$

When $q = \pm p/2$ there is no distinct set of solutions for y and f, this is known as gimbal lock. To avoid complications associated with gimbal lock it is common to switch to an alternate system. In this particular aerial tow system the issue of gimbal lock will not arise as the system necessitates the ATV fly at a lower altitude than the host aircraft resulting in cable segment attitude angles between $\pm p/2$.

The three-dimensional rotational coordinate transformation from the cable to the inertial coordinate system is represented by the following directional cosine matrix,

$$\left[\underline{\underline{C_{f,q,y}}}\right] = \begin{bmatrix} C_y C_q & -S_y C_f + C_y S_q S_f & S_y S_f + C_y S_q C_f \\ S_y C_q & C_y C_f + S_y S_q S_f & -C_y S_f + S_y S_q C_f \\ -S_q & C_q S_f & C_q C_f \end{bmatrix} \tag{3.6}$$

The position of the i^{th} segment's node in its coordinate system is by definition the length of the segment in the z-direction. Since the segments are a series of connected bodies the directional cosine matrix can be used to formulate the node's position in the inertial frame,

$$\begin{bmatrix} X_i \\ Y_i \\ Z_i \end{bmatrix} = \sum_{j=1}^{i} \left[\underline{\underline{C_{f_j,q_j,y_j}}}\right] \begin{bmatrix} 0 \\ 0 \\ l_j \end{bmatrix} \tag{3.7}$$

Expansion of equation 3.9 yields a more explicit form of the i^{th} segment position in the inertial frame,

$$\begin{aligned} X_i &= \sum_{j=1}^{i} l_j \left(S_{y_j} S_{f_j} + C_{y_j} S_{q_j} C_{f_j} \right) \\ Y_i &= \sum_{j=1}^{i} l_j \left(-C_{y_j} S_{f_j} + S_{y_j} S_{q_j} C_{f_j} \right) \quad (i = 1,2,\ldots,n) \\ Z_i &= \sum_{j=1}^{i} l_j \left(C_{q_j} C_{f_j} \right) \end{aligned} \tag{3.8}$$

As in the tow-dimensional case, the location of the node of a segment is dependant upon the angles of rotation of that segment and each preceding segment.

3.2.2 Lagrange Equations

The modeling of the cable is accomplished using the finite element method, just as with the two-dimensional case. As discussed previously, the method breaks the cable into an arbitrary number of segments, and each cable segment has its own coordinate system. The accuracy of the cable model improves with an increase in the number of segments for a given cable, so too does the difficulty of the derivation of the equations of motion for the cable.

Using Newton's method to derive the equations of motion for such a complex configuration would be fraught with danger, as it would require intense vector bookkeeping and multiple coupled rotation equations for each segment. The advantages of the Lagrange technique over Newton's method are even stronger for three-dimensional analysis than in the two-dimensional case. The added dimension greatly increases the system complexity and since the Lagrange technique has a standard process for the derivation of the equations of motion it is less likely that mistakes will be made in the derivation of the equations.

The bounds of the Lagrange equation are set by the degree of freedom of the system (refer to section 2.2.2). In three dimensions, the complete description of a cable segment is composed of its nodal position and its orientation (i.e. angle of twist). In the Cartesian coordinate system the position of the node is defined by its x, y, and z-coordinates. Due to the fact that the segment length is fixed the coordinates are not independent. The Cartesian constraint equations are shown below,

$$l_i^2 = \left(X_i - \sum_{j=1}^{i-1} X_j \right)^2 + \left(Y_i - \sum_{j=1}^{i-1} Y_j \right)^2 + \left(Z_i - \sum_{j=1}^{i-1} Z_j \right)^2 \quad (i = 1,2,\ldots,n) \tag{3.9}$$

The Cartesian coordinates alone cannot specify the angle of twist of the segment. Therefore, there are in actuality four coordinates necessary to define the system, and being that there is one constraint equation each cable segment has three degrees of freedom.

It is possible to completely define the position and orientation of a segment using the Euler angles. In this case, there are three angles which completely define the segment and there are no constraint equations. Therefore, the Euler angles of each segment are the independent generalized coordinates of the system. For the two-dimensional case the independent generalized coordinates were the attitude angles of rotation and since there was only one angle per segment the generalized coordinate consisted of just one variable. However, for the three-dimensional model each segment requires three angles for complete description of orientation. As a result, for a cable modeled by n segments there are $3n$ generalized coordinates made up of y, q, and f for each segment. (This assumes that each cable segment is free to fully rotate about the preceding segment. The validity of this assumption will be discussed in a later section).

For the three-dimensional system, Lagrange's equations represent an equation for each of the $3n$ degrees of freedom,

$$\frac{d}{dt}\left(\frac{\partial T}{\partial \dot{q}_i} \right) - \frac{\partial T}{\partial q_i} = Q_i \quad (i = 1,2,\ldots,3n) \tag{3.9}$$

$$Q_i = \sum_{j=1}^{n}\left[F_{X\,j}\frac{\partial X_j}{\partial q_i} + F_{Y\,j}\frac{\partial Y_j}{\partial q_i} + \left(F_{Z\,j} + m_j g\right)\frac{\partial Z_j}{\partial q_i} + M_{f\,j}\frac{\partial f_j}{\partial q_i} + M_{q\,j}\frac{\partial q_j}{\partial q_i} + M_{y\,j}\frac{\partial y_j}{\partial q_i}\right] \qquad (i = 1,2,\ldots,3n) \qquad (3.10)$$

Note that the generalized force, *Q*, contains applied forces, applied moments, and inertial forces as per the discussion in section 2.2.2.

Equation 3.9 represents a set of 3*n* equations. In which the generalized coordinate is made up of three independent variables. It may be presented more clearly rewritten as three sets of *n* equations, in which the generalized coordinate for each is an independent variable,

$$\begin{aligned} \frac{d}{dt}\left(\frac{\partial T}{\partial \dot{f}_i}\right) - \frac{\partial T}{\partial f_i} &= Q_{f_i} \\ \frac{d}{dt}\left(\frac{\partial T}{\partial \dot{q}_i}\right) - \frac{\partial T}{\partial q_i} &= Q_{q_i} \qquad (i = 1,2,\ldots,n) \\ \frac{d}{dt}\left(\frac{\partial T}{\partial \dot{y}_i}\right) - \frac{\partial T}{\partial y_i} &= Q_{y_i} \end{aligned} \qquad (3.11)$$

$$\begin{aligned} Q_{f\,i} &= \sum_{j=1}^{n} F_{X\,j}\frac{\partial X_j}{\partial f_i} + F_{Y\,j}\frac{\partial Y_j}{\partial f_i} + \left(F_{Z\,j} + m_j g\right)\frac{\partial Z_j}{\partial f_i} + M_{f\,j}\frac{\partial f_j}{\partial f_i} \\ Q_{q\,i} &= \sum_{j=1}^{n} F_{X\,j}\frac{\partial X_j}{\partial q_i} + F_{Y\,j}\frac{\partial Y_j}{\partial q_i} + \left(F_{Z\,j} + m_j g\right)\frac{\partial Z_j}{\partial q_i} + M_{q\,j}\frac{\partial q_j}{\partial q_i} \qquad (i = 1,2,\ldots,n) \\ Q_{y\,i} &= \sum_{j=1}^{n} F_{X\,j}\frac{\partial X_j}{\partial y_i} + F_{Y\,j}\frac{\partial Y_j}{\partial y_i} + \left(F_{Z\,j} + m_j g\right)\frac{\partial Z_j}{\partial y_i} + M_{y\,j}\frac{\partial y_j}{\partial y_i} \end{aligned} \qquad (3.12)$$

Thus, each segment will contain three equations of motion. Note that the applied moments and the moments produced by the applied forces are about the axis of rotation of their respective generalized coordinate, $\dot{f}_i$, $\dot{q}_i$, and $\dot{y}_i$.

The method for deriving the equations of motion is the same as that carried out in the two-dimensional cable dynamic section. The only difference is the more complex kinetic energy equation and the increase in the number of generalized coordinates of the system. The kinetic energy is made up of rotational and translational kinetic energy. The nodes, being point masses, have no inertia and thus no rotational kinetic energy. As a result, the derivation of the equations of motion relies solely on the translation kinetic energy of the system as a function of the generalized coordinates.

The kinetic energy can be found by calculating the square of velocity for the node of each segment as a function of the generalized coordinates, equation 2.9. The velocity components are simply the time rate of change of position

$$\begin{aligned}
\dot{X}_i &= \sum_{j=1}^{i} l_j \left[\dot{f}_j \left(S_{y_j} C_{f_j} - C_{y_j} S_{q_j} S_{f_j}\right) + \dot{q}_j \left(C_{y_j} C_{q_j} C_{f_j}\right) + \dot{y}_j \left(C_{y_j} S_{f_j} - S_{y_j} S_{q_j} C_{f_j}\right)\right] \\
\dot{Y}_i &= \sum_{j=1}^{i} l_j \left[\dot{f}_j \left(-C_{y_j} C_{f_j} - S_{y_j} S_{q_j} S_{f_j}\right) + \dot{q}_j \left(S_{y_j} C_{q_j} C_{f_j}\right) + \dot{y}_j \left(S_{y_j} S_{f_j} + C_{y_j} S_{q_j} C_{f_j}\right)\right] \\
\dot{Z}_i &= \sum_{j=1}^{i} l_j \left[\dot{f}_j \left(-C_{q_j} S_{f_j}\right) + \dot{q}_j \left(-S_{q_j} C_{f_j}\right)\right] \\
&\qquad\qquad for \quad (i = 1, 2 \ldots, n)
\end{aligned} \tag{3.13}$$

Thus, the square of velocity for the k^{th} segment is as follows,

$$
\begin{aligned}
V_k^2 &= \left(\dot{X}_k^2 + \dot{Y}_k^2 + \dot{Z}_k^2\right) = \sum_{i=1}^{k}\sum_{j=1}^{k}\Big\{ \\
&\dot{f}_i\Big[\dot{f}_j\left(C_{y_j-y_i}\left(S_{f_i}S_{f_j}S_{q_i}S_{q_j} + C_{f_i}C_{f_j}\right) + S_{y_j-y_i}\left(C_{f_i}S_{f_j}S_{q_j} - S_{f_i}C_{f_j}S_{q_i}\right) + S_{f_i}S_{f_j}C_{q_i}C_{q_j}\right) + \\
&\quad \dot{q}_j\left(-C_{y_j-y_i}S_{f_i}C_{f_j}S_{q_i}C_{q_j} - S_{y_j-y_i}C_{f_i}C_{f_j}C_{q_j} + S_{f_i}C_{f_j}C_{q_i}S_{q_j}\right) + \\
&\quad \dot{y}_j\left(-C_{y_j-y_i}\left(S_{f_i}S_{f_j}S_{q_i} + C_{f_i}C_{f_j}S_{q_j}\right) + S_{y_j-y_i}\left(S_{f_i}C_{f_j}S_{q_i}S_{q_j} - C_{f_i}S_{f_j}\right)\right)\Big] + \\
&\dot{q}_i\Big[\dot{f}_j\left(-C_{y_j-y_i}C_{f_i}S_{f_j}C_{q_i}S_{q_j} + S_{y_j-y_i}C_{f_i}C_{f_j}C_{q_i} + C_{f_i}S_{f_j}S_{q_i}C_{q_j}\right) + \\
&\quad \dot{q}_j\left(C_{y_j-y_i}C_{f_i}C_{f_j}C_{q_i}C_{q_j} + C_{f_i}C_{f_j}S_{q_i}S_{q_j}\right) + \\
&\quad \dot{y}_j\left(C_{y_j-y_i}C_{f_i}S_{f_j}C_{q_i} - S_{y_j-y_i}C_{f_i}C_{f_j}C_{q_i}S_{q_j}\right)\Big] + \\
&\dot{y}_i\Big[\dot{f}_j\left(C_{y_j-y_i}\left(-C_{f_i}C_{f_j}S_{q_i} - S_{f_i}S_{f_j}S_{q_j}\right) + S_{y_j-y_i}\left(-C_{f_i}S_{f_j}S_{q_i}S_{q_j} + S_{f_i}C_{f_j}\right)\right) + \\
&\quad \dot{q}_j\left(C_{y_j-y_i}S_{f_i}C_{f_j}C_{q_j} + S_{y_j-y_i}C_{f_i}C_{f_j}S_{q_i}C_{q_j}\right) + \\
&\quad \dot{y}_j\left(C_{y_j-y_i}\left(C_{f_i}C_{f_j}S_{q_i}S_{q_j} + S_{f_i}S_{f_j}\right) + S_{y_j-y_i}\left(C_{f_i}S_{f_j}S_{q_i} - S_{f_i}C_{f_j}S_{q_j}\right)\right)\Big]\Big\}
\end{aligned}
\tag{3.14}
$$

Furthermore, the three-dimensional kinetic energy equation is represented as a function of the independent generalized coordinates below,

$$
\begin{aligned}
T &= \frac{1}{2}\sum_{k=1}^{n} m_k V_k^2 = \frac{1}{2}\sum_{k=1}^{n}\sum_{i=1}^{k}\sum_{j=1}^{k} m_k \Big\{ \\
&\dot{f}_i\Big[\dot{f}_j\left(C_{y_j-y_i}\left(S_{f_i}S_{f_j}S_{q_i}S_{q_j} + C_{f_i}C_{f_j}\right) + S_{y_j-y_i}\left(C_{f_i}S_{f_j}S_{q_j} - S_{f_i}C_{f_j}S_{q_i}\right) + S_{f_i}S_{f_j}C_{q_i}C_{q_j}\right) + \\
&\quad \dot{q}_j\left(-C_{y_j-y_i}S_{f_i}C_{f_j}S_{q_i}C_{q_j} - S_{y_j-y_i}C_{f_i}C_{f_j}C_{q_j} + S_{f_i}C_{f_j}C_{q_i}S_{q_j}\right) + \\
&\quad \dot{y}_j\left(-C_{y_j-y_i}\left(S_{f_i}S_{f_j}S_{q_i} + C_{f_i}C_{f_j}S_{q_j}\right) + S_{y_j-y_i}\left(S_{f_i}C_{f_j}S_{q_i}S_{q_j} - C_{f_i}S_{f_j}\right)\right)\Big] + \\
&\dot{q}_i\Big[\dot{f}_j\left(-C_{y_j-y_i}C_{f_i}S_{f_j}C_{q_i}S_{q_j} + S_{y_j-y_i}C_{f_i}C_{f_j}C_{q_i} + C_{f_i}S_{f_j}S_{q_i}C_{q_j}\right) + \\
&\quad \dot{q}_j\left(C_{y_j-y_i}C_{f_i}C_{f_j}C_{q_i}C_{q_j} + C_{f_i}C_{f_j}S_{q_i}S_{q_j}\right) + \\
&\quad \dot{y}_j\left(C_{y_j-y_i}C_{f_i}S_{f_j}C_{q_i} - S_{y_j-y_i}C_{f_i}C_{f_j}C_{q_i}S_{q_j}\right)\Big] + \\
&\dot{y}_i\Big[\dot{f}_j\left(C_{y_j-y_i}\left(-C_{f_i}C_{f_j}S_{q_i} - S_{f_i}S_{f_j}S_{q_j}\right) + S_{y_j-y_i}\left(-C_{f_i}S_{f_j}S_{q_i}S_{q_j} + S_{f_i}C_{f_j}\right)\right) + \\
&\quad \dot{q}_j\left(C_{y_j-y_i}S_{f_i}C_{f_j}C_{q_j} + S_{y_j-y_i}C_{f_i}C_{f_j}S_{q_i}C_{q_j}\right) + \\
&\quad \dot{y}_j\left(C_{y_j-y_i}\left(C_{f_i}C_{f_j}S_{q_i}S_{q_j} + S_{f_i}S_{f_j}\right) + S_{y_j-y_i}\left(C_{f_i}S_{f_j}S_{q_i} - S_{f_i}C_{f_j}S_{q_j}\right)\right)\Big]\Big\}
\end{aligned}
\tag{3.15}
$$

Equation 3.15 is the basis from which Lagrange's equations will be derived. All one needs to do is compare equation 3.15 and 2.12 to grasp the increase in complexity from a

system existing in two to three-dimensions. With the cable kinetic energy equation derived the derivation of Lagrange's equations for each set of generalized coordinates can commence.

3.2.2.1 Bank angle

The implementation of the Lagrange equation in the three-dimensional cable model must be accomplished for each angle necessary for cable orientation definition. For the bank angle generalized coordinate the derivation is as follows.

The derivative of kinetic energy with respect to the bank angle and the time rate of change of the bank angle of the i^{th} cable segment yield the following,

$$\begin{aligned}
&\frac{\partial T}{\partial f_i} = \sum_{k=1}^{n}\sum_{j=1}^{k} m_k \Big\{ \\
&\dot{f}_i \Big[\dot{f}_j \Big(C_{y_j - y_i}\Big(C_{f_i} S_{f_j} S_{q_i} S_{q_j} - S_{f_i} C_{f_j}\Big) + S_{y_j - y_i}\Big(-S_{f_i} S_{f_j} S_{q_j} - C_{f_i} C_{f_j} S_{q_i}\Big) + C_{f_i} S_{f_j} C_{q_i} C_{q_j}\Big) + \\
&\quad \dot{q}_j \Big(-C_{y_j - y_i} C_{f_i} C_{f_j} S_{q_i} C_{q_j} + S_{y_j - y_i} S_{f_i} C_{f_j} C_{q_j} + C_{f_i} C_{f_j} C_{q_i} S_{q_j}\Big) + \\
&\quad \dot{y}_j \Big(-C_{y_j - y_i}\Big(C_{f_i} S_{f_j} S_{q_i} - S_{f_i} C_{f_j} S_{q_j}\Big) + S_{y_j - y_i}\Big(C_{f_i} C_{f_j} S_{q_i} S_{q_j} + S_{f_i} S_{f_j}\Big)\Big)\Big] + \\
&\dot{q}_i \Big[\dot{f}_j \Big(C_{y_j - y_i} S_{f_i} S_{f_j} C_{q_i} S_{q_j} - S_{y_j - y_i} S_{f_i} C_{f_j} C_{q_i} - S_{f_i} S_{f_j} S_{q_i} C_{q_j}\Big) + \\
&\quad \dot{q}_j \Big(-C_{y_j - y_i} S_{f_i} C_{f_j} C_{q_i} C_{q_j} - S_{f_i} C_{f_j} S_{q_i} S_{q_j}\Big) + \\
&\quad \dot{y}_j \Big(-C_{y_j - y_i} S_{f_i} S_{f_j} C_{q_i} + S_{y_j - y_i} S_{f_i} C_{f_j} C_{q_i} S_{q_j}\Big)\Big] + \\
&\dot{y}_i \Big[\dot{f}_j \Big(C_{y_j - y_i}\Big(S_{f_i} C_{f_j} S_{q_i} - C_{f_i} S_{f_j} S_{q_j}\Big) + S_{y_j - y_i}\Big(S_{f_i} S_{f_j} S_{q_i} S_{q_j} + C_{f_i} C_{f_j}\Big)\Big) + \\
&\quad \dot{q}_j \Big(C_{y_j - y_i} C_{f_i} C_{f_j} C_{q_j} - S_{y_j - y_i} S_{f_i} C_{f_j} S_{q_i} C_{q_j}\Big) + \\
&\quad \dot{y}_j \Big(C_{y_j - y_i}\Big(-S_{f_i} C_{f_j} S_{q_i} S_{q_j} + C_{f_i} S_{f_j}\Big) + S_{y_j - y_i}\Big(-S_{f_i} S_{f_j} S_{q_i} - C_{f_i} C_{f_j} S_{q_j}\Big)\Big)\Big]\Big\}
\end{aligned} \tag{3.16}$$

$$\frac{\partial T}{\partial \dot{f}_i} = \sum_{k=1}^{n}\sum_{j=1}^{k} m_k \Big\{$$
$$\dot{f}_j \Big(C_{y_j - y_i}\Big(S_{f_i} S_{f_j} S_{q_i} S_{q_j} + C_{f_i} C_{f_j}\Big) + S_{y_j - y_i}\Big(C_{f_i} S_{f_j} S_{q_j} - S_{f_i} C_{f_j} S_{q_i}\Big) + S_{f_i} S_{f_j} C_{q_i} C_{q_j}\Big) + \quad (3.17)$$
$$\dot{q}_j \Big(-C_{y_j - y_i} S_{f_i} C_{f_j} S_{q_i} C_{q_j} - S_{y_j - y_i} C_{f_i} C_{f_j} C_{q_j} + S_{f_i} C_{f_j} C_{q_i} S_{q_j}\Big) +$$
$$\dot{y}_j \Big(-C_{y_j - y_i}\Big(S_{f_i} S_{f_j} S_{q_i} + C_{f_i} C_{f_j} S_{q_j}\Big) + S_{y_j - y_i}\Big(S_{f_i} C_{f_j} S_{q_i} S_{q_j} - C_{f_i} S_{f_j}\Big)\Big)\Big\}$$

Finally evaluating the time rate of change of equation 3.17 produces,

$$\frac{d}{dt}\left(\frac{\partial T}{\partial \dot{f}_i}\right) = \sum_{k=1}^{n}\sum_{j=1}^{k} m_k \Big\{$$
$$\ddot{f}_j \Big(C_{y_j - y_i}\Big(S_{f_i} S_{f_j} S_{q_i} S_{q_j} + C_{f_i} C_{f_j}\Big) + S_{y_j - y_i}\Big(C_{f_i} S_{f_j} S_{q_j} - S_{f_i} C_{f_j} S_{q_i}\Big) + S_{f_i} S_{f_j} C_{q_i} C_{q_j}\Big) +$$
$$\ddot{q}_j \Big(-C_{y_j - y_i} S_{f_i} C_{f_j} S_{q_i} C_{q_j} - S_{y_j - y_i} C_{f_i} C_{f_j} C_{q_j} + S_{f_i} C_{f_j} C_{q_i} S_{q_j}\Big) +$$
$$\ddot{y}_j \Big(-C_{y_j - y_i}\Big(S_{f_i} S_{f_j} S_{q_i} + C_{f_i} C_{f_j} S_{q_j}\Big) + S_{y_j - y_i}\Big(S_{f_i} C_{f_j} S_{q_i} S_{q_j} - C_{f_i} S_{f_j}\Big)\Big) +$$
$$2\dot{f}_j \dot{q}_j \Big(C_{y_j - y_i} S_{f_i} S_{f_j} S_{q_i} C_{q_j} + S_{y_j - y_i} C_{f_i} S_{f_j} C_{q_j} - S_{f_i} S_{f_j} C_{q_i} S_{q_j}\Big) +$$
$$2\dot{q}_j \dot{y}_j \Big(S_{y_j - y_i} S_{f_i} C_{f_j} S_{q_i} C_{q_j} - C_{y_j - y_i} C_{f_i} C_{f_j} C_{q_j}\Big) +$$
$$2\dot{y}_j \dot{f}_j \Big(C_{y_j - y_i}\Big(-S_{f_i} C_{f_j} S_{q_i} + C_{f_i} S_{f_j} S_{q_j}\Big) + S_{y_j - y_i}\Big(-S_{f_i} S_{f_j} S_{q_i} S_{q_j} - C_{f_i} C_{f_j}\Big)\Big) +$$
$$\dot{f}_j^2 \Big(C_{y_j - y_i}\Big(S_{f_i} C_{f_j} S_{q_i} S_{q_j} - C_{f_i} S_{f_j}\Big) + S_{y_j - y_i}\Big(C_{f_i} C_{f_j} S_{q_j} + S_{f_i} S_{f_j} S_{q_i}\Big) + S_{f_i} C_{f_j} C_{q_i} C_{q_j}\Big) +$$
$$\dot{q}_j^2 \Big(C_{y_j - y_i} S_{f_i} C_{f_j} S_{q_i} S_{q_j} + S_{y_j - y_i} C_{f_i} C_{f_j} S_{q_j} + S_{f_i} C_{f_j} C_{q_i} C_{q_j}\Big) +$$
$$\dot{y}_j \Big(S_{y_j - y_i}\Big(S_{f_i} S_{f_j} S_{q_i} + C_{f_i} C_{f_j} S_{q_j}\Big) + C_{y_j - y_i}\Big(S_{f_i} C_{f_j} S_{q_i} S_{q_j} - C_{f_i} S_{f_j}\Big)\Big) +$$
$$\dot{f}_i \Big[\dot{f}_j \Big(C_{y_j - y_i}\Big(C_{f_i} S_{f_j} S_{q_i} S_{q_j} - S_{f_i} C_{f_j}\Big) + S_{y_j - y_i}\Big(-S_{f_i} S_{f_j} S_{q_j} - C_{f_i} C_{f_j} S_{q_i}\Big) + C_{f_i} S_{f_j} C_{q_i} C_{q_j}\Big) +$$
$$\dot{q}_j \Big(-C_{y_j - y_i} C_{f_i} C_{f_j} S_{q_i} C_{q_j} + S_{y_j - y_i} S_{f_i} C_{f_j} C_{q_j} + C_{f_i} C_{f_j} C_{q_i} S_{q_j}\Big) +$$
$$\dot{y}_j \Big(-C_{y_j - y_i}\Big(C_{f_i} S_{f_j} S_{q_i} - S_{f_i} C_{f_j} S_{q_j}\Big) + S_{y_j - y_i}\Big(C_{f_i} C_{f_j} S_{q_i} S_{q_j} + S_{f_i} S_{f_j}\Big)\Big)\Big] +$$
$$\dot{q}_i \Big[\dot{f}_j \Big(C_{y_j - y_i} S_{f_i} S_{f_j} C_{q_i} S_{q_j} - S_{y_j - y_i} S_{f_i} C_{f_j} C_{q_i} - S_{f_i} S_{f_j} S_{q_i} C_{q_j}\Big) +$$
$$\dot{q}_j \Big(-C_{y_j - y_i} S_{f_i} C_{f_j} C_{q_i} C_{q_j} - S_{f_i} C_{f_j} S_{q_i} S_{q_j}\Big) +$$
$$\dot{y}_j \Big(-C_{y_j - y_i} S_{f_i} S_{f_j} C_{q_i} + S_{y_j - y_i} S_{f_i} C_{f_j} C_{q_i} S_{q_j}\Big)\Big] +$$
$$\dot{y}_i \Big[\dot{f}_j \Big(C_{y_j - y_i}\Big(S_{f_i} C_{f_j} S_{q_i} - C_{f_i} S_{f_j} S_{q_j}\Big) + S_{y_j - y_i}\Big(S_{f_i} S_{f_j} S_{q_i} S_{q_j} + C_{f_i} C_{f_j}\Big)\Big) +$$
$$\dot{q}_j \Big(C_{y_j - y_i} C_{f_i} C_{f_j} C_{q_j} - S_{y_j - y_i} S_{f_i} C_{f_j} S_{q_i} C_{q_j}\Big) +$$
$$\dot{y}_j \Big(C_{y_j - y_i}\Big(-S_{f_i} C_{f_j} S_{q_i} S_{q_j} + C_{f_i} S_{f_j}\Big) + S_{y_j - y_i}\Big(-S_{f_i} S_{f_j} S_{q_i} - C_{f_i} C_{f_j} S_{q_j}\Big)\Big)\Big]\Big\}$$
(3.18)

Note that, just as in the two-dimensional case, the term representing the derivative of kinetic energy with respect to generalized coordinate, equation 3.16, is completely canceled by the some of the terms in the time rate of change of the derivative of kinetic energy with respect to the time rate of change of the generalized coordinate, equation 3.18.

Combining equations 3.16 and 3.18 results in the series representation of the left hand side of the Lagrange's equations for the bank angle of the three-dimensional finite element modeled cable,

$$\begin{aligned}
&\frac{d}{dt}\left(\frac{\partial T}{\partial \dot{f}_i}\right)-\frac{\partial T}{\partial f_i}=\sum_{k=1}^{n}\sum_{j=1}^{k} m_k\Big\{\\
&\ddot{f}_j\left(C_{y_j-y_i}\left(S_{f_i}S_{f_j}S_{q_i}S_{q_j}+C_{f_i}C_{f_j}\right)+S_{y_j-y_i}\left(C_{f_i}S_{f_j}S_{q_j}-S_{f_i}C_{f_j}S_{q_i}\right)+S_{f_i}S_{f_j}C_{q_i}C_{q_j}\right)+\\
&\ddot{q}_j\left(-C_{y_j-y_i}S_{f_i}C_{f_j}S_{q_i}C_{q_j}-S_{y_j-y_i}C_{f_i}C_{f_j}C_{q_j}+S_{f_i}C_{f_j}C_{q_i}S_{q_j}\right)+\\
&\ddot{y}_j\left(-C_{y_j-y_i}\left(S_{f_i}S_{f_j}S_{q_i}+C_{f_i}C_{f_j}S_{q_j}\right)+S_{y_j-y_i}\left(S_{f_i}C_{f_j}S_{q_i}S_{q_j}-C_{f_i}S_{f_j}\right)\right)+\\
&2\dot{f}_j\dot{q}_j\left(C_{y_j-y_i}S_{f_i}S_{f_j}S_{q_i}C_{q_j}+S_{y_j-y_i}C_{f_i}S_{f_j}C_{q_j}-S_{f_i}S_{f_j}C_{q_i}S_{q_j}\right)+\\
&2\dot{q}_j\dot{y}_j\left(S_{y_j-y_i}S_{f_i}C_{f_j}S_{q_i}C_{q_j}-C_{y_j-y_i}C_{f_i}C_{f_j}C_{q_j}\right)+\\
&2\dot{y}_j\dot{f}_j\left(C_{y_j-y_i}\left(-S_{f_i}C_{f_j}S_{q_i}+C_{f_i}S_{f_j}S_{q_j}\right)+S_{y_j-y_i}\left(-S_{f_i}S_{f_j}S_{q_i}S_{q_j}-C_{f_i}C_{f_j}\right)\right)+\\
&\dot{f}_j^2\left(C_{y_j-y_i}\left(S_{f_i}C_{f_j}S_{q_i}S_{q_j}-C_{f_i}S_{f_j}\right)+S_{y_j-y_i}\left(C_{f_i}C_{f_j}S_{q_j}+S_{f_i}S_{f_j}S_{q_i}\right)+S_{f_i}C_{f_j}C_{q_i}C_{q_j}\right)+\\
&\dot{q}_j^2\left(C_{y_j-y_i}S_{f_i}C_{f_j}S_{q_i}S_{q_j}+S_{y_j-y_i}C_{f_i}C_{f_j}S_{q_j}+S_{f_i}C_{f_j}C_{q_i}C_{q_j}\right)+\\
&\dot{y}_j\left(S_{y_j-y_i}\left(S_{f_i}S_{f_j}S_{q_i}+C_{f_i}C_{f_j}S_{q_j}\right)+C_{y_j-y_i}\left(S_{f_i}C_{f_j}S_{q_i}S_{q_j}-C_{f_i}S_{f_j}\right)\right)\Big\}=Q_{f_i}\\
&\qquad\qquad\qquad\qquad\qquad\qquad\qquad\qquad\qquad\qquad for\ \left(i=1,2,\ldots,n\right)
\end{aligned}\tag{3.19}$$

To fully develop the equations of motion the generalized force equation as a function of bank angle is evaluated in accordance with equation 3.12.

$$Q_{f_i} = M_{f_i} + \sum_{j=i}^{n} \Big[F_{X_j} l_i \left(C_{f_i} S_{y_i} - S_{f_i} S_{q_i} C_{y_i} \right) + F_{Y_j} l_i \left(- C_{f_i} C_{y_i} - S_{f_i} S_{q_i} S_{y_i} \right) + \left(F_{Z_j} + m_j g \right) l_i \left(- S_{f_i} C_{q_i} \right) \Big] \qquad \text{for} \quad (i = 1, 2, \ldots, n) \tag{3.20}$$

The implementation of the Lagrange equations for the bank angle generalized coordinate is complete, however to attain the full system equations of motion Lagrange's equations must be derived for the two remaining generalized coordinates.

3.2.2.2 Attitude Angle

This section investigates the application of the Lagrange equations for the attitude angle generalized coordinate. The Lagrange equation term representing the derivative of kinetic energy with respect to the attitude angle and the rate of change of the attitude angle of the i^{th} cable segment is as follows,

$$\begin{aligned}
\frac{\partial T}{\partial q_i} = \sum_{k=1}^{n} \sum_{j=1}^{k} m_k \Big\{ & \\
\dot{f}_i \Big[\dot{f}_j & \left(C_{y_j - y_i} S_{f_i} S_{f_j} C_{q_i} S_{q_j} - S_{y_j - y_i} S_{f_i} C_{f_j} C_{q_i} - S_{f_i} S_{f_j} S_{q_i} C_{q_j} \right) + \\
& \dot{q}_j \left(- C_{y_j - y_i} S_{f_i} C_{f_j} C_{q_i} C_{q_j} - S_{f_i} C_{f_j} S_{q_i} S_{q_j} \right) + \\
& \dot{y}_j \left(- C_{y_j - y_i} S_{f_i} S_{f_j} C_{q_i} + S_{y_j - y_i} S_{f_i} C_{f_j} C_{q_i} S_{q_j} \right) \Big] + \\
\dot{q}_i \Big[\dot{f}_j & \left(C_{y_j - y_i} C_{f_i} S_{f_j} S_{q_i} S_{q_j} - S_{y_j - y_i} C_{f_i} C_{f_j} S_{q_i} + C_{f_i} S_{f_j} C_{q_i} C_{q_j} \right) + \\
& \dot{q}_j \left(- C_{y_j - y_i} C_{f_i} C_{f_j} S_{q_i} C_{q_j} + C_{f_i} C_{f_j} C_{q_i} S_{q_j} \right) + \\
& \dot{y}_j \left(- C_{y_j - y_i} C_{f_i} S_{f_j} S_{q_i} + S_{y_j - y_i} C_{f_i} C_{f_j} S_{q_i} S_{q_j} \right) \Big] + \\
\dot{y}_i \Big[\dot{f}_j & \left(- C_{y_j - y_i} C_{f_i} C_{f_j} C_{q_i} - S_{y_j - y_i} C_{f_i} S_{f_j} C_{q_i} S_{q_j} \right) + \\
& \dot{q}_j \left(S_{y_j - y_i} C_{f_i} C_{f_j} C_{q_i} C_{q_j} \right) + \\
& \dot{y}_j \left(C_{y_j - y_i} C_{f_i} C_{f_j} C_{q_i} S_{q_j} + S_{y_j - y_i} C_{f_i} S_{f_j} C_{q_i} \right) \Big] \Big\}
\end{aligned} \tag{3.21}$$

$$\frac{\partial T}{\partial \dot{q}_i} = \sum_{k=1}^{n}\sum_{j=1}^{k} m_k \Big\{ \dot{f}_j \Big(-C_{y_j - y_i} C_{f_i} S_{f_j} C_{q_i} S_{q_j} + S_{y_j - y_i} C_{f_i} C_{f_j} C_{q_i} + C_{f_i} S_{f_j} S_{q_i} C_{q_j} \Big) + \dot{q}_j \Big(C_{y_j - y_i} C_{f_i} C_{f_j} C_{q_i} C_{q_j} + C_{f_i} C_{f_j} S_{q_i} S_{q_j} \Big) + \dot{y}_j \Big(C_{y_j - y_i} C_{f_i} S_{f_j} C_{q_i} - S_{y_j - y_i} C_{f_i} C_{f_j} C_{q_i} S_{q_j} \Big) \Big\} \quad (3.22)$$

Taking the time rate of change of the equation 3.22 produces the first term in Lagrange's equations for the attitude angle generalized coordinate,

$$
\begin{aligned}
\frac{d}{dt}\left(\frac{\partial T}{\partial \dot{q}_i}\right) = \sum_{k=1}^{n}\sum_{j=1}^{k} m_k \Big\{ & \\
& \ddot{f}_j\left(-C_{y_j-y_i}C_{f_i}S_{f_j}C_{q_i}S_{q_j} + S_{y_j-y_i}C_{f_i}C_{f_j}C_{q_i} + C_{f_i}S_{f_j}S_{q_i}C_{q_j}\right) + \\
& \ddot{q}_j\left(C_{y_j-y_i}C_{f_i}C_{f_j}C_{q_i}C_{q_j} + C_{f_i}C_{f_j}S_{q_i}S_{q_j}\right) + \\
& \ddot{y}_j\left(C_{y_j-y_i}C_{f_i}S_{f_j}C_{q_i} - S_{y_j-y_i}C_{f_i}C_{f_j}C_{q_i}S_{q_j}\right) + \\
& 2\dot{f}_j\dot{q}_j\left(-C_{y_j-y_i}C_{f_i}S_{f_j}C_{q_i}C_{q_j} - C_{f_i}S_{f_j}S_{q_i}S_{q_j}\right) + \\
& 2\dot{q}_j\dot{y}_j\left(-S_{y_j-y_i}C_{f_i}C_{f_j}C_{q_i}C_{q_j}\right) + \\
& 2\dot{y}_j\dot{f}_j\left(C_{y_j-y_i}C_{f_i}C_{f_j}C_{q_i} + S_{y_j-y_i}C_{f_i}S_{f_j}C_{q_i}S_{q_j}\right) + \\
& \dot{f}_j^2\left(-C_{y_j-y_i}C_{f_i}C_{f_j}C_{q_i}S_{q_j} - S_{y_j-y_i}C_{f_i}S_{f_j}C_{q_i} + C_{f_i}C_{f_j}S_{q_i}C_{q_j}\right) + \\
& \dot{q}_j^2\left(-C_{y_j-y_i}C_{f_i}C_{f_j}C_{q_i}S_{q_j} + C_{f_i}C_{f_j}S_{q_i}C_{q_j}\right) + \\
& \dot{y}_j^2\left(-S_{y_j-y_i}C_{f_i}S_{f_j}C_{q_i} - C_{y_j-y_i}C_{f_i}C_{f_j}C_{q_i}S_{q_j}\right) + \\
\dot{f}_i\Big[& \dot{f}_j\left(C_{y_j-y_i}S_{f_i}S_{f_j}C_{q_i}S_{q_j} - S_{y_j-y_i}S_{f_i}C_{f_j}C_{q_i} - S_{f_i}S_{f_j}S_{q_i}C_{q_j}\right) + \\
& \dot{q}_j\left(-C_{y_j-y_i}S_{f_i}C_{f_j}C_{q_i}C_{q_j} - S_{f_i}C_{f_j}S_{q_i}S_{q_j}\right) + \\
& \dot{y}_j\left(-C_{y_j-y_i}S_{f_i}S_{f_j}C_{q_i} + S_{y_j-y_i}S_{f_i}C_{f_j}C_{q_i}S_{q_j}\right)\Big] + \\
\dot{q}_i\Big[& \dot{f}_j\left(C_{y_j-y_i}C_{f_i}S_{f_j}S_{q_i}S_{q_j} - S_{y_j-y_i}C_{f_i}C_{f_j}S_{q_i} + C_{f_i}S_{f_j}C_{q_i}C_{q_j}\right) + \\
& \dot{q}_j\left(-C_{y_j-y_i}C_{f_i}C_{f_j}S_{q_i}C_{q_j} + C_{f_i}C_{f_j}C_{q_i}S_{q_j}\right) + \\
& \dot{y}_j\left(-C_{y_j-y_i}C_{f_i}S_{f_j}S_{q_i} + S_{y_j-y_i}C_{f_i}C_{f_j}S_{q_i}S_{q_j}\right)\Big] + \\
\dot{y}_i\Big[& \dot{f}_j\left(-C_{y_j-y_i}C_{f_i}C_{f_j}C_{q_i} - S_{y_j-y_i}C_{f_i}S_{f_j}C_{q_i}S_{q_j}\right) + \\
& \dot{q}_j\left(S_{y_j-y_i}C_{f_i}C_{f_j}C_{q_i}C_{q_j}\right) + \\
& \dot{y}_j\left(C_{y_j-y_i}C_{f_i}C_{f_j}C_{q_i}S_{q_j} + S_{y_j-y_i}C_{f_i}S_{f_j}C_{q_i}\right)\Big]\Big\}
\end{aligned}
\tag{3.23}
$$

Again, the time rate of change of the derivative of kinetic energy with respect to the time rate of change of the generalized coordinate, equation 3.23, contains terms that are equal to the derivative of kinetic energy with respect to the generalized coordinate, equation 3.21.

Combining equation 3.21 and 3.23 appropriately produces the left hand side of Lagrange's equations for the attitude angle generalized coordinate,

$$
\begin{aligned}
&\frac{d}{dt}\left(\frac{\partial T}{\partial \dot{q}_i}\right)-\frac{\partial T}{\partial q_i}=\sum_{k=1}^{n}\sum_{j=1}^{k} m_k\Big\{\\
&\ddot{f}_j\left(-C_{y_j-y_i}C_{f_i}S_{f_j}C_{q_i}S_{q_j}+S_{y_j-y_i}C_{f_i}C_{f_j}C_{q_i}+C_{f_i}S_{f_j}S_{q_i}C_{q_j}\right)+\\
&\ddot{q}_j\left(C_{y_j-y_i}C_{f_i}C_{f_j}C_{q_i}C_{q_j}+C_{f_i}C_{f_j}S_{q_i}S_{q_j}\right)+\\
&\ddot{y}_j\left(C_{y_j-y_i}C_{f_i}S_{f_j}C_{q_i}-S_{y_j-y_i}C_{f_i}C_{f_j}C_{q_i}S_{q_j}\right)+\\
&2\dot{f}_j\dot{q}_j\left(-C_{y_j-y_i}C_{f_i}S_{f_j}C_{q_i}C_{q_j}-C_{f_i}S_{f_j}S_{q_i}S_{q_j}\right)+\\
&2\dot{q}_j\dot{y}_j\left(-S_{y_j-y_i}C_{f_i}C_{f_j}C_{q_i}C_{q_j}\right)+\\
&2\dot{y}_j\dot{f}_j\left(C_{y_j-y_i}C_{f_i}C_{f_j}C_{q_i}+S_{y_j-y_i}C_{f_i}S_{f_j}C_{q_i}S_{q_j}\right)+\\
&\dot{f}_j^{\,2}\left(-C_{y_j-y_i}C_{f_i}C_{f_j}C_{q_i}S_{q_j}-S_{y_j-y_i}C_{f_i}S_{f_j}C_{q_i}+C_{f_i}C_{f_j}S_{q_i}C_{q_j}\right)+\\
&\dot{q}_j^{\,2}\left(-C_{y_j-y_i}C_{f_i}C_{f_j}C_{q_i}S_{q_j}+C_{f_i}C_{f_j}S_{q_i}C_{q_j}\right)+\\
&\dot{y}_j^{\,2}\left(-S_{y_j-y_i}C_{f_i}S_{f_j}C_{q_i}-C_{y_j-y_i}C_{f_i}C_{f_j}C_{q_i}S_{q_j}\right)\Big\}=Q_{q_i}
\end{aligned}
\tag{3.24}
$$

The right hand side of Lagrange's equations is the derivation of the generalized force for the i^{th} segment. The evaluation of equation 3.12 for the attitude angle generalized coordinate results in,

$$
Q_{q\,i}=M_{q\,i}+\sum_{j=i}^{n}\left[F_{X\,j}l_i\left(C_{f_i}C_{q_i}C_{y_i}\right)+F_{Y\,j}l_i\left(C_{f_i}C_{q_i}S_{y_i}\right)+\left(F_{Z\,j}+m_j g\right)l_i\left(-C_{f_i}S_{q_i}\right)\right] \tag{3.25}
$$
$$
for\quad (i=1,2,\ldots,n)
$$

Thus, concludes the derivation of the equations of motion for the attitude angle. However, there still remains one generalized coordinate not yet applied to the Lagrange equations.

3.2.2.3 Heading Angle

The final generalized coordinate is the heading angle. The equations of motion for the heading angle are derived in the same fashion as that of the other Euler angles. The

derivation of the Lagrange equations for the heading angle of the i^{th} segment as shown in equation 3.11 is presented in detail in the remainder of this section.

The derivative of kinetic energy with respect to the heading angle and time rate of change of heading angle of the cable segment is evaluated below,

$$\begin{aligned}
\frac{\partial T}{\partial y_i} = \sum_{k=1}^{n}\sum_{j=1}^{k} m_k \Big\{ & \\
\dot{f}_i \Big[\dot{f}_j \Big(& S_{y_j - y_i} \left(S_{f_i} S_{f_j} S_{q_i} S_{q_j} + C_{f_i} C_{f_j} \right) - C_{y_j - y_i} \left(C_{f_i} S_{f_j} S_{q_j} - S_{f_i} C_{f_j} S_{q_i} \right) \Big) + \\
& \dot{q}_j \left(- S_{y_j - y_i} S_{f_i} C_{f_j} S_{q_i} C_{q_j} + C_{y_j - y_i} C_{f_i} C_{f_j} C_{q_j} \right) + \\
& \dot{y}_j \left(- S_{y_j - y_i} \left(S_{f_i} S_{f_j} S_{q_i} + C_{f_i} C_{f_j} S_{q_j} \right) - C_{y_j - y_i} \left(S_{f_i} C_{f_j} S_{q_i} S_{q_j} - C_{f_i} S_{f_j} \right) \right) \Big] + \\
\dot{q}_i \Big[\dot{f}_j \Big(& - S_{y_j - y_i} C_{f_i} S_{f_j} C_{q_i} S_{q_j} - C_{y_j - y_i} C_{f_i} C_{f_j} C_{q_i} \Big) + \\
& \dot{q}_j \left(S_{y_j - y_i} C_{f_i} C_{f_j} C_{q_i} C_{q_j} \right) + \\
& \dot{y}_j \left(S_{y_j - y_i} C_{f_i} S_{f_j} C_{q_i} + C_{y_j - y_i} C_{f_i} C_{f_j} C_{q_i} S_{q_j} \right) \Big] + \\
\dot{y}_i \Big[\dot{f}_j \Big(& S_{y_j - y_i} \left(- C_{f_i} C_{f_j} S_{q_i} - S_{f_i} S_{f_j} S_{q_j} \right) - C_{y_j - y_i} \left(- C_{f_i} S_{f_j} S_{q_i} S_{q_j} + S_{f_i} C_{f_j} \right) \Big) + \\
& \dot{q}_j \left(S_{y_j - y_i} S_{f_i} C_{f_j} C_{q_j} - C_{y_j - y_i} C_{f_i} C_{f_j} S_{q_i} C_{q_j} \right) + \\
& \dot{y}_j \left(S_{y_j - y_i} \left(C_{f_i} C_{f_j} S_{q_i} S_{q_j} + S_{f_i} S_{f_j} \right) - C_{y_j - y_i} \left(C_{f_i} S_{f_j} S_{q_i} - S_{f_i} C_{f_j} S_{q_j} \right) \Big) \Big] \Big\}
\end{aligned} \tag{3.26}$$

$$\begin{aligned}
\frac{\partial T}{\partial \dot{y}_i} = \sum_{k=1}^{n}\sum_{j=1}^{k} m_k \Big\{ & \\
& \dot{f}_j \Big(C_{y_j - y_i} \left(- C_{f_i} C_{f_j} S_{q_i} - S_{f_i} S_{f_j} S_{q_j} \right) + S_{y_j - y_i} \left(- C_{f_i} S_{f_j} S_{q_i} S_{q_j} + S_{f_i} C_{f_j} \right) \Big) + \\
& \dot{q}_j \left(C_{y_j - y_i} S_{f_i} C_{f_j} C_{q_j} + S_{y_j - y_i} C_{f_i} C_{f_j} S_{q_i} C_{q_j} \right) + \\
& \dot{y}_j \left(C_{y_j - y_i} \left(C_{f_i} C_{f_j} S_{q_i} S_{q_j} + S_{f_i} S_{f_j} \right) + S_{y_j - y_i} \left(C_{f_i} S_{f_j} S_{q_i} - S_{f_i} C_{f_j} S_{q_j} \right) \right) \Big\}
\end{aligned} \tag{3.27}$$

The first term of Lagrange's equations is attained by taking the time rate of change of equation 3.27. The results are as follows,

$$
\begin{aligned}
\frac{d}{dt}\left(\frac{\partial T}{\partial \dot{y}_i}\right) = \sum_{k=1}^{n}\sum_{j=1}^{k} m_k \Big\{ & \\
& \ddot{f}_j \left(C_{y_j-y_i}\left(-C_{f_i}C_{f_j}S_{q_i} - S_{f_i}S_{f_j}S_{q_j}\right) + S_{y_j-y_i}\left(-C_{f_i}S_{f_j}S_{q_i}S_{q_j} + S_{f_i}C_{f_j}\right)\right) + \\
& \ddot{q}_j \left(C_{y_j-y_i}S_{f_i}C_{f_j}C_{q_j} + S_{y_j-y_i}C_{f_i}C_{f_j}S_{q_i}C_{q_j}\right) + \\
& \ddot{y}_j \left(C_{y_j-y_i}\left(C_{f_i}C_{f_j}S_{q_i}S_{q_j} + S_{f_i}S_{f_j}\right) + S_{y_j-y_i}\left(C_{f_i}S_{f_j}S_{q_i} - S_{f_i}C_{f_j}S_{q_j}\right)\right) + \\
& 2\dot{f}_j\dot{q}_j \left(-C_{y_j-y_i}S_{f_i}S_{f_j}C_{q_j} - S_{y_j-y_i}C_{f_i}S_{f_j}S_{q_i}C_{q_j}\right) + \\
& 2\dot{q}_j\dot{y}_j \left(-S_{y_j-y_i}S_{f_i}C_{f_j}C_{q_j} + C_{y_j-y_i}C_{f_i}C_{f_j}S_{q_i}C_{q_j}\right) + \\
& 2\dot{y}_j\dot{f}_j \left(C_{y_j-y_i}\left(-C_{f_i}S_{f_j}S_{q_i}S_{q_j} + S_{f_i}C_{f_j}\right) + S_{y_j-y_i}\left(C_{f_i}C_{f_j}S_{q_i} + S_{f_i}S_{f_j}S_{q_j}\right)\right) + \\
& \dot{f}_j^2 \left(C_{y_j-y_i}\left(C_{f_i}S_{f_j}S_{q_i} - S_{f_i}C_{f_j}S_{q_j}\right) + S_{y_j-y_i}\left(-C_{f_i}C_{f_j}S_{q_i}S_{q_j} - S_{f_i}S_{f_j}\right)\right) + \\
& \dot{q}_j^2 \left(-C_{y_j-y_i}S_{f_i}C_{f_j}S_{q_j} - S_{y_j-y_i}C_{f_i}C_{f_j}S_{q_i}S_{q_j}\right) + \\
& \dot{y}_j^2 \left(-S_{y_j-y_i}\left(C_{f_i}C_{f_j}S_{q_i}S_{q_j} + S_{f_i}S_{f_j}\right) + C_{y_j-y_i}\left(C_{f_i}S_{f_j}S_{q_i} - S_{f_i}C_{f_j}S_{q_j}\right)\right) + \\
\dot{f}_i\Big[& \dot{f}_j \left(S_{y_j-y_i}\left(S_{f_i}S_{f_j}S_{q_i}S_{q_j} + C_{f_i}C_{f_j}\right) - C_{y_j-y_i}\left(C_{f_i}S_{f_j}S_{q_j} - S_{f_i}C_{f_j}S_{q_i}\right)\right) + \\
& \dot{q}_j \left(-S_{y_j-y_i}S_{f_i}C_{f_j}S_{q_i}C_{q_j} + C_{y_j-y_i}C_{f_i}C_{f_j}C_{q_j}\right) + \\
& \dot{y}_j \left(-S_{y_j-y_i}\left(S_{f_i}S_{f_j}S_{q_i} + C_{f_i}C_{f_j}S_{q_j}\right) - C_{y_j-y_i}\left(S_{f_i}C_{f_j}S_{q_i}S_{q_j} - C_{f_i}S_{f_j}\right)\right)\Big] + \\
\dot{q}_i\Big[& \dot{f}_j \left(-S_{y_j-y_i}C_{f_i}S_{f_j}C_{q_i}S_{q_j} - C_{y_j-y_i}C_{f_i}C_{f_j}C_{q_i}\right) + \\
& \dot{q}_j \left(S_{y_j-y_i}C_{f_i}C_{f_j}C_{q_i}C_{q_j}\right) + \\
& \dot{y}_j \left(S_{y_j-y_i}C_{f_i}S_{f_j}C_{q_i} + C_{y_j-y_i}C_{f_i}C_{f_j}C_{q_i}S_{q_j}\right)\Big] + \\
\dot{y}_i\Big[& \dot{f}_j \left(S_{y_j-y_i}\left(-C_{f_i}C_{f_j}S_{q_i} - S_{f_i}S_{f_j}S_{q_j}\right) - C_{y_j-y_i}\left(-C_{f_i}S_{f_j}S_{q_i}S_{q_j} + S_{f_i}C_{f_j}\right)\right) + \\
& \dot{q}_j \left(S_{y_j-y_i}S_{f_i}C_{f_j}C_{q_j} - C_{y_j-y_i}C_{f_i}C_{f_j}S_{q_i}C_{q_j}\right) + \\
& \dot{y}_j \left(S_{y_j-y_i}\left(C_{f_i}C_{f_j}S_{q_i}S_{q_j} + S_{f_i}S_{f_j}\right) - C_{y_j-y_i}\left(C_{f_i}S_{f_j}S_{q_i} - S_{f_i}C_{f_j}S_{q_j}\right)\Big]\Big\}\right.
\end{aligned}
\tag{3.28}
$$

As with the previous derivations of Lagrange's equations for the cable system the time rate of change of the derivative of kinetic energy with respect to the time rate of change of the generalized coordinate contains terms that are equal to the derivative of kinetic energy with respect to the generalized coordinate, somewhat simplifying the equations of motion.

Combining equation 3.26 and 3.28 appropriately produce the left hand side of the Lagrange's equations of the heading angle generalized coordinate.

$$\begin{aligned}
&\frac{d}{dt}\left(\frac{\partial T}{\partial \dot{y}_i}\right)-\frac{\partial T}{\partial y_i}=\sum_{k=1}^{n}\sum_{j=1}^{k} m_k\Big\{\\
&\ddot{f}_j\left(C_{y_j-y_i}\left(-C_{f_i}C_{f_j}S_{q_i}-S_{f_i}S_{f_j}S_{q_j}\right)+S_{y_j-y_i}\left(-C_{f_i}S_{f_j}S_{q_i}S_{q_j}+S_{f_i}C_{f_j}\right)\right)+\\
&\ddot{q}_j\left(C_{y_j-y_i}S_{f_i}C_{f_j}C_{q_j}+S_{y_j-y_i}C_{f_i}C_{f_j}S_{q_i}C_{q_j}\right)+\\
&\ddot{y}_j\left(C_{y_j-y_i}\left(C_{f_i}C_{f_j}S_{q_i}S_{q_j}+S_{f_i}S_{f_j}\right)+S_{y_j-y_i}\left(C_{f_i}S_{f_j}S_{q_i}-S_{f_i}C_{f_j}S_{q_j}\right)\right)+\\
&2\dot{f}_j\dot{q}_j\left(-C_{y_j-y_i}S_{f_i}S_{f_j}C_{q_j}-S_{y_j-y_i}C_{f_i}S_{f_j}S_{q_i}C_{q_j}\right)+\\
&2\dot{q}_j\dot{y}_j\left(-S_{y_j-y_i}S_{f_i}C_{f_j}C_{q_j}+C_{y_j-y_i}C_{f_i}C_{f_j}S_{q_i}C_{q_j}\right)+\\
&2\dot{y}_j\dot{f}_j\left(C_{y_j-y_i}\left(-C_{f_i}S_{f_j}S_{q_i}S_{q_j}+S_{f_i}C_{f_j}\right)+S_{y_j-y_i}\left(C_{f_i}C_{f_j}S_{q_i}+S_{f_i}S_{f_j}S_{q_j}\right)\right)+\\
&\dot{f}_j^2\left(C_{y_j-y_i}\left(C_{f_i}S_{f_j}S_{q_i}-S_{f_i}C_{f_j}S_{q_j}\right)+S_{y_j-y_i}\left(-C_{f_i}C_{f_j}S_{q_i}S_{q_j}-S_{f_i}S_{f_j}\right)\right)+\\
&\dot{q}_j^2\left(-C_{y_j-y_i}S_{f_i}C_{f_j}S_{q_j}-S_{y_j-y_i}C_{f_i}C_{f_j}S_{q_i}S_{q_j}\right)+\\
&\dot{y}_j^2\left(-S_{y_j-y_i}\left(C_{f_i}C_{f_j}S_{q_i}S_{q_j}+S_{f_i}S_{f_j}\right)+C_{y_j-y_i}\left(C_{f_i}S_{f_j}S_{q_i}-S_{f_i}C_{f_j}S_{q_j}\right)\right)\Big\}=Q_{y_i}
\end{aligned} \tag{3.29}$$

The final addition to the dynamics equations are the effect of the applied loads on the heading angle. The generalized force for the heading angle is derived in accordance with equation 3.12 and result in the following,

$$Q_{y_i}=M_{y_i}+\sum_{j=i}^{n}\left[F_{X_j}l_i\left(S_{f_i}C_{y_i}-C_{f_i}S_{q_i}S_{y_i}\right)+F_{Y_j}l_i\left(S_{f_i}S_{y_i}+C_{f_i}S_{q_i}C_{y_i}\right)\right] \quad for\ \ (i=1,2,\ldots,n) \tag{3.30}$$

The equations of motion of the cable segments are dependant upon the equations of motion of the Euler angles of each segment. Simulation of the cable motion requires simultaneous solution of the angular acceleration of the generalized coordinates for all cable segments.

3.2.2.4 Cable Equations of Motions

We have yet to discuss the three-dimensional aerodynamic applied loads, but neglecting that, the equations of motion for the three-dimensional cable have been derived, although they are not in a convenient form. We can rewrite the equations of motion in matrix form for an arbitrary number of cable segments as was done in the two-dimensional case. The fully three-dimensional nonlinear differential equations of motion for a cable of n segments can be written in the following form,

$$\begin{bmatrix} A_1 & A_2 & A_3 \\ A_4 & A_5 & A_6 \\ A_7 & A_8 & A_9 \end{bmatrix}\begin{bmatrix} \ddot{f} \\ \ddot{q} \\ \ddot{y} \end{bmatrix} + \begin{bmatrix} B_1 & B_2 & B_3 \\ B_4 & B_5 & B_6 \\ B_7 & B_8 & B_9 \end{bmatrix}\begin{bmatrix} \dot{f}^2 \\ \dot{q}^2 \\ \dot{y}^2 \end{bmatrix} + \begin{bmatrix} C_1 & C_2 & C_3 \\ C_4 & C_5 & C_6 \\ C_7 & C_8 & C_9 \end{bmatrix}\begin{bmatrix} \dot{f}\dot{q} \\ \dot{q}\dot{y} \\ \dot{y}\dot{f} \end{bmatrix} = \begin{bmatrix} Q_f \\ Q_q \\ Q_y \end{bmatrix} \qquad (3.31)$$

where A, B, C, and Q are augmented matrices. In other words, matrix A is composed of nine submatrices of size n x n. Thus A is of size $3n$ x $3n$. The same is true for matrix B and C. A, B, and C are coefficient matrices. The generalized force column matrix, Q, is an augmented matrix of size $3n$ x 1. The values of the matrices components are taken directly from the results of the derivation of the Lagrange equation carried out in the previous sections, and combine to form a set of $3n$ equations of motion.

The A, B, and C matrices in equation 3.31 are represented by the equations below, where i and j are the row and column of the matrices.

$$A_{1_{i,j}} = \underline{m}_{i,j} l_i l_j \left[C_{y_j - y_i} \left(S_{f_i} S_{f_j} S_{q_i} S_{q_j} + C_{f_i} C_{f_j} \right) + S_{y_j - y_i} \left(C_{f_i} S_{f_j} S_{q_j} - S_{f_i} C_{f_j} S_{q_i} \right) + S_{f_i} S_{f_j} C_{q_i} C_{q_j} \right] \qquad (3.32)$$

$$A_{2_{i,j}} = \underline{m}_{i,j} l_i l_j \left(- C_{y_j - y_i} S_{f_i} C_{f_j} S_{q_i} C_{q_j} - S_{y_j - y_i} C_{f_i} C_{f_j} C_{q_j} + S_{f_i} C_{f_j} C_{q_i} S_{q_j} \right) \qquad (3.33)$$

$$A_{3_{i,j}} = \underline{m}_{i,j} l_i l_j \left[-C_{y_j - y_i} \left(S_{f_i} S_{f_j} S_{q_i} + C_{f_i} C_{f_j} S_{q_j} \right) + S_{y_j - y_i} \left(S_{f_i} C_{f_j} S_{q_i} S_{q_j} - C_{f_i} S_{f_j} \right) \right] \tag{3.34}$$

$$A_{4_{i,j}} = A_{2_{j,i}} \tag{3.35}$$

$$A_{5_{i,j}} = \underline{m}_{i,j} l_i l_j \left(C_{y_j - y_i} C_{f_i} C_{f_j} C_{q_i} C_{q_j} + C_{f_i} C_{f_j} S_{q_i} S_{q_j} \right) \tag{3.36}$$

$$A_{6_{i,j}} = \underline{m}_{i,j} l_i l_j \left(C_{y_j - y_i} C_{f_i} S_{f_j} C_{q_i} - S_{y_j - y_i} C_{f_i} C_{f_j} C_{q_i} S_{q_j} \right) \tag{3.37}$$

$$A_{7_{i,j}} = A_{3_{j,i}} \tag{3.38}$$

$$A_{8_{i,j}} = A_{6_{j,i}} \tag{3.39}$$

$$A_{9_{i,j}} = \underline{m}_{i,j} l_i l_j \left[C_{y_j - y_i} \left(C_{f_i} C_{f_j} S_{q_i} S_{q_j} + S_{f_i} S_{f_j} \right) + S_{y_j - y_i} \left(C_{f_i} S_{f_j} S_{q_i} - S_{f_i} C_{f_j} S_{q_j} \right) \right] \tag{3.40}$$

$$B_{1_{i,j}} = \underline{m}_{i,j} l_i l_j \left[C_{y_j - y_i} \left(S_{f_i} C_{f_j} S_{q_i} S_{q_j} - C_{f_i} S_{f_j} \right) + S_{y_j - y_i} \left(C_{f_i} C_{f_j} S_{q_j} + S_{f_i} S_{f_j} S_{q_i} \right) + S_{f_i} C_{f_j} C_{q_i} C_{q_j} \right] \tag{3.41}$$

$$B_{2_{i,j}} = \underline{m}_{i,j} l_i l_j \left(C_{y_j - y_i} S_{f_i} C_{f_j} S_{q_i} S_{q_j} + S_{y_j - y_i} C_{f_i} C_{f_j} S_{q_j} + S_{f_i} C_{f_j} C_{q_i} C_{q_j} \right) \tag{3.42}$$

$$B_{3_{i,j}} = \underline{m}_{i,j} l_i l_j \left[-C_{y_j - y_i} \left(S_{f_i} S_{f_j} S_{q_i} + C_{f_i} C_{f_j} S_{q_j} \right) + S_{y_j - y_i} \left(S_{f_i} C_{f_j} S_{q_i} S_{q_j} - C_{f_i} S_{f_j} \right) \right] \tag{3.43}$$

$$B_{4_{i,j}} = \underline{m}_{i,j} l_i l_j \left(-C_{y_j - y_i} C_{f_i} C_{f_j} C_{q_i} S_{q_j} - S_{y_j - y_i} C_{f_i} S_{f_j} C_{q_i} + C_{f_i} C_{f_j} S_{q_i} C_{q_j} \right) \tag{3.44}$$

$$B_{5_{i,j}} = \underline{m}_{i,j} l_i l_j \left(-C_{y_j - y_i} C_{f_i} C_{f_j} C_{q_i} S_{q_j} + C_{f_i} C_{f_j} S_{q_i} C_{q_j} \right) \tag{3.45}$$

$$B_{6_{i,j}} = \underline{m}_{i,j} l_i l_j \left(- C_{y_j - y_i} C_{f_i} C_{f_j} C_{q_i} S_{q_j} - S_{y_j - y_i} C_{f_i} S_{f_j} C_{q_i} \right) \tag{3.46}$$

$$B_{7_{i,j}} = \underline{m}_{i,j} l_i l_j \left[- C_{y_j - y_i} \left(S_{f_i} C_{f_j} S_{q_j} - C_{f_i} S_{f_j} S_{q_i} \right) - S_{y_j - y_i} \left(C_{f_i} C_{f_j} S_{q_i} S_{q_j} + S_{f_i} S_{f_j} \right) \right] \tag{3.47}$$

$$B_{8_{i,j}} = \underline{m}_{i,j} l_i l_j \left(- C_{y_j - y_i} S_{f_i} C_{f_j} S_{q_j} - S_{y_j - y_i} C_{f_i} C_{f_j} S_{q_i} S_{q_j} \right) \tag{3.48}$$

$$B_{9_{i,j}} = \underline{m}_{i,j} l_i l_j \left[C_{y_j - y_i} \left(C_{f_i} S_{f_j} S_{q_i} - S_{f_i} C_{f_j} S_{q_j} \right) - S_{y_j - y_i} \left(C_{f_i} C_{f_j} S_{q_i} S_{q_j} + S_{f_i} S_{f_j} \right) \right] \tag{3.49}$$

$$C_{1_{i,j}} = 2\underline{m}_{i,j} l_i l_j \left(C_{y_j - y_i} S_{f_i} S_{f_j} S_{q_i} C_{q_j} + S_{y_j - y_i} C_{f_i} S_{f_j} C_{q_j} - S_{f_i} S_{f_j} C_{q_i} S_{q_j} \right) \tag{3.50}$$

$$C_{2_{i,j}} = 2\underline{m}_{i,j} l_i l_j \left(- C_{y_j - y_i} C_{f_i} C_{f_j} C_{q_j} + S_{y_j - y_i} S_{f_i} C_{f_j} S_{q_i} C_{q_j} \right) \tag{3.51}$$

$$C_{3_{i,j}} = 2\underline{m}_{i,j} l_i l_j \left[C_{y_j - y_i} \left(C_{f_i} S_{f_j} S_{q_j} - S_{f_i} C_{f_j} S_{q_i} \right) - S_{y_j - y_i} \left(S_{f_i} S_{f_j} S_{q_i} S_{q_j} + C_{f_i} C_{f_j} \right) \right] \tag{3.52}$$

$$C_{4_{i,j}} = 2\underline{m}_{i,j} l_i l_j \left(- C_{y_j - y_i} C_{f_i} S_{f_j} C_{q_i} C_{q_j} - C_{f_i} S_{f_j} S_{q_i} S_{q_j} \right) \tag{3.53}$$

$$C_{5_{i,j}} = 2\underline{m}_{i,j} l_i l_j \left(- S_{y_j - y_i} C_{f_i} C_{f_j} C_{q_i} C_{q_j} \right) \tag{3.54}$$

$$C_{6_{i,j}} = 2\underline{m}_{i,j} l_i l_j \left(C_{y_j - y_i} C_{f_i} C_{f_j} C_{q_i} + S_{y_j - y_i} C_{f_i} S_{f_j} C_{q_i} S_{q_j} \right) \tag{3.55}$$

$$C_{7_{i,j}} = 2\underline{m}_{i,j} l_i l_j \left(- C_{y_j - y_i} S_{f_i} S_{f_j} S_{q_j} - S_{y_j - y_i} C_{f_i} S_{f_j} S_{q_i} C_{q_j} \right) \tag{3.56}$$

$$C_{8_{i,j}} = 2\underline{m}_{i,j} l_i l_j \left(C_{y_j - y_i} C_{f_i} C_{f_j} S_{q_i} C_{q_j} - S_{y_j - y_i} S_{f_i} C_{f_j} C_{q_j} \right) \tag{3.57}$$

$$C_{9_{i,j}} = 2\underline{m}_{i,j} l_i l_j \left[C_{y_j - y_i} \left(-C_{f_i} S_{f_j} S_{q_i} S_{q_j} + S_{f_i} C_{f_j} \right) + S_{y_j - y_i} \left(C_{f_i} C_{f_j} S_{q_i} + S_{f_i} S_{f_j} S_{q_j} \right) \right] \tag{3.58}$$

Recall the mass distribution for the lumped mass modeled segment from equation 2.33,

$$\underline{m}_{i,j} = \sum_{k=\max(i,j)}^{n} m_k$$

The resulting matrix equation is quite complex, but then again so is the system that the equations are modeling. The equations were set up independent of the number of system segments. As a result, the addition of segments is easily accomplished (however, it will increase the computational workload). The angular acceleration of each segment can be calculated given known initial conditions such as the magnitude of the angles and angular velocity. To solve the equations of motion the matrices need to be populated, as per equations 3.20, 3.25, 3.30, and 3.33 through 3.58, and the *A* matrix must be inverted and appropriately applied to equation 3.31. There is an issue in the inversion of the *A* matrix but that will be discussed in a later section.

The model of the connected cable segments allows for complete rotational freedom for each segment. This assumption is valid with the exception of the twisting or rotation about the *z*-axis of the cable segment. In an actual cable the torsion resistance would not allow for free twisting. One could then introduce an additional constraint equation that would restrict twisting. However the kinetic energy associated with the twisting in the modeled cable segment is zero due to the fact that the segment has no inertia through the segment *z*-axis. The derivation of the equations of motion for cable using the Lagrange

technique is based on the kinetic energy; therefore, the free rotation of the segment about its *z*-axis is of no consequence. The utilization of the twisting constraint equation would reduce the degree of freedom of the system but it would also complicate the derivation. As a result, this will be left for future work.

The equations of motion to this point are sufficient to perform a dynamic simulation of an ideal three-dimensional cable. The final step to complete the full cable dynamic simulation is the modeling of the applied loads produced by the frictional fluid forces. These forces can then be introduced into the Q matrix which would allow a dynamic simulation of a cable in a fluid.

3.2.3 Aerodynamic Modeling

Hoerner's crossflow method for calculating cable drag is fundamentally applicable in the analysis of the three-dimensional cable model; the cable is composed of straight segments with circular cross-sections, and the flight conditions produce subcritical Reynolds number about the cable. However, direct application does not account for flow in the transverse direction.

In short, the crossflow method predicts the frictional and pressure forces produced by the fluid flow relative to the cable. The friction and pressure drag are calculated via the components of the flow that are normal and tangent to the cable. This is evident from the two-dimensional crossflow drag equations produced by Hoerner. This concept can be extended to three-dimensional flow with only slight modifications.

In the cable segment frame, the *z*-axis is tangent and the *x* and *y*-axes are perpendicular to the cable segment. Therefore, the magnitude of the normal velocity is dependant solely on the velocity of the fluid in the *x* and *y*-coordinate direction. The pressure drag is a function of the magnitude of the normal velocity and the friction drag is a function of the magnitude of the overall velocity.

The modification of the crossflow-principle for three-dimensional flow on the j^{th} cable segment is as follows:

$$
\begin{aligned}
F_{x_j} &= -\frac{1}{2}\rho d l_j V_{x_j}\left(\pi c_f \sqrt{V_{x_j}^2 + V_{y_j}^2 + V_{z_j}^2} + c_p \sqrt{V_{x_j}^2 + V_{y_j}^2}\right) \\
F_{y_j} &= -\frac{1}{2}\rho d l_j V_{y_j}\left(\pi c_f \sqrt{V_{x_j}^2 + V_{y_j}^2 + V_{z_j}^2} + c_p \sqrt{V_{x_j}^2 + V_{y_j}^2}\right) \\
F_{z_j} &= -\frac{1}{2}\rho d l_j V_{z_j}\left(\pi c_f \sqrt{V_{x_j}^2 + V_{y_j}^2 + V_{z_j}^2}\right)
\end{aligned}
\tag{3.59}
$$

where, ρ, d, c_f, and c_p are air density, cable diameter, frictional coefficient, and pressure coefficient, respectively; F_x, F_y, and F_z are the aerodynamic forces, and V_x, V_y, and V_z are the flow field velocity relative to the cable segment in the cable segment frame.

The fluid velocity relative to the cable is a result of the freestream flow, U_0, V_0, and W_0, and the motion of the cable system. The reference flight conditions as well as the equations calculating the segment node velocity are in the inertial frame. The application of equation 3.59 requires that the inertial velocity be converted to the cable segment coordinate system. Thus a rotational coordinate transformation is necessary,

$$\begin{bmatrix} V_{x\,j} \\ V_{y\,j} \\ V_{z\,j} \end{bmatrix} = \left[\underline{\underline{C_{f,q,y\,j}}}\right]^T \begin{bmatrix} U_0 + \dot{X}_j \\ V_0 + \dot{Y}_j \\ W_0 + \dot{Z}_j \end{bmatrix} \tag{3.60}$$

The drag loads are applied at the node of a given segment producing moments about the point of rotation of the segment. The resulting moments are inherently calculated in Lagrange's equations via the generalized force equations, equation 3.12. However, the forces in the generalized force equation are in the inertial frame. As a result, the drag forces calculated by the modified crossflow method require the rotational transformation as shown below,

$$\begin{bmatrix} F_{X\,j} \\ F_{Y\,j} \\ F_{Z\,j} \end{bmatrix} = \left[\underline{\underline{C_{f,q,y\,j}}}\right] \begin{bmatrix} F_{x\,j} \\ F_{y\,j} \\ F_{z\,j} \end{bmatrix} \tag{3.61}$$

The application of the friction forces of each cable segment to the generalized force equations, equations 3.20, 3.25, and 3.30, complete the system equations of motion for a cable in a fluid. The angular acceleration of each segment can be calculated by the manipulation of equation 3.31 given that the appropriate initial conditions, such as segment orientation and Euler angular velocities, of each segment are known. The ordinary differential equations can be utilized in combination with a numerical integration routine to produce a simulation that predicts the dynamics of a cable in a fluid field.

3.3 Arial Tow Vehicle

The three-dimensional flight dynamics and analysis of simple aircraft have been well documented. As a result, the simulation of the ATV alone would simply be an application of the aircraft equations of motion, resulting in a general flight simulator. However, the addition of the cable to the ATV introduces complexities for both the cable and ATV dynamics. The system equations of motion must be derived and solved simultaneously for both the cable and ATV.

In this configuration, the ATV is attached to the base of the cable, and the ATV is free to rotate about the cable-ATV hitch point. The ATV has a center of mass, at which the inertial and aerodynamic forces are applied, that is a fixed distance from its rotation point. It is possible, then, to describe the location of the ATV center of mass by the Euler angles of the imaginary line connecting the cable-ATV hitch point to the ATV center of mass, and like the cable segments the energy of the ATV can be described as a function of these Euler angles. Therefore, it is feasible to model the ATV as an additional segment to the cable. The parameters such as the mass and length of the segment are dictated by the configuration of the aircraft, and the applied loads on the ATV segment will be determined by the aircraft aerodynamics.

Modeling the ATV as a cable segment takes advantage of the equations that have already been derived to model the individual and coupled dynamics of connected bodies. However, the total energy of the ATV is not entirely represented by the translational kinetic and potential energies. Unlike the lumped mass cable segments defined in the

previous section the ATV has rotation kinetic energy. As a result, the system equations of motion will require expansion.

3.3.1 Coordinate System

The additional ATV segment has a coordinate system that is defined in the same manner as that of the cable segments. The origin of the ATV segment frame is at the cable-ATV hitch point and its z-axis passes through the ATV center of mass. However, the equations representing the aerodynamics of the ATV, as they are defined in Nelson and Raymer, are in the general body fixed frame of the aircraft. In this orthogonal coordinate system the origin is at the aircraft center of mass; the *x*-axis points from the origin towards the nose of the aircraft; the *y*-axis points towards the starboard side; and the z-axis points towards the bottom of the aircraft (presumably towards the ground). As a result, the ATV segment will have two coordinate systems, the ATV segment frame and the ATV aircraft frame.

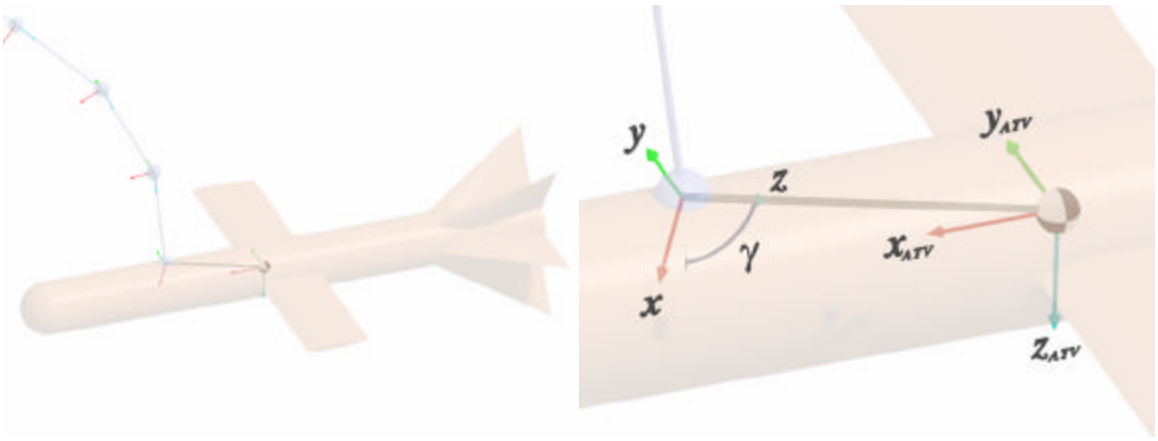

Figure 3.3 ATV coordinate systems

The ATV segment is geometrically defined from the cable-ATV hitch point to the ATV center of gravity. Thus, the ATV segment and the ATV aircraft coordinate system

differ in rotation by a fixed attitude angle, ? (this makes the reasonable assumption that the cable-ATV hitch point is in the *xz* plane). The aircraft aerodynamics that predicts the applied loads on the aircraft will be in the ATV aircraft frame, yet the generalized force equations require the forces be in the inertial frame. A rotational transformation is able to accommodate the change from one coordinate system to the next. Rotating from the ATV aircraft frame to the inertial frame is accomplished thru a series of transformations, first from the ATV aircraft to the ATV segment frame followed by the transformation from the ATV segment frame to the inertial frame.

Due to the fact that the ATV aircraft and ATV segment frame differ by a fixed angle in the *xz*-plane, the rotational transformation between the two is simply represented by a rotation about the aircraft *y*-axis.

$$\begin{bmatrix} x \\ y \\ z \end{bmatrix} = \begin{bmatrix} C_g & 0 & S_g \\ 0 & 1 & 0 \\ -S_g & 0 & C_g \end{bmatrix} \begin{bmatrix} x_{ATV} \\ y_{ATV} \\ z_{ATV} \end{bmatrix} = \underline{\underline{[C_g]}} \begin{bmatrix} x_{ATV} \\ y_{ATV} \\ z_{ATV} \end{bmatrix} \tag{3.62}$$

where, x_{ATV}, y_{ATV}, and z_{ATV} are the coordinates directions of the ATV aircraft frame.

The ATV segment has the full three-degrees of freedom in rotation. Therefore, the rotational transformation from the ATV segment frame to the inertial frame is the same as that derived in equation 3.6. The rotational transformation from the ATV aircraft to the inertial frame is as follows,

$$\begin{bmatrix} X \\ Y \\ Z \end{bmatrix} = \underline{\underline{[C_{f,q,y_{n+1}}]}} \underline{\underline{[C_g]}} \begin{bmatrix} x_{ATV} \\ y_{ATV} \\ z_{ATV} \end{bmatrix} \tag{3.63}$$

This transformation will allow the use of standard aircraft aerodynamic techniques to be used in calculating the generalized forces on the ATV segment due to the freestream flow and the shape and motion of the ATV.

3.3.2 Lagrange Equations

Lagrange's equations are based upon the total energy of the system, which in this system includes kinetic and potential energy. The kinetic energy is composed of both translational and rotational kinetic energy. The derivation of the cable segment equations of motion was simplified in that the segment nodes have no inertia and thus the segment has no rotational kinetic energy. The same is not true for the ATV segment. The ATV segment node is the ATV center of gravity and its inertia is derived from the ATV inertia. Therefore, the derivation of the equations of motion for the ATV segment is broken into two parts, translational and rotational kinetic energy. Due to the similarities in the model of the ATV segment and the cable segment, the derivation due to the translational kinetic energy is identical to that derived in the previous section; leaving only the derivation of the Lagrange equations due to the rotational kinetic energy, see equation 2.41.

Recall equation 2.43 presents the rotational kinetic energy equation of a rigid body,

$$T_{rot} = \frac{1}{2}\{w\}^T [I]\{w\}$$

where, *?* and *I* are the angular velocity vector and inertia matrix of the rigid body, respectively. The angular velocity vector of the ATV segment is dependant upon the generalized coordinates and their time derivatives, as follows,

$$\{w\} = \begin{bmatrix} w_x \\ w_y \\ w_z \end{bmatrix} = \begin{bmatrix} \dot{f} - \dot{y} S_q \\ \dot{q} C_f + \dot{y} C_q S_f \\ -\dot{q} S_f + \dot{y} C_q C_f \end{bmatrix} \tag{3.64}$$

The ATV inertial matrix is a three by three matrix as follows,

$$[I'] = \begin{bmatrix} I'_{xx} & I'_{xy} & I'_{xz} \\ I'_{yx} & I'_{yy} & I'_{yz} \\ I'_{zx} & I'_{zy} & I'_{zz} \end{bmatrix} \tag{3.65}$$

Note that, in the notation used, I'_{xy} is equivalent to I'_{yx}. Also note, that due to the aircraft symmetry the component of inertia I'_{xy} and I'_{yz} are equal to zero (this aircraft symmetry exists in most aircraft).

The inertia matrix for the ATV is in the ATV aircraft frame; however the equations of motion are derived for the Euler angles which dictate the position and motion of the system segments. Therefore, the inertia matrix in the kinetic energy equation must be that of the ATV segment not the ATV itself. The two coordinate systems differ by the fixed rotation angle, ?. The ATV segment inertia matrix is calculated from the ATV inertia as follows,

$$[I] = \left[\underline{\underline{C_g}}\right][I']\left[\underline{\underline{C_g}}\right]^T \tag{3.66}$$

Since this transformation is accomplished via a fixed angle it need only be calculated once, in other words it does not affect the derivation of the rotational equations of motion since the angle is not a function of time or generalized coordinates. The rotation of the

inertia matrix to the ATV segment frame does not affect the inertial symmetry (i.e I_{xy} and I_{xz} are zero).

The substitution of the three-dimensional angular velocity vector, equation 3.64, and the inertia matrix into the kinetic energy equation, equation 2.43, produces the segment rotational kinetic energy equation in terms of the generalized coordinates.,

$$T_{rot} = \frac{1}{2}\begin{bmatrix} \dot{f} - \dot{y} S_q \\ \dot{q} C_f + \dot{y} C_q S_f \\ -\dot{q} S_f + \dot{y} C_q C_f \end{bmatrix}^T \begin{bmatrix} I_{xx} & 0 & I_{xz} \\ 0 & I_{yy} & 0 \\ I_{zx} & 0 & I_{zz} \end{bmatrix} \begin{bmatrix} \dot{f} - \dot{y} S_q \\ \dot{q} C_f + \dot{y} C_q S_f \\ -\dot{q} S_f + \dot{y} C_q C_f \end{bmatrix} \tag{3.67}$$

The expansion of equation 3.67 and the application of it to every segment produce the rotational kinetic energy equation for the three-dimensional cable and ATV system,

$$\begin{aligned} T_{rot} = \frac{1}{2}\sum_{i=1}^{n+1}\Big[& I_{xx_i}\left(\dot{f}_i^2 + \dot{y}_i^2 S_{q_i}^2 - 2\dot{f}_i \dot{y}_i S_{q_i}\right) + \\ & I_{yy_i}\left(\dot{q}_i^2 C_{f_i}^2 + \dot{y}_i^2 C_{q_i}^2 S_{f_i}^2 + 2\dot{q}_i \dot{y}_i C_{f_i} S_{f_i} C_{q_i}\right) + \\ & I_{zz_i}\left(\dot{y}_i^2 C_{q_i}^2 C_{f_i}^2 + \dot{q}_i^2 S_{f_i}^2 - 2\dot{q}_i \dot{y}_i C_{f_i} S_{f_i} C_{q_i}\right) + \\ & 2I_{xz_i}\left(\dot{f}_i \dot{y}_i C_{f_i} C_{q_i} - \dot{f}_i \dot{q}_i S_{f_i} - \dot{y}_i^2 C_{f_i} C_{q_i} S_{q_i} + \dot{y}_i \dot{q}_i S_{f_i} S_{q_i}\right)\Big] \end{aligned} \tag{3.68}$$

Note that equation 3.68 accounts for each segment in the system cable and ATV alike. The equation would be greatly simplified under the condition that the cable segments were modeled using the lumped mass technique as the inertia components would be zero for i=1,2,…,n. However, this simplification will not be applied until after the equations of motion have been derived to increase robustness.

The effects of inertia on the dynamic response of the system is found by applying Lagrange's equation to the rotational kinetic energy equation for each generalized

coordinate, i.e. the Euler angles (bank angle, attitude angle, and heading angle) of each segment.

3.3.2.1 Bank Angle

The rotational bank angle equation of motion for the i^{th} segment is produced by evaluating Lagrange's equations for the appropriate generalized coordinate with respect to rotational kinetic energy,

$$\frac{d}{dt}\left(\frac{\partial T_{rot}}{\partial \dot{f}_i}\right)-\frac{\partial T_{rot}}{\partial f_i} \tag{3.69}$$

The derivative of rotational kinetic energy with respect to the bank angle and the time rate of change of the bank angle of the i^{th} segment are as follows,

$$\begin{aligned}\frac{\partial T_{rot}}{\partial f_i} = {} & I_{yy_i}\left[-\dot{q}_i^{\,2}C_{f_i}S_{f_i}+\dot{y}_i^{\,2}C_{f_i}S_{f_i}C_{q_i}^2+\dot{q}_i\dot{y}_i C_{q_i}\left(C_{f_i}^2-S_{f_i}^2\right)\right]+ \\ & I_{zzi}\left[-\dot{y}_i^{\,2}C_{f_i}S_{f_i}C_{q_i}^2+\dot{q}_i^{\,2}C_{f_i}S_{f_i}-\dot{q}_i\dot{y}_i C_{q_i}\left(C_{f_i}^2-S_{f_i}^2\right)\right]+ \\ & I_{xz_i}\left(-\dot{f}_i\dot{y}_i S_{f_i}C_{q_i}-\dot{f}_i\dot{q}_i C_{f_i}+\dot{y}_i^{\,2}S_{f_i}C_{q_i}S_{q_i}+\dot{y}_i\dot{q}_i C_{f_i}S_{q_i}\right)\end{aligned} \tag{3.70}$$

$$\frac{\partial T_{rot}}{\partial \dot{f}_i} = I_{xx_i}\left(\dot{f}_i-\dot{y}_i S_{q_i}\right)+I_{xz_i}\left(\dot{y}_i C_{f_i}C_{q_i}-\dot{q}_i S_{f_i}\right) \tag{3.71}$$

The time rate of change of equation 3.71 produces the final term of Lagrange's equations,

$$\begin{aligned}\frac{d}{dt}\left(\frac{\partial T_{rot}}{\partial \dot{f}_i}\right) = {} & I_{xx_i}\left(\ddot{f}_i-\ddot{y}_i S_{q_i}-\dot{y}_i\dot{q}_i C_{q_i}\right)+ \\ & I_{xz_i}\left(\ddot{y}_i C_{f_i}C_{q_i}-\dot{y}_i\dot{f}_i S_{f_i}C_{q_i}-\dot{y}_i\dot{q}_i C_{f_i}S_{q_i}-\ddot{q}_i S_{f_i}-\dot{q}_i\dot{f}_i C_{f_i}\right)\end{aligned} \tag{3.72}$$

The substitution of equations 3.70 and 3.72 into equation 3.69 yields the rotational equation of motion for the i_{th} segment due to bank angle rotation,

$$\begin{aligned}\frac{d}{dt}\left(\frac{\partial T_{rot}}{\partial \dot{f}_i}\right)-\frac{\partial T_{rot}}{\partial f_i} = \\ & I_{xx_i}\left(\ddot{f}_i-\ddot{y}_i S_{q_i}-\dot{y}_i\dot{q}_i C_{q_i}\right)+ \\ & I_{yy_i}\left[\dot{q}_i^2 C_{f_i}S_{f_i}-\dot{y}_i^2 C_{f_i}S_{f_i}C_{q_i}^2-\dot{q}_i\dot{y}_i C_{q_i}\left(C_{f_i}^2-S_{f_i}^2\right)\right]+ \\ & I_{zz_i}\left[\dot{y}_i^2 C_{f_i}S_{f_i}C_{q_i}^2-\dot{q}_i^2 C_{f_i}S_{f_i}+\dot{q}_i\dot{y}_i C_{q_i}\left(C_{f_i}^2-S_{f_i}^2\right)\right]+ \\ & I_{xz_i}\left(\ddot{y}_i C_{f_i}C_{q_i}-2\dot{y}_i\dot{q}_i C_{f_i}S_{q_i}-\ddot{q}_i S_{f_i}+\dot{y}_i^2 S_{f_i}C_{q_i}S_{q_i}\right) \\ & \qquad for\quad (i=1,2,\ldots n+1)\end{aligned} \tag{3.73}$$

3.3.2.2 Attitude Angle

The rotational attitude angle equation of motion for the i^{th} segment is produced by evaluating Lagrange's equations for the appropriate generalized coordinate with respect to rotational kinetic energy,

$$\frac{d}{dt}\left(\frac{\partial T_{rot}}{\partial \dot{q}_i}\right)-\frac{\partial T_{rot}}{\partial q_i} \tag{3.74}$$

The derivative of rotational kinetic energy with respect to the attitude angle and the time rate of change of the attitude angle of the i^{th} segment are as follows,

$$\begin{aligned}\frac{\partial T_{rot}}{\partial q_i} = & I_{xx_i}\left(\dot{y}_i^2 C_{q_i}S_{q_i}-\dot{f}_i\dot{y}_i C_{q_i}\right)+ \\ & I_{yy_i}\left(-\dot{y}_i^2 C_{q_i}S_{q_i}S_{f_i}^2-\dot{q}_i\dot{y}_i C_{f_i}S_{f_i}S_{q_i}\right)+ \\ & I_{zz_i}\left(-\dot{y}_i^2 C_{f_i}^2 C_{q_i}S_{q_i}+\dot{q}_i\dot{y}_i C_{f_i}S_{f_i}S_{q_i}\right)+ \\ & I_{xz_i}\left[-\dot{f}_i\dot{y}_i C_{f_i}S_{q_i}-\dot{y}_i^2 C_{f_i}\left(C_{q_i}^2-S_{q_i}^2\right)+\dot{y}_i\dot{q}_i S_{f_i}C_{q_i}\right]\end{aligned} \tag{3.75}$$

$$\frac{\partial T_{rot}}{\partial \dot{q}_i} = I_{yy_i}\left(\dot{q}_i C_{f_i}^2 + \dot{y}_i C_{f_i} S_{f_i} C_{q_i}\right) + I_{zz_i}\left(\dot{q}_i S_{f_i}^2 - \dot{y}_i C_{f_i} S_{f_i} C_{q_i}\right) + I_{xz_i}\left(-\dot{f}_i S_{f_i} + \dot{y}_i S_{f_i} S_{q_i}\right) \tag{3.76}$$

The time rate of change of equation 3.76 is as follows,

$$\begin{aligned}\frac{d}{dt}\left(\frac{\partial T_{rot}}{\partial \dot{q}_i}\right) = \\ I_{yy_i}\left[\ddot{q}_i C_{f_i}^2 - 2\dot{q}_i \dot{f}_i C_{f_i} S_{f_i} + \ddot{y}_i C_{f_i} S_{f_i} C_{q_i} - \dot{y}_i \dot{q}_i C_{f_i} S_{f_i} S_{q_i} + \dot{y}_i \dot{f}_i C_{q_i}\left(C_{f_i}^2 - S_{f_i}^2\right)\right] + \\ I_{zz_i}\left[\ddot{q}_i S_{f_i}^2 + 2\dot{q}_i \dot{f}_i C_{f_i} S_{f_i} - \ddot{y}_i C_{f_i} S_{f_i} C_{q_i} + \dot{y}_i \dot{q}_i C_{f_i} S_{f_i} S_{q_i} - \dot{y}_i \dot{f}_i C_{q_i}\left(C_{f_i}^2 - S_{f_i}^2\right)\right] + \\ I_{xz_i}\left(-\ddot{f}_i S_{f_i} - \dot{f}_i^2 C_{f_i} + \ddot{y}_i S_{f_i} S_{q_i} + \dot{y}_i \dot{f}_i C_{f_i} S_{q_i} + \dot{y}_i \dot{q}_i S_{f_i} C_{q_i}\right)\end{aligned} \tag{3.77}$$

The substitution of equation 3.75 and 3.77 into equation 3.74 yields the rotational equation of motion of the i_{th} segment due to attitude angle rotation,

$$\begin{aligned}\frac{d}{dt}\left(\frac{\partial T_{rot}}{\partial \dot{q}_i}\right) - \frac{\partial T_{rot}}{\partial q_i} = \\ I_{xx_i}\left(-\dot{y}_i^2 C_{q_i} S_{q_i} + \dot{f}_i \dot{y}_i C_{q_i}\right) + \\ I_{yy_i}\left[\ddot{q}_i C_{f_i}^2 - 2\dot{q}_i \dot{f}_i C_{f_i} S_{f_i} + \ddot{y}_i C_{f_i} S_{f_i} C_{q_i} + \dot{y}_i \dot{f}_i C_{q_i}\left(C_{f_i}^2 - S_{f_i}^2\right) + \dot{y}_i^2 S_{f_i}^2 C_{q_i} S_{q_i}\right] + \\ I_{zz_i}\left[\ddot{q}_i S_{f_i}^2 + 2\dot{q}_i \dot{f}_i C_{f_i} S_{f_i} - \ddot{y}_i C_{f_i} S_{f_i} C_{q_i} - \dot{y}_i \dot{f}_i C_{q_i}\left(C_{f_i}^2 - S_{f_i}^2\right) + \dot{y}_i^2 C_{f_i}^2 C_{q_i} S_{q_i}\right] + \\ I_{xz_i}\left[-\ddot{f}_i S_{f_i} - \dot{f}_i^2 C_{f_i} + \ddot{y}_i S_{f_i} S_{q_i} + 2\dot{f}_i \dot{y}_i C_{f_i} S_{q_i} + \dot{y}_i^2 C_{f_i}\left(C_{q_i}^2 - S_{q_i}^2\right)\right] \\ for \quad (i = 1, 2, \ldots n+1)\end{aligned} \tag{3.78}$$

3.3.2.3 Heading Angle

The rotational heading angle equation of motion for the i^{th} segment is produced by evaluating Lagrange's equations for the appropriate generalized coordinate with respect to rotational kinetic energy,

$$\frac{d}{dt}\left(\frac{\partial T_{rot}}{\partial \dot{y}_i}\right)-\frac{\partial T_{rot}}{\partial y_i} \tag{3.79}$$

The derivative of rotational kinetic energy with respect to the heading angle and the time rate of change of the heading angle of the i^{th} segment are as follows,

$$\frac{\partial T_{rot}}{\partial y_i}=0 \tag{3.80}$$

$$\begin{aligned}\frac{\partial T_{rot}}{\partial \dot{y}_i}=&\left[I_{xx_i}\left(\dot{y}_i S_{q_i}^2-\dot{f}_i S_{q_i}\right)+\right.\\ &I_{yy_i}\left(\dot{y}_i C_{q_i}^2 S_{f_i}^2+\dot{q}_i C_{f_i} S_{f_i} C_{q_i}\right)+\\ &I_{zz_i}\left(\dot{y}_i C_{q_i}^2 C_{f_i}^2-\dot{q}_i C_{f_i} S_{f_i} C_{q_i}\right)+\\ &\left.I_{xz_i}\left(\dot{f}_i C_{f_i} C_{q_i}-2\dot{y}_i C_{f_i} C_{q_i} S_{q_i}+\dot{q}_i S_{f_i} S_{q_i}\right)\right]\end{aligned} \tag{3.81}$$

The time rate of change of equation 3.81 is as follows,

$$\begin{aligned}\frac{d}{dt}\left(\frac{\partial T_{rot}}{\partial \dot{y}_i}\right)=&\\ &I_{xx_i}\left(\ddot{y}_i S_{q_i}^2+2\dot{y}_i\dot{q}_i C_{q_i} S_{q_i}-\ddot{f}_i S_{q_i}-\dot{f}_i\dot{q}_i C_{q_i}\right)+\\ &I_{yy_i}\left[\ddot{y}_i S_{f_i}^2 C_{q_i}^2+2\dot{y}_i\dot{f}_i C_{f_i} S_{f_i} C_{q_i}^2-2\dot{y}_i\dot{q}_i S_{f_i}^2 C_{q_i} S_{q_i}+\right.\\ &\left.\ddot{q}_i C_{f_i} S_{f_i} C_{q_i}+\dot{q}_i\dot{f}_i C_{q_i}\left(C_{f_i}^2-S_{f_i}^2\right)-\dot{q}_i^2 C_{f_i} S_{f_i} S_{q_i}\right]+\\ &I_{zz_i}\left[\ddot{y}_i C_{f_i}^2 C_{q_i}^2-2\dot{y}_i\dot{f}_i C_{f_i} S_{f_i} C_{q_i}^2-2\dot{y}_i\dot{q}_i C_{f_i}^2 C_{q_i} S_{q_i}-\right.\\ &\left.\ddot{q}_i C_{f_i} S_{f_i} C_{q_i}-\dot{q}_i\dot{f}_i C_{q_i}\left(C_{f_i}^2-S_{f_i}^2\right)+\dot{q}_i^2 C_{f_i} S_{f_i} S_{q_i}\right]+\\ &I_{xz_i}\left[\ddot{f}_i C_{f_i} C_{q_i}-\dot{f}_i^2 S_{f_i} C_{q_i}+\ddot{q}_i S_{f_i} S_{q_i}+\dot{q}_i^2 S_{f_i} C_{q_i}-\right.\\ &\left.2\ddot{y}_i C_{f_i} C_{q_i} S_{q_i}+2\dot{y}_i\dot{f}_i S_{f_i} C_{q_i} S_{q_i}-2\dot{y}_i\dot{q}_i C_{f_i}\left(C_{q_i}^2-S_{q_i}^2\right)\right]\end{aligned} \tag{3.82}$$

The left hand side of Lagrange's equations for the heading generalized coordinates is equal to equation 3.82 since the rotational kinetic energy equation is not a function of heading angle.

$$\begin{aligned}\frac{d}{dt}\left(\frac{\partial T_{rot}}{\partial \dot{y}_i}\right)-\frac{\partial T_{rot}}{\partial y_i}=&\\ &I_{xx_i}\left(\ddot{y}_i S_{q_i}^2+2\dot{y}_i\dot{q}_i C_{q_i}S_{q_i}-\ddot{f}_i S_{q_i}-\dot{f}_i\dot{q}_i C_{q_i}\right)+\\ &I_{yy_i}\left[\ddot{y}_i S_{f_i}^2 C_{q_i}^2+2\dot{y}_i\dot{f}_i C_{f_i}S_{f_i}C_{q_i}^2-2\dot{y}_i\dot{q}_i S_{f_i}^2 C_{q_i}S_{q_i}+\right.\\ &\qquad\left.\ddot{q}_i C_{f_i}S_{f_i}C_{q_i}+\dot{q}_i\dot{f}_i C_{q_i}\left(C_{f_i}^2-S_{f_i}^2\right)-\dot{q}_i^2 C_{f_i}S_{f_i}S_{q_i}\right]+\\ &I_{zz_i}\left[\ddot{y}_i C_{f_i}^2 C_{q_i}^2-2\dot{y}_i\dot{f}_i C_{f_i}S_{f_i}C_{q_i}^2-2\dot{y}_i\dot{q}_i C_{f_i}^2 C_{q_i}S_{q_i}-\right.\\ &\qquad\left.\ddot{q}_i C_{f_i}S_{f_i}C_{q_i}-\dot{q}_i\dot{f}_i C_{q_i}\left(C_{f_i}^2-S_{f_i}^2\right)+\dot{q}_i^2 C_{f_i}S_{f_i}S_{q_i}\right]+\\ &I_{xz_i}\left[\ddot{f}_i C_{f_i}C_{q_i}-\dot{f}_i^2 S_{f_i}C_{q_i}+\ddot{q}_i S_{f_i}S_{q_i}+\dot{q}_i^2 S_{f_i}C_{q_i}-\right.\\ &\qquad\left.2\ddot{y}_i C_{f_i}C_{q_i}S_{q_i}+2\dot{y}_i\dot{f}_i S_{f_i}C_{q_i}S_{q_i}-2\dot{y}_i\dot{q}_i C_{f_i}\left(C_{q_i}^2-S_{q_i}^2\right)\right]\\ &\qquad\qquad for\quad (i=1,2,\ldots n+1)\end{aligned} \tag{3.83}$$

3.3.2.4 Rotational Equations of Motion

The results of the previous three sections produce the rigid body rotational equations of motion for the n+1 segments of the cable and ATV system. The set of differential equations is best illustrated in matrix form, as follows,

$$\begin{bmatrix} A_{rot_1} & A_{rot_2} & A_{rot_3}\\ A_{rot_4} & A_{rot_5} & A_{rot_6}\\ A_{rot_7} & A_{rot_8} & A_{rot_9}\end{bmatrix}\begin{bmatrix}\ddot{f}\\ \ddot{q}\\ \ddot{y}\end{bmatrix}+\begin{bmatrix} B_{rot_1} & B_{rot_2} & B_{rot_3}\\ B_{rot_4} & B_{rot_5} & B_{rot_6}\\ B_{rot_7} & B_{rot_8} & B_{rot_9}\end{bmatrix}\begin{bmatrix}\dot{f}^2\\ \dot{q}^2\\ \dot{y}^2\end{bmatrix}+\begin{bmatrix} C_{rot_1} & C_{rot_2} & C_{rot_3}\\ C_{rot_4} & C_{rot_5} & C_{rot_6}\\ C_{rot_7} & C_{rot_8} & C_{rot_9}\end{bmatrix}\begin{bmatrix}\dot{f}\dot{q}\\ \dot{q}\dot{y}\\ \dot{y}\dot{f}\end{bmatrix} \tag{3.84}$$

Where, A_{rot}, B_{rot}, and C_{rot} are augmented rotational coefficients matrices of size n+1 by n+1. These matrices are purely diagonal due to the fact that the angular velocity of one

segment is independent of all other segments. The following equations represents the diagonal terms of the coefficients matrices for $i = 1 \ldots n+1$,

$$A_{rot_{1_{i,i}}} = I_{xx_i} \tag{3.85}$$

$$A_{rot_{2_{i,i}}} = -I_{xz_i} S_{f_i} \tag{3.86}$$

$$A_{rot_{3_{i,i}}} = -I_{xx_i} S_{q_i} + I_{xz_i} C_{q_i} C_{f_i} \tag{3.87}$$

$$A_{rot_4} = A_{rot_2} \tag{3.88}$$

$$A_{rot_{5_{i,i}}} = I_{yy_i} C_{f_i}^2 + I_{zz_i} S_{f_i}^2 \tag{3.89}$$

$$A_{rot_{6_{i,j}}} = \left(I_{yy_i} - I_{zz_i}\right) C_{f_i} S_{f_i} C_{q_i} + I_{xz_i} S_{f_i} S_{q_i} \tag{3.90}$$

$$A_{rot_7} = A_{rot_3} \tag{3.91}$$

$$A_{rot_8} = A_{rot_6} \tag{3.92}$$

$$A_{rot_{9_{i,j}}} = I_{xx_i} S_{q_i}^2 + \left(I_{yy_i} S_{f_i}^2 - I_{zz_i} C_{f_i}^2\right) C_{q_i}^2 - 2 I_{xz_i} C_{f_i} C_{q_i} S_{q_i} \tag{3.93}$$

$$B_{rot_1} = 0 \tag{3.94}$$

$$B_{rot_{2_{i,j}}} = \left(I_{yy_i} - I_{zz_i}\right) C_{f_i} S_{f_i} \tag{3.95}$$

$$B_{rot_{3_{i,i}}} = \left(I_{zz_i} - I_{yy_i}\right) C_{f_i} S_{f_i} C_{q_i}^2 - I_{xz_i} C_{f_i} \tag{3.96}$$

$$B_{rot_{4_{i,j}}} = -I_{xz_i} C_{f_i} \tag{3.97}$$

$$B_{rot_5} = 0 \tag{3.98}$$

$$B_{rot_{6_{i,j}}} = \left(-I_{xx_i} + I_{yy_i} S_{f_i}^2 - I_{zz_i} C_{f_i}^2\right) C_{q_i} S_{q_i} + I_{xz_i} C_{f_i} C_{2q_i} \tag{3.99}$$

$$B_{rot_{7_{i,j}}} = I_{xz_i} S_{f_i} C_{q_i} \tag{3.100}$$

$$B_{rot_{8_{i,i}}} = \left(I_{zz_i} - I_{yy_i}\right) C_{f_i} S_{f_i} S_{q_i} + I_{xz_i} S_{f_i} C_{q_i} \tag{3.101}$$

$$B_{rot_9} = 0 \tag{3.102}$$

$$C_{rot_1} = 0 \tag{3.103}$$

$$C_{rot_{2_{i,i}}} = \left(-I_{xx_i} - I_{yy_i} C_{2f_i} + I_{zz_i} C_{2f_i}\right) C_{q_i} - 2I_{xz_i} C_{f_i} S_{q_i} \tag{3.104}$$

$$C_{rot_3} = 0 \tag{3.105}$$

$$C_{rot_{4_{i,i}}} = 2\left(I_{zz_i} - I_{yy_i}\right) C_{f_i} S_{f_i} \tag{3.106}$$

$$C_{rot_5} = 0 \tag{3.107}$$

$$C_{rot_{6_{i,i}}} = \left(I_{xx_i} + I_{yy_i} C_{2f_i} - I_{zz_i} C_{2f_i}\right) C_{q_i} + 2I_{xz_i} C_{f_i} S_{q_i} \tag{3.108}$$

$$C_{rot_{7_{i,i}}} = \left(-I_{xx_i} + I_{yy_i} C_{2f_i} - I_{zz_i} C_{2f_i}\right) C_{q_i} \tag{3.109}$$

$$C_{rot_{8_{i,i}}} = 2\left(I_{xx_i} - I_{yy_i} S_{f_i}^2 - I_{zz_i} C_{f_i}^2\right) C_{q_i} S_{q_i} - 2I_{xz_i} C_{f_i} C_{2q_i} \tag{3.110}$$

$$C_{rot_{9_{i,i}}} = 2\left(I_{yy_i} - I_{zz_i}\right)C_{f_i}S_{f_i}C_{q_i}^2 + 2I_{xz_i}S_{f_i}C_{q_i}S_{q_i} \tag{3.111}$$

Note that the rotational equations of motion are about the velocity vector of the generalized coordinates. Recall that the three rotation vectors ($\dot{f}$, $\dot{q}$, and $\dot{y}$) are non-orthogonal and order dependant. A transformation can be applied to the derived rotation equations of motion in order to get the three non-orthogonal equations about an orthogonal rotational system. The transformation is as follows,

$$\begin{bmatrix} M_x \\ M_y \\ M_z \end{bmatrix} = \begin{bmatrix} 1 & 0 & 0 \\ S_f T_q & C_f & S_f / C_q \\ C_f T_q & -S_f & C_f / C_q \end{bmatrix} \begin{bmatrix} M_f \\ M_q \\ M_y \end{bmatrix} \tag{3.112}$$

Being that the coefficient matrices of equation 3.84 are diagonal the system rotation equations are uncoupled, thus there are *n*+1 independent equations. Imagine there is only one body and its rotational equations of motion are represented by equation 3.84 in response to the moments $M_{\dot{f}}$, $M_{\dot{q}}$, and $M_{\dot{y}}$. The rigid body rotational equations of motion in Cartesian coordinates can be attained by applying the transformation of equation 3.112 to the rigid body rotation equations. Simplifying the result using equation 3.64 produces in the following rotation equations in Cartesian coordinates,

$$\begin{aligned} I_{xx}\dot{w}_x + w_y w_z\left(I_z - I_y\right) + I_{xz}\left(\dot{w}_z + w_x w_y\right) &= M_x \\ I_{yy}\dot{w}_y + w_z w_y\left(I_x - I_z\right) + I_{xz}\left(w_z^2 - w_x^2\right) &= M_y \\ I_{zz}\dot{w}_z + w_x w_y\left(I_y - I_x\right) + I_{xz}\left(\dot{w}_x - w_y w_z\right) &= M_z \end{aligned} \tag{3.113}$$

Equation 3.113 is equal to the rotational equations of motion for a rigid body as derived by Newton's laws. The Cartesian coordinate rigid body rotation equations

cannot be used directly as the equations of motion for nodal translation are also about the Euler angular velocity vectors. The transformation only serves to validate the derived rotational equations of motion.

The complete set of equations of motion for the segments in the cable-ATV system are presented in two parts, translation and rotation of the center of mass of the segments. The translational and rotational equations of motion for each segment are represented by equation 3.31 and 3.84, respectively. Thus, the complete equations of motion for the segments are obtained simply by combining the two equations. This is accomplished simply by superimposing the rotational matrices, equation 3.85-111, onto the translational matrices, equation 3.32-58. For example, matrix A_1 is now of the form,

$$A_{1_{i,j}} = A_{rot_1} d_{i,j} + \underline{m}_{i,j} l_i l_j \left[C_{y_j - y_i} \left(S_{f_i} S_{f_j} S_{q_i} S_{q_j} + C_{f_i} C_{f_j} \right) + S_{y_j - y_i} \left(C_{f_i} S_{f_j} S_{q_j} - S_{f_i} C_{f_j} S_{q_i} \right) + S_{f_i} S_{f_j} C_{q_i} C_{q_j} \right] \quad (3.114)$$
$$for \quad (i = 1,2,\ldots,n+1)$$

Where, the kronecker delta insures that the rotational coefficient is applied on the diagonal of the matrix.

The rotational equations of motion apply to each of the segments in the system. However, in the current configuration the only segment that has a nonzero inertia is the ATV segment, $i = n+1$. As a result, the values of the rotational coefficients for the cable segment will be trivial (this is not be the case for a system in which the cable segment model has a distributed mass).

The n+1 row of the augmented matrices represents the ATV dynamic effect of the motion of each cable segment on the ATV segment, and the n+1 column of the augmented matrices represents the dynamic effect of the ATV segment on the motion of each of the cable segments. The nonlinear system equations of motion can be solved simultaneously for the angular acceleration of each segment given that the initial conditions, such as the Euler angles, Euler rates, and generalized forces are known. The generalized force equations for each segment are dependant upon the applied forces on the segment. Thus the evaluation of the aerodynamic forces and moments is needed to produce a realistic simulation of the system.

3.3.3 Generalized Forces

Being that the ATV is modeled in the same fashion as the cable segments the generalized force equations are the same as those of the cable segments, equations 3.20, 3.25, and 3.30. There is, however, a difference in the model for the applied forces and moments between the two types of segments. The calculation of the Aerodynamic forces and moments on the ATV are accomplished using linearized small-disturbance theory, Nelson[14]; where in, the aerodynamic forces and moments are calculated based upon the aircraft reference flight conditions and the small deviations about the reference condition. The aircraft aerodynamics are represented by stability derivatives that approximate the affects of the deviations from the reference flight condition due to various parameters such as perturbation velocities and angular rate of rotation. The aircraft fixed frame equations for the aerodynamic forces, F_{XATV}, F_{YATV}, and F_{ZATV}, and moments, L, M, and N, are as follows,

$$
\begin{aligned}
F_{XATV} &= X_0 + m\left(X_u u + X_w w\right) \\
F_{YATV} &= Y_0 + m\left(Y_v v + Y_p p + Y_r r\right) \\
F_{ZATV} &= Z_0 + m\left(Z_u u + Z_w w + Z_{\dot{w}} \dot{w} + Z_q q\right) \\
L &= L_0 + I_X \left(L_v v + L_p p + L_r r\right) \\
M &= M_0 + I_Y \left(M_u u + M_w w + M_{\dot{w}} \dot{w} + M_q q\right) \\
N &= N_0 + I_Z \left(N_v v + N_p p + N_r r\right)
\end{aligned}
\tag{3.115}
$$

where, m is mass, I_X, I_Y, and I_Z are mass moment of inertia, and X_u, X_w,…, N_r are the stability derivatives of the aircraft. The perturbation velocities u, v, and w are the velocity difference between the ATV and reference freestream,

$$
\begin{bmatrix} u \\ v \\ w \end{bmatrix} = \left[\underline{\underline{C_g}}\right]^T \left[\underline{\underline{C_{f,q,y_{n+1}}}}\right]^T \begin{bmatrix} U_0 + \dot{X}_{n+1} \\ V_0 + \dot{Y}_{n+1} \\ W_0 + \dot{Z}_{n+1} \end{bmatrix} - \begin{bmatrix} U_0 \\ V_0 \\ W_0 \end{bmatrix} \tag{3.116}
$$

The angular rotation rates of the aircraft p, q, and r, are about the orthogonal aircraft fixed frame,

$$
\begin{bmatrix} p \\ q \\ r \end{bmatrix} = \left[\underline{\underline{C_g}}\right]^T \begin{bmatrix} w_{x_{n+1}} \\ w_{y_{n+1}} \\ w_{z_{n+1}} \end{bmatrix} = \left[\underline{\underline{C_g}}\right]^T \begin{bmatrix} \dot{f}_{n+1} - \dot{y}_{n+1} S_{q_{n+1}} \\ \dot{q}_{n+1} C_{f_{n+1}} + \dot{y}_{n+1} C_{q_{n+1}} S_{f_{n+1}} \\ -\dot{q}_{n+1} S_{f_{n+1}} + \dot{y}_{n+1} C_{q_{n+1}} C_{f_{n+1}} \end{bmatrix} \tag{3.117}
$$

Note that the aerodynamic moments of equation 3.115 are about the orthogonal ATV fixed frame, yet the moments in the generalized force equations are in the non-orthogonal generalized coordinate system. Therefore, the aerodynamic moments must be calculated and then translated into the proper frame prior to the implementation of the generalized force equations. The first step is to translate the moments in the orthogonal aircraft frame to the orthogonal ATV segment frame,

$$\begin{bmatrix} M_x \\ M_y \\ M_z \end{bmatrix} = \underline{\underline{[C_g]}} \begin{bmatrix} L \\ M \\ N \end{bmatrix} \tag{3.118}$$

Next, the translation matrix in equation 3.112 configures the aerodynamic moments into the proper non-orthogonal generalized coordinate system,

$$\begin{aligned} \begin{bmatrix} M_f \\ M_q \\ M_y \end{bmatrix} &= \begin{bmatrix} 1 & 0 & 0 \\ S_f T_q & C_f & S_f / C_q \\ C_f T_q & -S_f & C_f / C_q \end{bmatrix}^{-1} \begin{bmatrix} M_x \\ M_y \\ M_z \end{bmatrix} \\ &= \begin{bmatrix} 1 & 0 & 0 \\ 0 & C_f & -S_f \\ -S_q & S_f C_q & C_f C_q \end{bmatrix} \underline{\underline{[C_g]}} \begin{bmatrix} L \\ M \\ N \end{bmatrix} \end{aligned} \tag{3.119}$$

At this point the aerodynamic forces and moments can be correctly applied to the derived generalized force equations, and the simulation of the cable-ATV system is attainable.

Using small disturbance theory to model the aerodynamics of the ATV allows for the simulation of the cable-tow system for an array of towed aircraft. The aerodynamics of the ATV due to its size and shape can be quickly quantified and easily applied to the simulation without having to rederive the equations of motion.

3.4 Host Vehicle

As with the two-dimensional case, the assumption is made that the host aircraft is much greater in size than the ATV. As a result, the forces produce from the motion of the cable and ATV will be insignificant in comparison to the aerodynamic and thrust

forces of the host aircraft. That is not to say that the host vehicle dynamics are inconsequential. It is likely that the autopilot of the host aircraft will not be perfect and that disturbances in the flow will cause oscillations of the vehicle, which will, in turn, affect the motion of the cable and ATV. As a result, the motion of the host aircraft can be viewed as the movement of the host-cable attachment point.

3.4.1 Coordinate System

The movement of the host aircraft complicates the spatial definition of the system. Introducing the host vehicle coordinate system aids in the system evaluation. The host vehicle coordinate system is purely translational, its origin is at the host-cable connection point, and it is parallel to the inertial coordinate system. In the previous sections of this chapter the inertial and host vehicle coordinate systems have been coincident.

The *x*, *y*, and *z*-axes of the host frame are denoted by X', Y', and Z'. The node position for the i^{th} segment in the host frame is as follows,

$$\begin{bmatrix} X_i' \\ Y_i' \\ Z_i' \end{bmatrix} = \sum_{j=1}^{i} \left[\underline{\underline{C_{f_j q_j y_j}}} \right] \begin{bmatrix} 0 \\ 0 \\ l_j \end{bmatrix} \tag{3.120}$$

The position of the origin of the host frame in the inertial coordinate system is denoted by $\underline{x}$, $\underline{y}$, and $\underline{z}$. As a result, the equation for the node position of the i^{th} segment in the inertial frame can be rewritten as follows,

$$\begin{bmatrix} X_i \\ Y_i \\ Z_i \end{bmatrix} = \begin{bmatrix} \underline{x} \\ \underline{y} \\ \underline{z} \end{bmatrix} + \begin{bmatrix} X_i' \\ Y_i' \\ Z_i' \end{bmatrix} = \begin{bmatrix} \underline{x} \\ \underline{y} \\ \underline{z} \end{bmatrix} + \sum_{j=1}^{i} \left[\underline{\underline{C}}_{f_j, q_j, y_j} \right] \begin{bmatrix} 0 \\ 0 \\ l_j \end{bmatrix} \tag{3.120}$$

3.4.2 Lagrange Equations

The motion of the host vehicle can be made arbitrarily. For example, the *x*, *y*, and *z* components of velocity and acceleration of the host vehicle can be set as a harmonic function that represents a particular aircraft's longitudinal and lateral dynamics. It can also be set to model aircraft maneuvers such as coordinated turns or altitude changes.

The motion of the host aircraft alters the translational kinetic energy of the system as derived in equation 3.15. Therefore, the effect of the connecting point movement on the cable and ATV equations of motion is determined by deriving Lagrange's equations for the appropriate kinetic energy equation.

The kinetic energy equation is derived by first calculating the velocity of each segment in the inertial frame, as in the previous sections,

$$\begin{bmatrix} \dot{X}_i \\ \dot{Y}_i \\ \dot{Z}_i \end{bmatrix} = \begin{bmatrix} \dot{\underline{x}} \\ \dot{\underline{y}} \\ \dot{\underline{z}} \end{bmatrix} + \begin{bmatrix} \dot{X}_i' \\ \dot{Y}_i' \\ \dot{Z}_i' \end{bmatrix} \tag{3.121}$$

To calculate the translational kinetic energy the square of velocity must first be calculated.

$$V_k^2 = \left(\dot{X}_k^2 + \dot{Y}_k^2 + \dot{Z}_k^2\right) = \underline{\dot{x}}^2 + 2\underline{\dot{x}}\dot{X}_k' + \dot{X}_k'^2 + \underline{\dot{y}}^2 + 2\underline{\dot{y}}\dot{Y}_k' + \dot{Y}_k'^2 + \underline{\dot{z}}^2 + 2\underline{\dot{z}}\dot{Z}_k' + \dot{Z}_k'^2 \tag{3.122}$$

The kinetic energy of the system is made up of rotational and translational kinetic energy. The rotational kinetic energy equation remains unaffected by the translation of the host frame, and therefore will not be rederived. The kinetic energy equation for the system is as follows,

$$\begin{aligned} T &= T_{rot} + \frac{1}{2}\sum_{k=1}^{n} m_k V_k^2 = \\ T &= T_{rot} + \frac{1}{2}\sum_{k=1}^{n} m_k \left(\underline{\dot{x}}^2 + \underline{\dot{y}}^2 + \underline{\dot{z}}^2 + 2\underline{\dot{x}}\dot{X}_k' + 2\underline{\dot{y}}\dot{Y}_k' + 2\underline{\dot{z}}\dot{Z}_k'\right) + \\ &\quad \frac{1}{2}\sum_{k=1}^{n} m_k \left(\dot{X}_k'^2 + \dot{Y}_k'^2 + \dot{Z}_k'^2\right) \\ T &= T_{rot} + T_{host} + T_{seg} \end{aligned} \tag{3.123}$$

where, T_{seg} and T_{host} are the kinetic energy due to the translation of the rotation segments and the kinetic energy due to the translation of the host vehicle, respectively. Note that T_{seg} is equivalent to the translational kinetic energy of sections 3.2 and 3.3 when the inertial and host frame were coincident. The equations of motion of the aerial tow system can be found by applying Lagrange's equations to the total system kinetic energy or the superposition of Lagrange's equations applied to each of the kinetic energy term,

$$\begin{aligned} &\frac{d}{dt}\left[\frac{\partial\left(T_{rot} + T_{host} + T_{seg}\right)}{\partial\dot{q}_i}\right] - \frac{\partial\left(T_{rot} + T_{host} + T_{seg}\right)}{\partial q_i} = Q_i \\ &\frac{d}{dt}\left(\frac{\partial T_{host}}{\partial\dot{q}_i}\right) - \frac{\partial T_{host}}{\partial q_i} + \frac{d}{dt}\left(\frac{\partial\left(T_{seg} + T_{rot}\right)}{\partial\dot{q}_i}\right) - \frac{\partial\left(T_{seg} + T_{rot}\right)}{\partial q_i} = Q_i \\ &\qquad\qquad\qquad\qquad\qquad\qquad\qquad\qquad\qquad\qquad\qquad\qquad for \quad \left[i = 1,2,\ldots,3(n+1)\right] \end{aligned} \tag{3.124}$$

The derivation of the equations of motion due to T_{seg} and T_{rot} has been accomplished in previous sections. Therefore, the only remaining derivation is that of Lagrange's equations with respect to T_{host}. The equations of motion for the host-cable-ATV system are produced by the superposition of the results of Lagrange's equations for each of the kinetic energies.

The expansion of the kinetic energy due to the host vehicle motion is as follows,

$$\begin{aligned} T_{host} = & \frac{1}{2}\sum_{k=1}^{n+1}\sum_{i=1}^{k} m_k l_i \left\{ \underline{\dot{x}}^2 + \underline{\dot{y}}^2 + \underline{\dot{z}}^2 + \right. \\ & 2\underline{\dot{x}}\left[\dot{f}_i\left(S_{y_i}C_{f_i} - C_{y_i}S_{q_i}S_{f_i}\right) + \dot{q}_i\left(C_{y_i}C_{q_i}C_{f_i}\right) + \dot{y}_i\left(C_{y_i}S_{f_i} - S_{y_i}S_{q_i}C_{f_i}\right)\right] + \\ & 2\underline{\dot{y}}\left[\dot{f}_i\left(-C_{y_i}C_{f_i} - S_{y_i}S_{q_i}S_{f_i}\right) + \dot{q}_i\left(S_{y_i}C_{q_i}C_{f_i}\right) + \dot{y}_i\left(S_{y_i}S_{f_i} + C_{y_i}S_{q_i}C_{f_i}\right)\right] + \\ & \left. 2\underline{\dot{z}}\left[\dot{f}_i\left(-C_{q_i}S_{f_i}\right) + \dot{q}_i\left(-S_{q_i}C_{f_i}\right)\right]\right\} \end{aligned} \tag{3.125}$$

The application of equation 3.125 to Lagrange's equations returns the added effect of the host vehicle motion.

3.4.2.1 Bank Angle

The derivative of kinetic energy, due to host vehicle movement, with respect to bank angle and the time rate of change of bank angle is as follows,

$$\begin{aligned} \frac{\partial T_{host}}{\partial f_i} = & \sum_{k=i}^{n+1} m_k l_i \{ \\ & \underline{\dot{x}}\left[\dot{f}_i\left(-S_{y_i}S_{f_i} - C_{y_i}S_{q_i}C_{f_i}\right) + \dot{q}_i\left(-C_{y_i}C_{q_i}S_{f_i}\right) + \dot{y}_i\left(C_{y_i}C_{f_i} + S_{y_i}S_{q_i}S_{f_i}\right)\right] + \\ & \underline{\dot{y}}\left[\dot{f}_i\left(C_{y_i}S_{f_i} - S_{y_i}S_{q_i}C_{f_i}\right) + \dot{q}_i\left(-S_{y_i}C_{q_i}S_{f_i}\right) + \dot{y}_i\left(S_{y_i}C_{f_i} - C_{y_i}S_{q_i}S_{f_i}\right)\right] + \\ & \underline{\dot{z}}\left[\dot{f}_i\left(-C_{q_i}C_{f_i}\right) + \dot{q}_i\left(S_{q_i}S_{f_i}\right)\right]\} \end{aligned} \tag{3.126}$$

$$\frac{\partial T_{host}}{\partial \dot{f}_i} = \sum_{k=i}^{n+1} m_k l_i \left[\dot{\underline{x}} \left(S_{y_i} C_{f_i} - C_{y_i} S_{q_i} S_{f_i} \right) + \dot{\underline{y}} \left(-C_{y_i} C_{f_i} - S_{y_i} S_{q_i} S_{f_i} \right) + \dot{\underline{z}} \left(-C_{q_i} S_{f_i} \right) \right] \tag{3.127}$$

Time rate of change of equation 3.127 is as follows,

$$\begin{aligned} \frac{d}{dt}\left(\frac{\partial T_{host}}{\partial \dot{f}_i} \right) = \sum_{k=i}^{n+1} m_k l_i \{ & \\ & \ddot{\underline{x}} \left(S_{y_i} C_{f_i} - C_{y_i} S_{q_i} S_{f_i} \right) + \ddot{\underline{y}} \left(-C_{y_i} C_{f_i} - S_{y_i} S_{q_i} S_{f_i} \right) + \ddot{\underline{z}} \left(-C_{q_i} S_{f_i} \right) + \\ & \dot{\underline{x}} \left[\dot{f}_i \left(-S_{y_i} S_{f_i} - C_{y_i} S_{q_i} C_{f_i} \right) + \dot{q}_i \left(-C_{y_i} C_{q_i} S_{f_i} \right) + \dot{y}_i \left(C_{y_i} C_{f_i} + S_{y_i} S_{q_i} S_{f_i} \right) \right] + \\ & \dot{\underline{y}} \left[\dot{f}_i \left(C_{y_i} S_{f_i} - S_{y_i} S_{q_i} C_{f_i} \right) + \dot{q}_i \left(-S_{y_i} C_{q_i} S_{f_i} \right) + \dot{y}_i \left(S_{y_i} C_{f_i} - C_{y_i} S_{q_i} S_{f_i} \right) \right] + \\ & \dot{\underline{z}} \left[\dot{f}_i \left(-C_{q_i} C_{f_i} \right) + \dot{q}_i \left(S_{q_i} S_{f_i} \right) \right] \} \end{aligned} \tag{3.128}$$

The addition to the bank angle translation equations of motion due to the host vehicle translation is as follows,

$$\frac{d}{dt}\left(\frac{\partial T_{host}}{\partial \dot{f}_i} \right) - \frac{\partial T_{host}}{\partial f_i} = \sum_{k=i}^{n+1} m_k l_i \left[\ddot{\underline{x}} \left(S_{y_i} C_{f_i} - C_{y_i} S_{q_i} S_{f_i} \right) + \ddot{\underline{y}} \left(-C_{y_i} C_{f_i} - S_{y_i} S_{q_i} S_{f_i} \right) + \ddot{\underline{z}} \left(-C_{q_i} S_{f_i} \right) \right] \tag{3.129}$$

3.4.2.2 Attitude Angle

The derivative of kinetic energy, due to host vehicle movement, with respect to attitude angle and the time rate of change of attitude angle is as follows,

$$\frac{\partial T_{host}}{\partial q_i} = \sum_{k=i}^{n+1} m_k l_i \Big\{ \underline{\dot{x}}\Big[\dot{f}_i\left(-C_{y_i}C_{q_i}S_{f_i}\right)+\dot{q}_i\left(-C_{y_i}S_{q_i}C_{f_i}\right)+\dot{y}_i\left(-S_{y_i}C_{q_i}C_{f_i}\right)\Big]+ \underline{\dot{y}}\Big[\dot{f}_i\left(-S_{y_i}C_{q_i}S_{f_i}\right)+\dot{q}_i\left(-S_{y_i}S_{q_i}C_{f_i}\right)+\dot{y}_i\left(C_{y_i}C_{q_i}C_{f_i}\right)\Big]+ \underline{\dot{z}}\Big[\dot{f}_i\left(S_{q_i}S_{f_i}\right)+\dot{q}_i\left(-C_{q_i}C_{f_i}\right)\Big]\Big\} \tag{3.130}$$

$$\frac{\partial T_{host}}{\partial \dot{q}_i} = \sum_{k=i}^{n+1} m_k l_i \left[\underline{\dot{x}}\left(C_{y_i}C_{q_i}C_{f_i}\right)+\underline{\dot{y}}\left(S_{y_i}C_{q_i}C_{f_i}\right)+\underline{\dot{z}}\left(-S_{q_i}C_{f_i}\right)\right] \tag{3.131}$$

Time rate of change of equation 3.131 is as follows,

$$\frac{d}{dt}\left(\frac{\partial T_{host}}{\partial \dot{q}_i}\right) = \sum_{k=i}^{n+1} m_k l_i \Big\{ \underline{\ddot{x}}\left(C_{y_i}C_{q_i}C_{f_i}\right)+\underline{\ddot{y}}\left(S_{y_i}C_{q_i}C_{f_i}\right)+\underline{\ddot{z}}\left(-S_{q_i}C_{f_i}\right)+ \underline{\dot{x}}\Big[\dot{f}_i\left(-C_{y_i}C_{q_i}S_{f_i}\right)+\dot{q}_i\left(-C_{y_i}S_{q_i}C_{f_i}\right)+\dot{y}_i\left(-S_{y_i}C_{q_i}C_{f_i}\right)\Big]+ \underline{\dot{y}}\Big[\dot{f}_i\left(-S_{y_i}C_{q_i}S_{f_i}\right)+\dot{q}_i\left(-S_{y_i}S_{q_i}C_{f_i}\right)+\dot{y}_i\left(C_{y_i}C_{q_i}C_{f_i}\right)\Big]+ \underline{\dot{z}}\Big[\dot{f}_i\left(S_{q_i}S_{f_i}\right)+\dot{q}_i\left(-C_{q_i}C_{f_i}\right)\Big]\Big\} \tag{3.132}$$

The addition to the attitude angle translation equations of motion due to the host vehicle dynamics is as follows,

$$\frac{d}{dt}\left(\frac{\partial T_{host}}{\partial \dot{q}_i}\right)-\frac{\partial T_{host}}{\partial q_i} = \sum_{k=i}^{n+1} m_k l_i \left[\underline{\ddot{x}}\left(C_{y_i}C_{q_i}C_{f_i}\right)+\underline{\ddot{y}}\left(S_{y_i}C_{q_i}C_{f_i}\right)+\underline{\ddot{z}}\left(-S_{q_i}C_{f_i}\right)\right] \tag{3.133}$$

3.4.2.3 Heading Angle

The derivative of kinetic energy, due to host vehicle movement, with respect to heading angle and the time rate of change of heading angle is as follows,

$$\frac{\partial T_{host}}{\partial y_i} = \sum_{k=i}^{n+1} m_k l_i \Big\{ \\ \underline{\dot{x}}\Big[\dot{f}_i\left(C_{y_i}C_{f_i} + S_{y_i}S_{q_i}S_{f_i}\right) + \dot{q}_i\left(-S_{y_i}C_{q_i}C_{f_i}\right) + \dot{y}_i\left(-S_{y_i}S_{f_i} - C_{y_i}S_{q_i}C_{f_i}\right)\Big] + \\ \underline{\dot{y}}\Big[\dot{f}_i\left(S_{y_i}C_{f_i} - C_{y_i}S_{q_i}S_{f_i}\right) + \dot{q}_i\left(C_{y_i}C_{q_i}C_{f_i}\right) + \dot{y}_i\left(C_{y_i}S_{f_i} - S_{y_i}S_{q_i}C_{f_i}\right)\Big]\Big\} \quad (3.134)$$

$$\frac{\partial T_{host}}{\partial \dot{y}_i} = \sum_{k=i}^{n+1} m_k l_i \Big[\underline{\dot{x}}\left(C_{y_i}S_{f_i} - S_{y_i}S_{q_i}C_{f_i}\right) + \underline{\dot{y}}\left(S_{y_i}S_{f_i} + C_{y_i}S_{q_i}C_{f_i}\right)\Big] \quad (3.135)$$

Time rate of change of equation 3.135 is as follows,

$$\frac{d}{dt}\left(\frac{\partial T_{host}}{\partial \dot{f}_i}\right) = \sum_{k=i}^{n+1} m_k l_i \Big\{ \\ \underline{\ddot{x}}\left(C_{y_i}S_{f_i} - S_{y_i}S_{q_i}C_{f_i}\right) + \underline{\ddot{y}}\left(S_{y_i}S_{f_i} + C_{y_i}S_{q_i}C_{f_i}\right) + \\ \underline{\dot{x}}\Big[\dot{f}_i\left(C_{y_i}C_{f_i} + S_{y_i}S_{q_i}S_{f_i}\right) + \dot{q}_i\left(-S_{y_i}C_{q_i}C_{f_i}\right) + \dot{y}_i\left(-S_{y_i}S_{f_i} - C_{y_i}S_{q_i}C_{f_i}\right)\Big] + \\ \underline{\dot{y}}\Big[\dot{f}_i\left(S_{y_i}C_{f_i} - C_{y_i}S_{q_i}S_{f_i}\right) + \dot{q}_i\left(C_{y_i}C_{q_i}C_{f_i}\right) + \dot{y}_i\left(C_{y_i}S_{f_i} - S_{y_i}S_{q_i}C_{f_i}\right)\Big]\Big\} \quad (3.136)$$

Finally, the addition to the heading angle translation equations of motion due to the host vehicle dynamics is as follows,

$$\frac{d}{dt}\left(\frac{\partial T_{host}}{\partial \dot{y}_i}\right) - \frac{\partial T_{host}}{\partial y_i} = \sum_{k=i}^{n+1} m_k l_i \Big[\underline{\ddot{x}}\left(C_{y_i}S_{f_i} - S_{y_i}S_{q_i}C_{f_i}\right) + \underline{\ddot{y}}\left(S_{y_i}S_{f_i} + C_{y_i}S_{q_i}C_{f_i}\right)\Big] \quad (3.137)$$

3.4.3 Generalized Forces

The host vehicle motion alters the kinetic energy of the system consisting of just the cable and ATV. This change in kinetic energy adds to the cable-ATV system equations of motion. As with the two-dimensional case, the units of the equations resulting from the application of Lagrange's equations on T_{host}, equations 3.129, 3.133, and 3.137, have units of force times distance and the equations are similar in form to the generalized force

equations, equations 3.20, 3.25, and 3.30. As a result, the effects of the motion of the host vehicle can be thought of as an applied force due to the acceleration of the host vehicle. The resulting equations of motion for the cable and ATV system remain the same in the event the host vehicle moves the only change is in the generalized force equation,

$$\begin{aligned} Q_{f_i} = M_{f_i} + l_i \sum_{j=i}^{n+1} \Big\{ & \left(F_{X_j} - m_j \underline{\ddot{x}}\right)\left(-S_{f_i} S_{q_i} C_{y_i} + C_{f_i} S_{y_i}\right) + \\ & \left(F_{Y_j} - m_j \underline{\ddot{y}}\right)\left(-S_{f_i} S_{q_i} S_{y_i} - C_{f_i} C_{y_i}\right) + \\ & \left[F_{Z_j} + m_j (g - \underline{\ddot{z}})\right]\left(-S_{f_i} C_{q_i}\right) \Big\} \end{aligned} \tag{3.138}$$

$$\begin{aligned} Q_{q_i} = M_{q_i} + l_i \sum_{j=i}^{n+1} \Big\{ & \left(F_{X_j} - m_j \underline{\ddot{x}}\right)\left(C_{f_i} C_{q_i} C_{y_i}\right) + \left(F_{Y_j} - m_j \underline{\ddot{y}}\right)\left(C_{f_i} C_{q_i} S_{y_i}\right) + \\ & \left[F_{Z_j} + m_j (g - \underline{\ddot{z}})\right]\left(-C_{f_i} S_{q_i}\right) \Big\} \end{aligned} \tag{3.139}$$

$$\begin{aligned} Q_{y_i} = M_{y_i} + l_i \sum_{j=i}^{n+1} \Big[& \left(F_{X_j} - m_j \underline{\ddot{x}}\right)\left(-C_{f_i} S_{q_i} S_{y_i} + S_{f_i} C_{y_i}\right) + \\ & \left(F_{Y_j} - m_j \underline{\ddot{y}}\right)\left(C_{f_i} S_{q_i} C_{y_i} + S_{f_i} S_{y_i}\right) \Big] \end{aligned} \tag{3.140}$$

The motion of the host vehicle has no affect on the *A*, *B*, or *C* coefficient matrix in equation 3.28. The direct results of the derivation show that the moving host frame produces applied loads on each segment node proportional to the host vehicle acceleration. The indirect effect of the host vehicle motion is the added segment velocity which affects the applied aerodynamic forces and moments of the segment. Note that the derivation due to the host vehicle motion is independent of the functions used to model it, i.e. the displacement functions can be arbitrarily chosen to represent any number of host vehicle maneuvers.

At this point, the equations of motion for the three-dimensional aerial tow system are complete, and given a proper numerical integration program with a set of valid initial conditions a simulation of the three-dimensional aerial tow system can be accomplished. The simulation can be created for many freestream conditions and host vehicle maneuvers.

3.5 System Equations of Motion of an Alternate Segment Model

The equations of motion derived throughout this chapter up to now have been done so using the lumped mass segment model. It has been made clear in section 2.5 that the lumped mass model is a poor model when the number of segments is small, and it has been suggested that a better model for the segments would be the thin rod model. The thin rod model has its center of mass at mid-length and, unlike the lumped mass model, it has rotational inertia.

The equations of motion of the system for the thin rod segment model can be derived using Lagrange's equations, in the same fashion as that of the lumped mass segment model. Upon completing the derivation of the equations of motion one will find that equation 3.31 still holds true, recall equation 3.31,

$$\begin{bmatrix} A_1 & A_2 & A_3 \\ A_4 & A_5 & A_6 \\ A_7 & A_8 & A_9 \end{bmatrix} \begin{bmatrix} \ddot{f} \\ \ddot{q} \\ \ddot{y} \end{bmatrix} + \begin{bmatrix} B_1 & B_2 & B_3 \\ B_4 & B_5 & B_6 \\ B_7 & B_8 & B_9 \end{bmatrix} \begin{bmatrix} \dot{f}^2 \\ \dot{q}^2 \\ \dot{y}^2 \end{bmatrix} + \begin{bmatrix} C_1 & C_2 & C_3 \\ C_4 & C_5 & C_6 \\ C_7 & C_8 & C_9 \end{bmatrix} \begin{bmatrix} \dot{f}\dot{q} \\ \dot{q}\dot{y} \\ \dot{y}\dot{f} \end{bmatrix} = \begin{bmatrix} Q_f \\ Q_q \\ Q_y \end{bmatrix}$$

And just as in the two-dimensional case only the mass distribution of the coefficient matrices *A*, *B*, and *C* and the lever arm of the generalized force equations will differ from the equations derived for the lumped mass segment model.

The mass distribution of the coefficient matrices for the lumped mass model is given in equation 2.33 and the mass distribution for the thin rod model is given in 2.68, recall equation 2.68,

$$\underline{m}_{i,j} = -m_{\max(i,j)}\left(\frac{1}{2}+\frac{d_{i,j}}{4}\right)+\sum_{k=\max(i,j)}^{n+1} m_k$$

This remains the same for the two and three-dimensional case.

The generalized force equations are only slightly altered due to the fact that the inertial and applied forces on a segment are located at the segment's center of mass. Thus, the lever arm of the applied and inertial forces of the i^{th} segment is half the segment length.

$$\begin{aligned} Q_{f_i} = M_{f_i} + l_i \sum_{j=i}^{n+1} \Big\{ & \Big(F_{X_j} - m_j \underline{\ddot{x}}\Big)\Big(-S_{f_i} S_{q_i} C_{y_i} + C_{f_i} S_{y_i}\Big) + \\ & \Big(F_{Y_j} - m_j \underline{\ddot{y}}\Big)\Big(-S_{f_i} S_{q_i} S_{y_i} - C_{f_i} C_{y_i}\Big) + \\ & \Big[F_{Z_j} + m_j (g - \underline{\ddot{z}})\Big]\Big(-S_{f_i} C_{q_i}\Big)\Big\}\left(1-\frac{d_{i,j}}{2}\right) \end{aligned} \tag{3.141}$$

$$\begin{aligned} Q_{q_i} = M_{q_i} + l_i \sum_{j=i}^{n+1} \Big\{ & \Big(F_{X_j} - m_j \underline{\ddot{x}}\Big)\Big(C_{f_i} C_{q_i} C_{y_i}\Big) + \Big(F_{Y_j} - m_j \underline{\ddot{y}}\Big)\Big(C_{f_i} C_{q_i} S_{y_i}\Big) + \\ & \Big[F_{Z_j} + m_j (g - \underline{\ddot{x}})\Big]\Big(-C_{f_i} S_{q_i}\Big)\Big\}\left(1-\frac{d_{i,j}}{2}\right) \end{aligned} \tag{3.142}$$

$$\begin{aligned} Q_{y_i} = M_{y_i} + l_i \sum_{j=i}^{n+1} \Big[& \Big(F_{X_j} - m_j \underline{\ddot{x}}\Big)\Big(-C_{f_i} S_{q_i} S_{y_i} + S_{f_i} C_{y_i}\Big) + \\ & \Big(F_{Y_j} - m_j \underline{\ddot{y}}\Big)\Big(C_{f_i} S_{q_i} C_{y_i} + S_{f_i} S_{y_i}\Big)\Big]\left(1-\frac{d_{i,j}}{2}\right) \end{aligned} \tag{3.143}$$

Note, for equations 3.141 – 3.143 to be accurate for the ATV segment the ATV center of mass must coincide with the center of mass of the segment model.

The three-dimensional system equations of motion with the thin rod segment model can be attained by applying equations 3.32-3.58, 3.85-3.111, 3.141-3.143, and 2.68 with equation 3.31. Given proper initial conditions and an adequate numerical integration routine a simulation of the three-dimensional aerial towed system with the thin rod segment model can be produced. A comparison between the simulation results of the lumped mass and thin rod segment modeled systems with the same initial conditions will be analyzed in chapter five.

CHAPTER 4

FLIGHT PARAMETERS

4.1 Introduction

The driving force behind this work is the analysis of an aerial tow system in which the ATV is towed near the ocean surface. The derived equations of motion are general and would apply to a wide range of aerial tow systems. The parameters of the system that make it unique to the low altitude tow system are the length of separation between the host aircraft, the size, shape, and controllability of the ATV, and the shape of the terrain over which the ATV is being towed.

In order for the ATV to maintain a given height above the ocean surface it is necessary that the ATV be able the ocean waves. This can be accomplished by appropriately changing the applied forces on the aircraft as it cruises. For instance, if the ATV senses that it is flying too low it changes its aerodynamics to apply a vertical force to increase its altitude. This is attained in reality by attaching a radar altimeter and an autopilot to the ATV. A mathematical model of the ATV autopilot and the ocean terrain is necessary to simulate the altitude hold of the ATV above the ocean waves.

4.2 Ocean Surface Waveform

The ATV autopilot attempts to maintain a given altitude above the ocean surface as it is being towed by the host aircraft. A radar altimeter is equipped to the ATV and it measures the distance between the vehicle and the 'ground'. Numerically this distance is the difference between the ATV and a given surface directly below the ATV. The equations for the ATV position in the inertial frame have been derived in the previous sections, thus a model of the ocean is required to produce a mathematical model of the radar altimeter reading.

The shape of the ocean varies widely. It can range from placid to situations where there are swells of fifty feet in height. The shape of the waves depends on many parameters such as ocean current, wind speed, and wave height. As a result, there is no one algorithm that can be used to fit the shape of the ocean surface.

For our simulation we will model the ocean surface as a simple sine wave with variable amplitude and frequency. Therefore, the radar altimeter reading will be a result of the sine wave and the ATV altitude. The sine wave oscillates about some nominal altitude, in our case it is sea level. In the inertia frame sea level is a distance h_n in the z-direction. The vertical position of the wave, h, in the inertial frame is a function of time and inertial x-position, X,

$$h = A_o \sin\left(w_o t + 2pX / l\right) + h_n \tag{4.1}$$

where, A_o is the amplitude of oscillation. The wave frequency, w_0, as seen by the origin of the inertial frame is dependent upon its x-direction flight speed and the ocean wavelength, l, as follows:

$$w_o = U_0 / l \tag{4.2}$$

Note that the velocity of the ocean wave is neglected due to its comparatively small magnitude; however, it could be easily included by adding the wave velocity to the freestream flow, if the conditions deemed it necessary.

The wave model of equation 4.1 is two-dimensionally adequate, i.e. it holds as long as the ATV travels in the inertial xz-plane. If a side gust were to push the ATV in the y-direction this model would not account for transverse changes produced by neighboring waves. A fully three-dimensional waveform model is necessary to accommodate the three-dimensional motion of the ATV.

The transverse waves are modeled as a series of sine waves with the amplitude dictated by the amplitude of the longitudinal ocean wave at the point of intersection between the two waves. The transverse wavelength is assumed to be identical to the lateral wavelength. The resulting model is a surface where the z-position of the surface at any given point is a determined by its x and y-position and time. The wave surface in the inertial coordinated system is as follows:

$$h = A_o \sin\left(w_o t + 2pX / l\right)\sin\left(2p\ Y / l\right) + h_n \tag{4.3}$$

Figure 4.1 shows an isometric view and a contour plot of a general three-dimensional surface waveform.

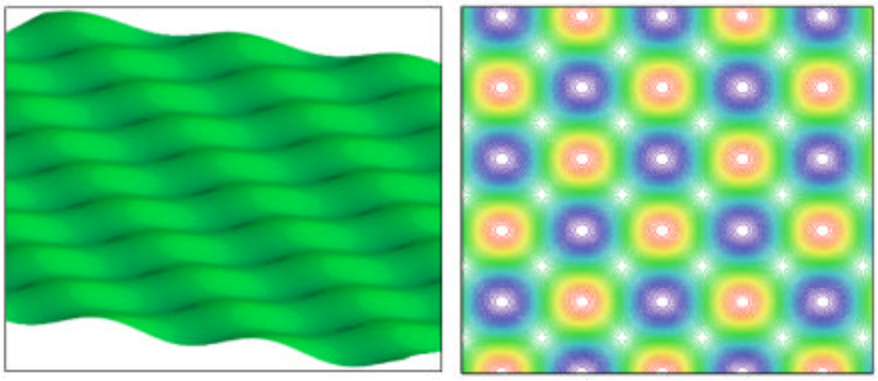

Figure 4.1 Three-dimensional ocean surface waveform

The mathematical model of the ATV radar altimeter reading is determined by the time and three-dimensional position of the ATV,

$$\Delta h = A_o \sin\left(w_o t + 2pX_{ATV}/l\right)\sin\left(2p\,Y_{ATV}/l\right) + h_n - Z_{ATV} \tag{4.4}$$

where, X_{ATV}, Y_{ATV}, and Z_{ATV} are the three-dimensional Cartesian coordinate position of the ATV in the inertial frame.

4.3 ATV Autopilot

For the ATV to track the ocean waves a control system is required. A wide variety of control schemes exist for general aviation aircraft and could be applied to the ATV for academic interest. However, there is no point in simulating an intricate control scheme in which its application is realistically unpractical. Often the ATV is basic in its design and does not possess the control surfaces necessary to equip a complex control system.

The configuration of the ATV used in the given tow system is similar to the towed targets used in weapons testing. As a result, the control system in this aerial tow system is a descendant of those commonly used in aerial tow targets. These aircraft differ from general aviation aircraft in that they have only one control surface, which is an all moving wing. Therefore, the aircraft autopilot corrects the incidence angle of the wing to appropriately adjust the aircraft lift.

A proportional derivative (pd) controller used to determine wing correction. The autopilot receives a signal from the radar altimeter and accelerometer to determine both the error signal (the difference in actual and desired ATV altitude) and time rate of change of the error signal. The given signals allow the autopilot to relay to the wing servo the appropriate wing rotation to minimize the altitude error. The ATV autopilot multiplies the signals by the designed gains to produce the change in wing incidence,

$$\Delta i_w = k_p \Delta h + k_d \Delta \dot{h} \tag{4.5}$$

where, k_p, k_d, and Di_w are the proportional gain, derivative gain, and wing angle correction, respectively. In all the subsequent simulations the control law remains fixed.

CHAPTER 5

SYSTEM SIMULATIONS

5.1 The Ideal Cable

The equations of motion for the two and three-dimensional cable were derived using Lagrange's energy based technique. Neglecting applied forces such as fluid drag the sole factors in the derivation are the potential and kinetic energy of the cable system. This ideal system is conservative. As a result, if the equations of motion are correctly derived and the numerical integration routine is adequate the system should maintain a constant energy during the simulation. Thus an initial test of the cable equations of motion and the numerical simulation can be produced by analyzing the results of the ideal cable system.

Another means of testing the derived equations is the comparison between the two and three-dimensional systems. The three-dimensional cable equations of motion are vastly more complex than that of the two-dimensional cable system. However, both should produce the same results given identical initial conditions. The initial conditions are chosen such that the three-dimensional equations of motion are not trivialized yet the motion is completely contained in one plane.

The initial conditions have each cable segment with the following Euler angles, phi, theta, and psi equal to 30, 55, and 20 degrees, respectively. The dynamics of the cable are a result of the inertial forces of the cable (initially the angular velocities are zero) and given the initial straight cable configuration the cable will move in a planar fashion. Being that the three-dimensional motion is planar it can be compared to the two-dimensional case. The initial cable angles for the two-dimensional system can be calculated such that the center of mass as well as the orientation of each of the segments is equal to that of the three-dimensional case. The three-dimensional initial conditions are match when the angles of the two-dimensional cable segments are set at 60.216 degrees.

If the equations of motion are correctly derived and the numerical integration routine adequate both the two and three-dimensional systems should have a constant energy and produce the same cable orientations over the duration of the simulation. The two and three-dimensional systems discussed are simulated with a 2000 foot cable that is broken into 25 segments. Figure 5.1 shows the simulation results of the two and three-dimensional system with both the lumped mass and thin rod segment model.

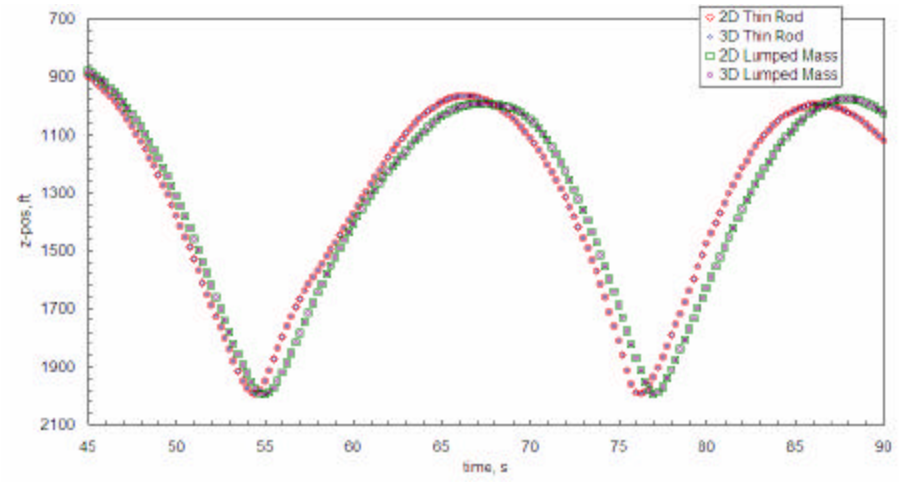

a)

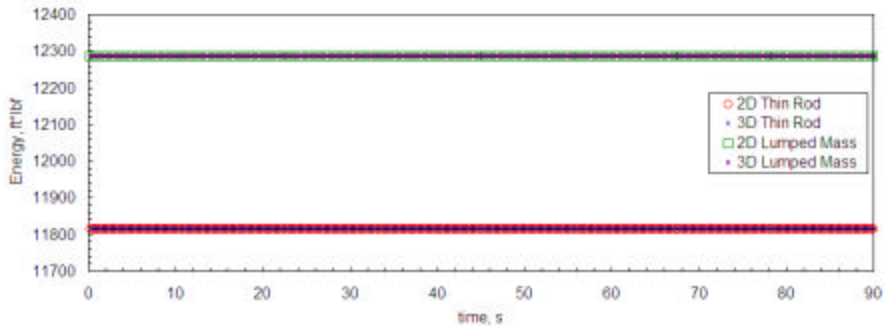

b)

Figure 5.1 Two and Three-dimensional ideal cable simulation results. The figure shows, a) the height of cable base, and b) the system energy versus time.

Figure 5.1a plots the vertical position (in the host vehicle frame) of the free end of the cable with respect to time. Note that the altitude of the free end of the cable is dependent upon the orientation of each of the previous segments. Figures 5.1a and 5.1b confirm that for each configuration the energy remains constant and that the two and three-dimensional systems return exactly the same results in both cable orientation and energy. However, while the two and three-dimensional equations of motion produce the same results the system with the lumped mass segment model and the system with the thin rod segment model do not. Which of the two systems is producing better results?

Recall that the simulations undertaken were modeled by breaking the cable into 25 segments. It is likely that as the cable is broken into more segments the simulation will yield more accurate results. Thus, a convergence test is needed to determine the proper number of segments for each of the segment models that will produce valid results.

5.2 Lumped Mass Versus Thin Rod Cable Model

The number of cable segments used in the ideal cable simulation was chosen arbitrarily. At this point the equations of motion have been derived to accurately predict the dynamics of each segment; however even if the equations of motion are correct that doesn't necessarily mean the system motion will reflect that of a continuous cable. In other words, the number of segments needed to accurately predict the cable motion is unknown. Thus, the segment number convergence test is conducted for both the lumped mass and thin rod cable segment models. The test for convergence begins by running the simulation with 10 segments and comparing the results with a simulation of 25 segments. Additional simulations are run continually increasing the number of cable segments of the system until the results begin to converge. It is then the proper number of segments necessary to model the dynamics of the cable can be determined.

The ideal system is helpful in supporting the validity of the equations of motion but the accuracy of the simulation is of most importance for the aerial towed system flight configuration. As a result, the convergence simulations include the cable friction forces and 100 pound weight which is added to the unfixed cable end to represent the ATV (note that in this simulation does not include the ATV segment or any ATV aerodynamic forces). The cable dimensions and drag coefficients as well as the reference flight

conditions are presented in table 5.1. (Note that at the given reference flight speed and cable diameter the Reynolds number is indeed subcritical.)

Cable Parameters			Reference Conditions		
Diameter	d	0.065 in	Velocity	U_0	100 knots
Mass per unit length		0.00036 slug/ft	Air density	ρ	0.00238 slug/ft^3
Friction coefficient	c_f	0.00573			
Pressure coefficient	c_p	1.1			

Table 5.1 Cable parameters and reference flight conditions

The initial cable configuration has the cable hanging perfectly vertical. It is then introduced to a fluid moving at 100 knots. As time progresses the friction forces exerted on the cable will induce motion, and at some point the inertial forces (including the 100 pound weight) will balance the drag on the cable and the system will reach equilibrium. Figure 5.2 contains the results of the simulations with varying number of cable segments for both the lumped mass and thin rod cable models.

a)

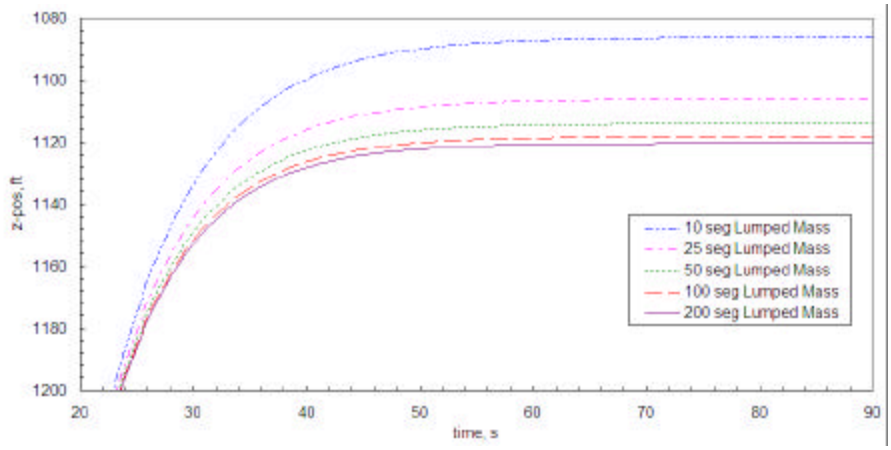

b)

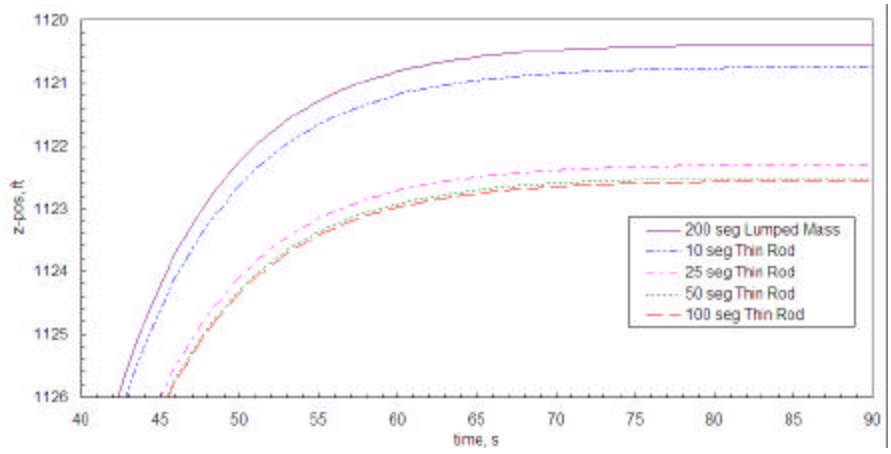

Figure 5.2 A cable in fluid flow simulation results. The cable is broken into various numbers of segments; the segments are modeled as, a) lumped masses, and b) thin rods.

Both systems respond to the aerodynamic drag applied to the cable by the freestream flow. As time increases the systems' dynamics slow and equilibrium is attained. The lumped mass and thin rod models produce different static locations as the number of segments change. The equilibrium positions begin to converge as the number of segments increase. However, the thin rod modeled system seems to be converging much quicker than the lumped mass system. The thin rod system has reached a reasonable convergence in just 25 segments (the altitude difference between the 25 and 100 segment

thin rod modeled system is just 4 inches). While it is apparent that even at 100 segments the lumped mass system has yet to converge.

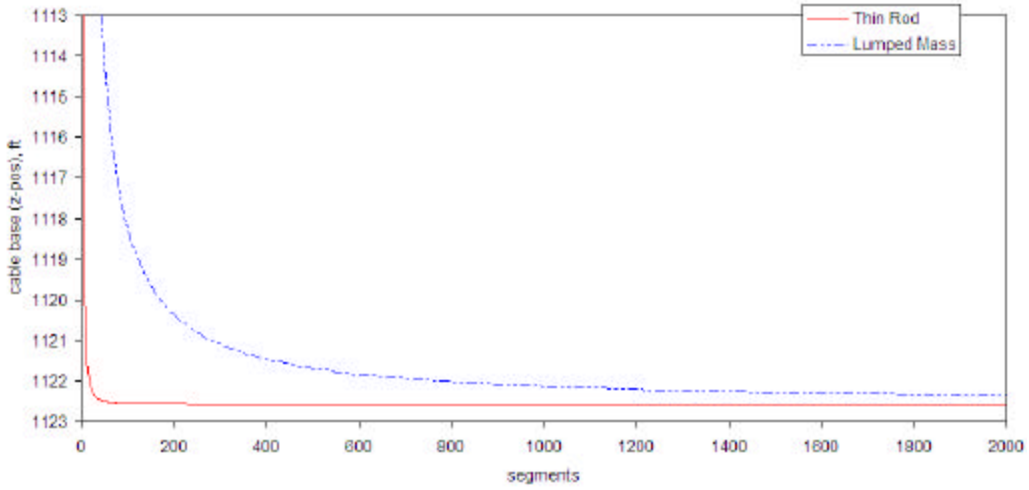

Figure 5.3 Cable base static positions versus number of cable segments

The vertical static position of the cable base is plotted versus number of cable segments for lumped mass and thin rod modeled systems in figure 5.3. It is clear from the figure that the thin rod modeled system converges with fewer segments than lumped mass system. Upon convergence, the simulation results for both cable segment modeled systems are similar, yet the computational workload varies greatly.

Figure 5.2b shows that the system simulation with the thin rod cable model produces slightly better results with 10 segments than with 200 segments of the system with the lumped mass cable model. While both systems produced roughly the same results, the computation time required to produce the 90 second simulation for the system using the lumped mass cable model with 200 segments was more than 35 minutes. On the other hand, the computation time required for the same simulation for the system using the thin

rod cable mode with 10 segments was less than 1 second. The thin rod model has an obvious advantage.

One of the factors attributing to the more accurate results of the thin rod cable model is simply the distribution of the cable mass. The lumped mass method places the all of the segment mass at the segment's end. Clearly a better approach would be to place the segment's mass in the middle of the segment. This is illustrated best by analyzing the potential energy of the cable. Imagine a cable is in the initial condition described in the ideal cable section (each segment is at an angle of 60.216 degrees). For the cable employing the lumped mass model, as the number of segment used to model the cable changes so too does the potential energy of the system. This is due to the mass placement of the lumped mass technique. For the system using the thin rod segment mode the potential energy remains exactly the same no matter how many segments the cable is broke into. Figure 5.4 depicts the potential energy of the static cable as it is broken into a various number of segments.

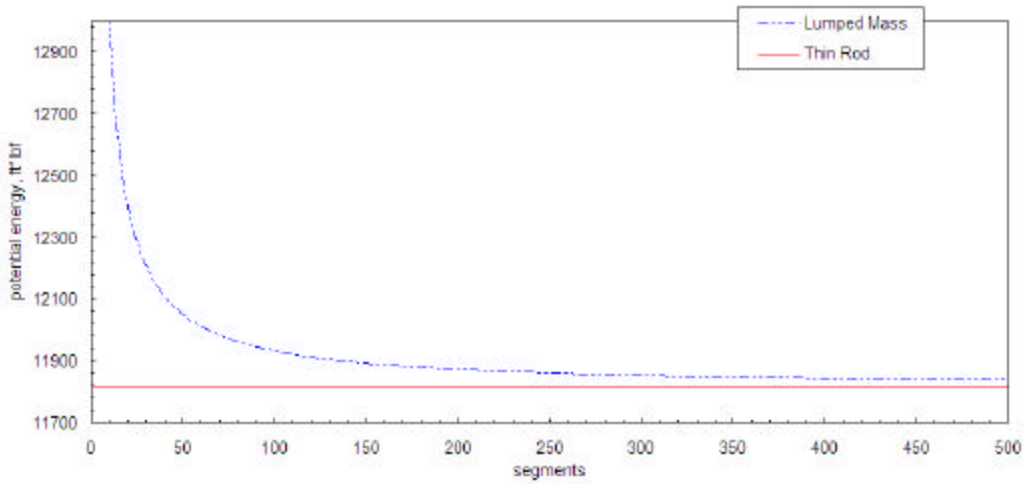

Figure 5.4 Potential energy versus number of cable segments.

As the number of segments increase in the lumped mass model the potential energy approaches that of the thin rod model. The thin rod potential energy is in fact the asymptote of the lumped mass model; the lumped mass model potential energy will never exactly match the potential energy of the thin rod mode but as the number of segments increase it will come ever closer. This illustrates a fundamental flaw in the lumped mass cable segment model.

The thin rod model produces much better results than that of the lumped mass mode simply because it is a better physical model. For the thin rod model the inertial and applied forces are localized at the center of each segment; the velocity of the segment is calculated at the center of the segment producing a more accurate drag prediction; and the thin rod segments have rotational inertial that produces a more realistic dynamic response. As a result, the thin rod segment model can produce a better simulation with fewer cable segments than the system using the lumped mass technique.

5.3 Simulation of the Cable-ATV System

The equations of motion governing the dynamics of the rigid body segments for both the cable and ATV have been derived for the two-dimensional system in chapters 2 and for the three-dimensional system in chapter 3. As discussed in those chapters, the applied forces on the towed aircraft are dictated by the aircraft's size and shape in the form of stability derivatives. The aircraft parameters for the ATV that will be simulated throughout the remainder of the paper are presented in table 5.2.

ATV data					
Moment of Inertia	I_x	0.128 slug ft^2	Fuselage diameter		8 in.
	I_y	6.127 slug ft^2	Mass	m	8.301 slugs
	I_z	6.121 slug ft^2		?	0
Longitudinal			Lateral		
Stability derivatives	X_0	-9.35 lbf	Stability derivatives	Y_β	-55.2 ft s^{-2}
	X_u	-0.054 s^{-1}		Y_p	0
	X_a	0		Y_r	1.742 ft s^{-1}
	Z_u	0		L_β	0
	Z_a	-176.1 ft s^{-2}		L_p	-19.265 s^{-1}
	Z_q	-1.045 ft s^{-1}		L_r	0
	M_u	0		N_β	291.1 s^{-2}
	M_a	-78.1 s^{-2}		N_p	0
	M_q	-1.103 s^{-1}		N_r	-2.414 s^{-1}

Table 5.2 Aerial towed aircraft parameters

5.3.1 Dimensional Comparison

One final test of the governing equations pits the two and three-dimensional full system equations of motion against one another. Just as in the ideal cable comparison the three-dimensional Euler angles of each cable segment are initialized with phi, theta, and psi at 30, 55, and 20 degrees, respectively, and the two-dimensional cable segments each have an angle of 60.216 degrees. The ATV segments in both the two and three-dimensional cases are oriented such that its initial angle of attack of the aircraft is equal to zero. However, to ensure that there is no lateral ATV motion in the three-dimensional case the freestream flow is rotated 20 degrees about the z-axis producing components of flow in the x and y-directions, and the ATV segment is oriented such that the initial sideslip angle is zero. The cable is 2000 feet in length and its remaining parameters are equal to those in table 5.1. The cable is modeled using the thin rod method and it is broken into 25 segments. The results of the simulations are presented in figure 5.5.

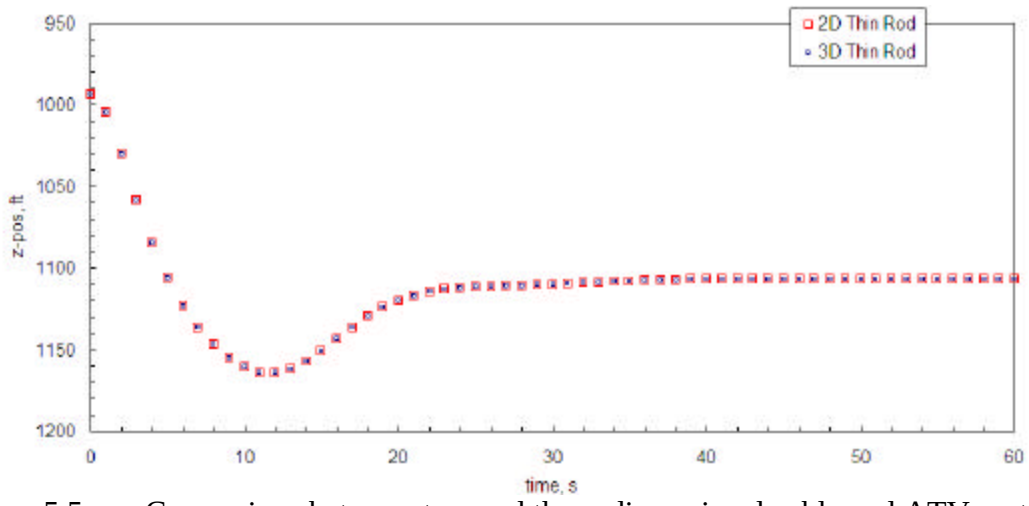

Figure 5.5 Comparison between two and three-dimensional cable and ATV system

Figure 5.5 plots the altitude of the center of mass of the ATV (in the host frame) over time. As time progresses the initially straight cable begins to curve due to the inertial and aerodynamic forces of the ATV and the drag force on each of the cable segments. Eventually the motion of the system dies out and the system finds equilibrium. Throughout the simulation both the two and three-dimensional systems produce exactly the same results.

5.3.2 Altitude Effects

The equilibrium configuration of the aerial tow system is largely dependant upon the length of the cable in the system. The equilibrium orientations of four configurations with varying cable length are presented in figure 5.6. The configurations give the system enough cable to allow the ATV to cruise 250, 500, 1000, and 2000 feet below the host aircraft. From the figure it is evident that the curve of the cable becomes more pronounced as the length of the cable increases, this is due to the fact that there is more cable for the air to act upon the cumulative cable drag arises as the driving force behind the shape of the static configuration.

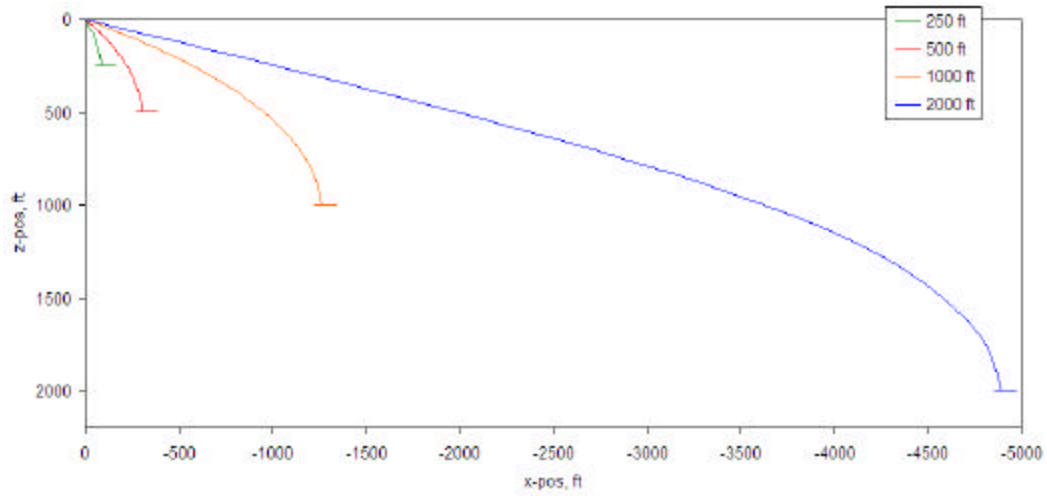

Figure 5.6 Host vehicle cruise altitude affect on static cable curvature and position

With the host vehicle cruising at an altitude of 250 feet the connecting cable is slightly curved. On the other hand when the host vehicle is at 2000 feet the cable is considerably more curved and the ATV cruises well aft of the host aircraft.

The equilibrium position of the system can be easily found by solving for the angles that reduce the generalized force vector to zero, and then conclusions about the effect of the cable length can be surmised. However, to determine the cable's affect on the dynamics of the system a simulations is necessary.

In an effort to test the dynamic motion of the aerially towed system four system configurations are simulated with variation in cable length. These configurations give the system enough cable to allow the ATV to cruise 250, 500, 1000, and 2000 feet below the host aircraft, just as in figure 5.6. The simulation begins with the system in equilibrium. As the simulation progresses the system is excited by the oscillation of the host aircraft. The amplitude and period of oscillation is such that it resembles the long period motion of general aviation aircraft. (This would be the type of oscillation that would be expected

if the host aircraft were disturbed in someway. The amplitude and period of the host vehicle oscillation is 10 feet and 30 seconds, respectively.) During the simulation the natural response of the system is recorded. Figure 5.7 presents the motion of the ATV as well as its static ATV position in the host frame.

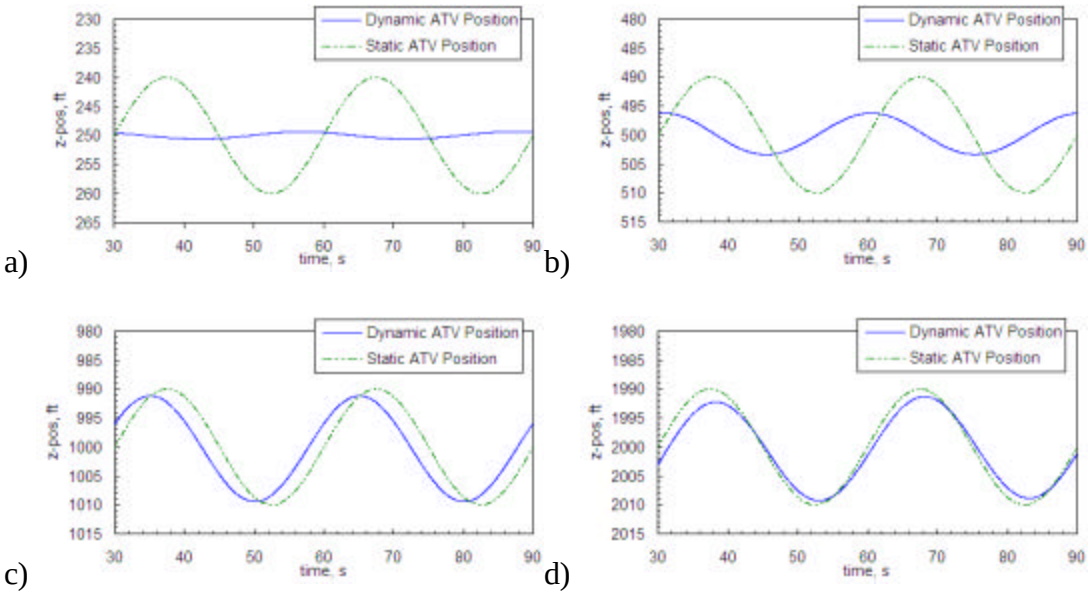

Figure 5.7 Dynamic response to host vehicle oscillation as viewed from the host vehicle coordinate system.

The shortest cable configuration results in the ATV following almost exactly the motion of the host vehicle. The ATV remains roughly 250 feet below the host aircraft at all times. Conversely, the ATV in the longest cable configuration is only slightly disturbed from its static location. Thus, as the cable length increases the response to the host oscillation decreases. The host vehicle displacement is accommodated by the flex of the curved cable; whereas the force of the host vehicle displacement is applied directly to the ATV through the straight cable. The dynamics of the curved cable absorb the motion of the ATV in a manner the straight cable configuration cannot.

The flex of the cable has an interesting effect on the horizontal motion of the ATV. Figure 5.8 traces out the path of the ATV in the *xz*-plane for each of the four systems. As the cable length increases an elliptical pattern emerges. This longitudinal motion is confirmed in research, Nakagawa and Obata[15], to be consistent with aerial tow system's having a curved cable configuration.

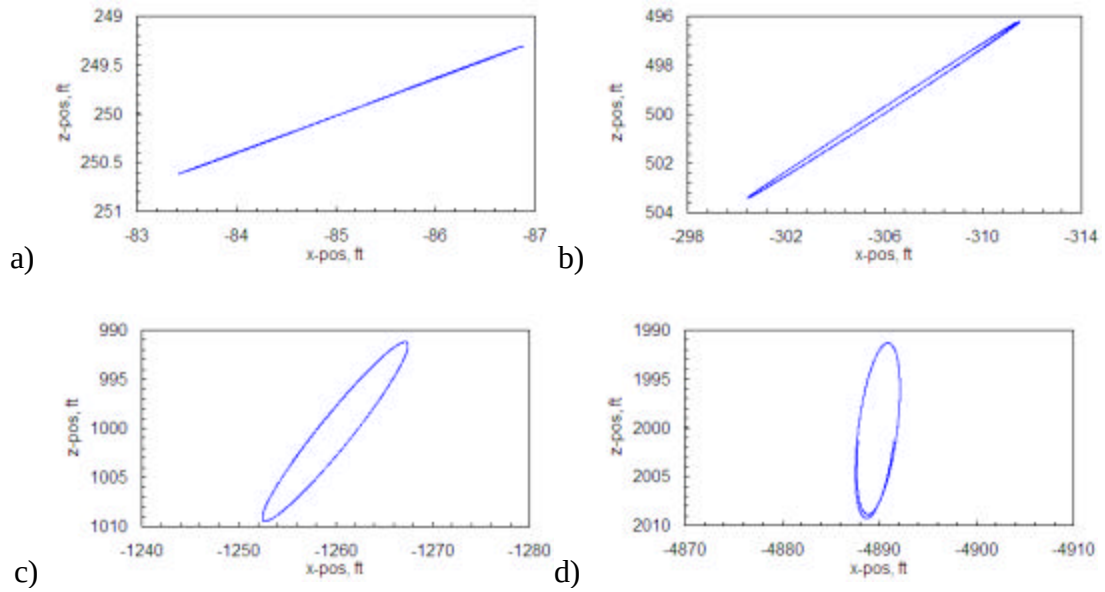

Figure 5.8 Elliptic oscillations in the *x* and *z*-direction, for a host vehicle altitude of a) 250 ft., b) 500 ft., c) 1000 ft., and d) 2000 ft.

Nakagawa and Obata[15] carried out the analysis of the longitudinal dynamic modes of the aerial tow system. They identified two dynamic longitudinal modes that have a large effect on the translation of the ATV. The two modes are the bowing and pendulum modes.

The bowing mode is actually the first vibration mode of the cable. In general the vibration modes of the cable have little effect on the motion of the ATV. However, in configurations in which the cable is curved the first vibration mode causes the ATV to

surge fore and aft as well as move vertically. The result is an elliptical ATV motion about its static location. Being that the bowing mode is a result of the curved cable configuration the elliptical motion is less pronounced in systems in which the cable curvature is small. The pendulum mode however is unaffected by the cable's shape.

The pendulum mode is as named because the resulting motion resembles that of a simple pendulum. The pendulum mode can be visualized as the static cable and ATV configuration swinging about the host-cable hitch point. As a result, it produces little dynamic interaction between the cable and the ATV. Thus, the pendulum mode rotates the system in an arching pattern around its equilibrium position with little effect on the shape of the cable or attitude of the ATV. (Note that the pendulum arch is small enough that its effect appears to be linear in the simulation results.)

The two dynamic modes produce coupled horizontal and vertical ATV motion of varying type. The bowing mode stimulates an elliptical motion while the pendulum mode creates an arching movement. As a result, the motion of the ATV will be a combination of the two and depending on the system configuration it is possible that one mode may be more pronounced that the other. This can be seen in figure 5.8. In the shortest cable configuration there is no visible elliptical motion, but just the oscillation of the pendulum mode. As the cable length increases the bowing mode becomes visible. The slanted ellipse of the remaining three configurations is a combination of the elliptical motion of the bowing mode and the slanting of the pendulum mode.

The length of the cable plays a critical role in determining the degree to which the ATV motion is coupled. The elliptical motion of the bowing mode is a result of the cable

curvature, and the cable curvature is increased as the cable length is increased. As a result, the bowing mode is more prevalent as the cable length increases. Also, the cumulative cable drag in the long cable configuration causes the ATV to cruise well aft of the host vehicle. Therefore, the slope of the arcing motion of the pendulum mode becomes more vertical than the short cable configuration.

The derived aerial tow system equations of motion and simulation produce results that correlate with those found by Nakagawa and Obata[15]. The motion of the ATV has been found to be coupled. That is no vertical motion can be attained without inducing horizontal motion. This leaves the question of how the coupled motion will affect the ability of the ATV to maintain its altitude over the ocean waves and since the cable length has a large effect on the degree of coupling which configuration will produce a better tracking of the waves. The system's wave tracking ability will be simulated in the following sections for various flight conditions.

5.4 ATV Wave Tracking

The goal of the aerial towed system is to safely tow the ATV in a manner that allows for atmospheric measurement in close proximity to the ocean surface. To gather insight into the behavior of the system, simulations are run with varying configurations and conditions. For instance, what effect may the oceanic wave conditions, connecting cable length, wind conditions, or host aircraft disturbance have on the system's ability to track the ocean waves? These cases will be simulated in the subsequent sections. Throughout the simulations the cable will be made discrete by breaking it into 25 segments each

modeled as a thin rod; the parameters of the cable and ATV as well as the reference flight conditions will conform to those presented previously in table 5.1 and 5.2.

5.4.1 Surface Waveform Variation

The utilization of the ATV autopilot presumably allows for system to track the ocean waves. From day to day the ocean waves may vary in amplitude and frequency depending on a myriad of factors. As a result, it is pertinent to know the effect the waves have on the system's ability to track them. This could potentially limit the conditions at which oceanic measurements are taken, or at least give the designers an idea of the quality of the results to be expected for a given condition.

The tracking of three waveforms is simulated and the results are presented in figure 5.9. Waveform 1 has an amplitude of 10 feet and a wavelength of 250 feet. Waveform 2 has an amplitude of 7.5 feet and a wavelength of 150 feet. Waveform 3 has an amplitude of 5 feet and a wavelength of 50 feet. In each simulation the system is configured with the host vehicle cruising at 1000 feet above the desired tracking altitude. In figure 5.9 the vertical ATV position as well as its desired position above the ocean waves is illustrated (ideally the 'ATV' path will exactly cover the 'Track' wave).

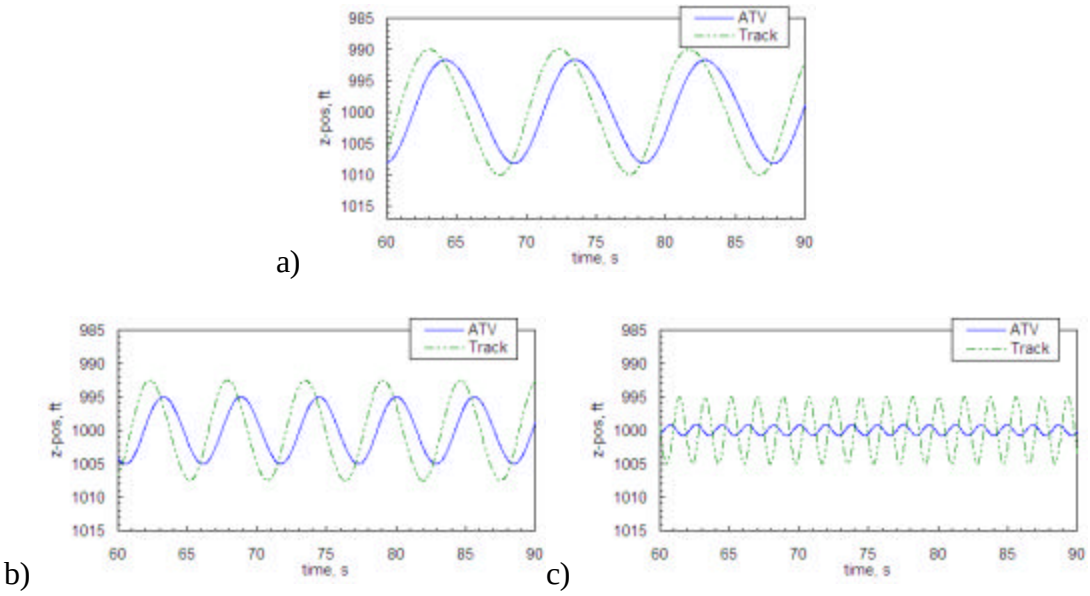

Figure 5.9 Tracking at with various ocean wavelengths

The results show the system tracking the first waveform relatively well, with only a small amplitude decrease and phase shift. However, as the wavelength decreases the system's lag of the tracking wave increases. The system dynamics are too sluggish to keep up with the increasing wave frequency. This inability to respond quickly causes the ATV oscillation to decrease in amplitude, as the wavelength decreases the autopilot and system dynamics filter out the ocean waveform.

The result of testing in conditions that produce small ocean wavelengths is poor tracking. Although, in general, as the ocean wavelength reduces so too does the amplitude. As long as the ATV is tracking the waves at an altitude slightly greater than that of the ocean wave amplitude there will be no resulting collision.

5.4.2 Host Aircraft Cruise Altitude

The host vehicle can cruise safely under the control of its autopilot at a range of altitudes. The length of cable required to place the ATV just above the ocean naturally

changes with the change in host vehicle cruising altitude. (However, this change is not proportional.) As discussed previously, the increase in the connecting cable length reduces the effect of the ATV's weight on the shape of the cable, thus the static profile of the system changes. The static configurations for the aerial tow systems in which the altitude difference between the host vehicle and the ATV are 250, 500, 1000, and 2000 feet is presented in Figure 5.6.

A simulation for the four configurations of varying host vehicle cruise altitude is accomplished to determine the effects of cable length on wave tracking quality.

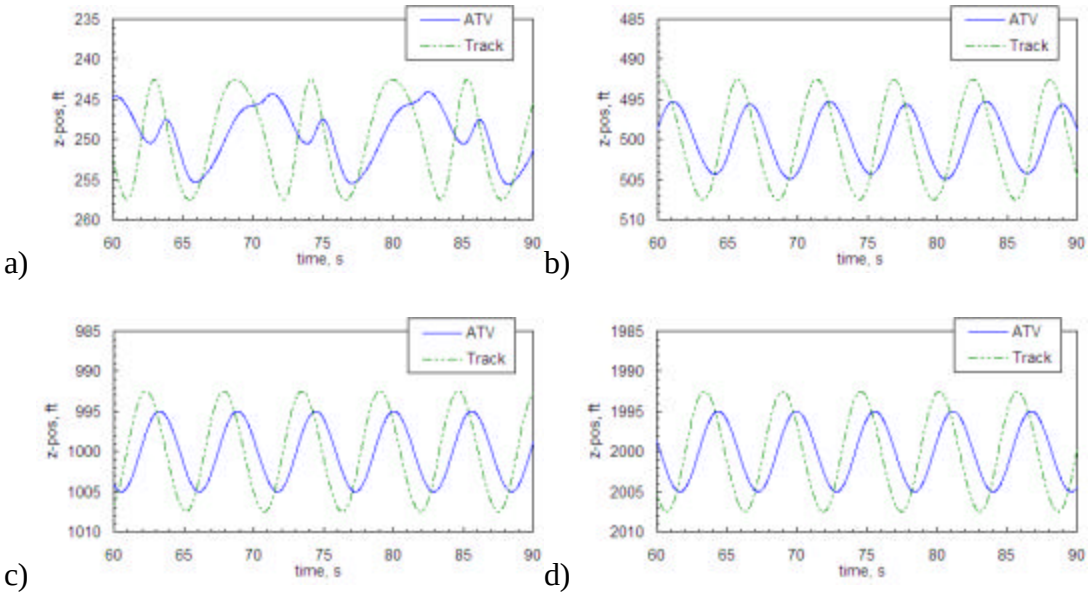

Figure 5.10 Host vehicle cruise altitude affect on wave tracing a) 250 ft., b) 500 ft., c) 1000 ft., and d) 2000 ft.

Figure 5.10 shows the results for simulations of four different systems attempting to follow surface waveform 2. The figure presents the actual 'ATV' path and the desired 'Track' wave. It is apparent from the figure that the system with the host aircraft cruising at 250 feet has the most difficulty tracking the waveform. As the host vehicle increases

in altitude the tracking is improved and the ATV amplitude of oscillation nears that of the wave. The remaining three systems, though largely different in cable length, both follow the waveform comparatively well.

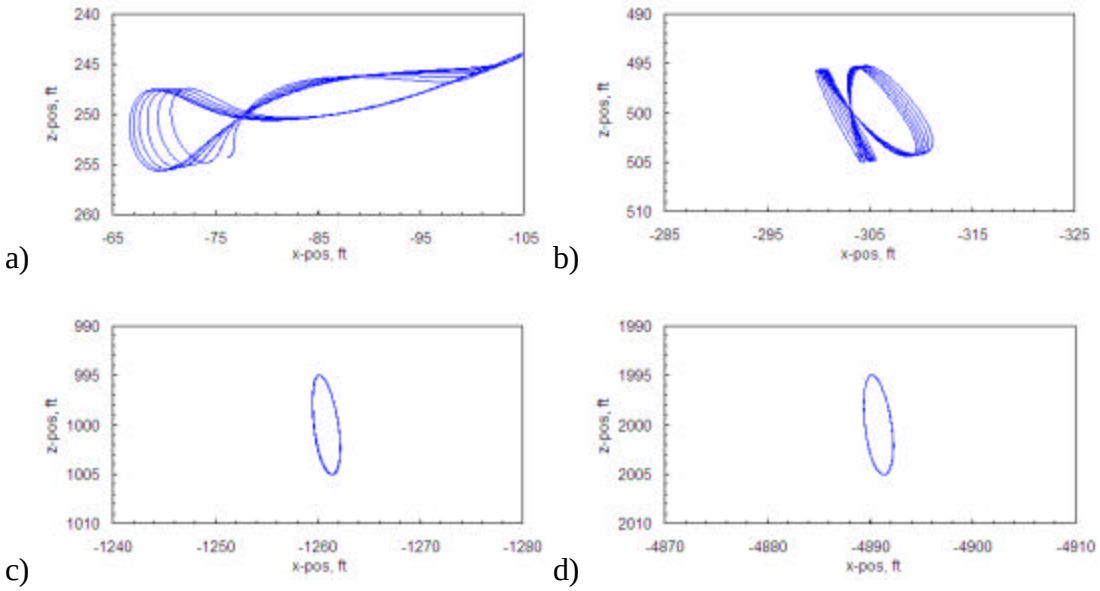

Figure 5.11 Elliptic oscillations in the *x* and *z*-direction, for a host vehicle altitude of a) 250 ft., b) 500 ft., c) 1000 ft., and d) 2000 ft.

The vertical and horizontal coupled motion of the four systems is revealed in figure 5.11. The longitudinal dynamic modes, discussed previously, are present as the ATV's autopilot attempts to track the wave, yet they are a bit more complicated than the pure natural response of the aerial tow system. This complication arises through the ATV autopilot. The autopilot attempts to increase and decrease the ATV altitude by changing the incidence angle of the wings as necessary. This change in lift and drag has an affect on the curvature of the connecting cable. During the wave tracking simulation the wing incidence angle ranges from positive to negative 12 degrees. When the wing has an angle of incidence of 12 degrees the weight of the plane is effectively lessened and the aircraft sees an increase in drag. The resulting drop in cable tension allows for a more curved

cable configuration. When the wing has a negative 12 degrees of incidence the weight of the ATV is effectively larger and the drag is increased. This causes greater cable tension and thus reduces the flex in the cable.

In the systems in which the tension of the cable is dominated by the inertial and aerodynamic forces of the ATV the change in the aircraft incidence angle will have a greater effect on cable curvature than in the systems in which the inertial and aerodynamic forces of the cable play a greater role in dictating the tension in the cable. That is to say, the curve of the cable will be more greatly affected by the change in incidence angle for the system with a short cable rather than with a long cable.

As a result the motion of the two systems with the shortest cables, as seen in figure 5.11a and figure 5.11b, is affected by the pendulum and bowing modes to different degrees at various points in the simulation depending on the incidence angle. The result is a more complex coupled motion than that produced in the natural response of the system, figure 5.8, in which the wing incidence angle remains zero throughout the simulation. In the systems in which the connecting cable is much longer the orientation of the cable is dominated by the cumulative drag on the cable and the inertial and aerodynamic forces of the ATV are less consequential. Thus, the long cable configurations remains highly curved regardless of the angle of incidence, which leads to similar motion between the controlled and uncontrolled response of the system.

The configuration in which the ATV is 250 feet below the host aircraft is in a straight cable configuration for the majority of the simulation. This causes the pendulum mode to be the more prevalent than the bowing mode, and since the ATV does not trail far aft of

the host vehicle the pendulum mode oscillation is largely in the horizontal direction. Thus, the corrective vertical motion is more highly coupled with horizontal motion than in the systems with a longer cable configuration.

The cable in the system in which the ATV is 500 feet below the host aircraft remains more curved than the previous system. As a result the coupled motion of the ATV is less affected by the pendulum mode, and the elliptical motion of the bowing mode is more prevalent. Under these conditions the autopilot can increase altitude of the ATV without the drastic horizontal displacement which results in better wave tracking.

In the long cable configuration the bowing mode is clearly dominant. The bowing mode produces an elliptical motion that is predominantly in the vertical direction. Thus, the pendulum's effect on the ATV oscillation is minimized. Together, these two modes in the long cable configurations produce little fore-aft ATV oscillation.

In general aerial tow situations, there is no clear drawback to the coupled horizontal and vertical motion of the ATV. However, when the aerial tow system is attempting to track ocean waves the coupled motion complicates the process. During tracking the autopilot attempts to correct the altitude of the ATV but the vertical correction induces a horizontal surge of the ATV. This horizontal motion results in, essentially, increasing or decreasing the frequency of the coming wave. In our system the degree to which the vertical motion produces a horizontal motion is dictated by the curve of the cable. The horizontal and vertical coupling is at its most detrimental when the connecting cable is short, roughly 250 feet. In this configuration the autopilot cannot track the ocean waves. However, increasing the cable reduces the autopilots effect on the cable curvature and

produces better wave tracking. Connection cables of significant length to allow the host vehicle to cruise 500, 1000, and 2000 feet above the ATV produced good wave tracking results.

5.4.3 Lateral Motion

The previous simulations of variable waveforms and host vehicle altitudes were simulated using the two-dimensional system since all of the motion was longitudinal. However, to simulate the effects of lateral motion it is necessary to use the three-dimensional equations of motion and waveform. In this instance the ATV is tracking the longitudinal waves (waveform 2) as it is hit by a side gust. The side gust has a magnitude of 10 knots and persists for 10 seconds. The simulation allows for analysis of the lateral response of the ATV and its ability to maintain tracking of the ocean surface.

Due to the fact that the same ATV configuration is used in each simulation, the gust produces the same ATV aerodynamic side force for all system configurations. The difference between the simulations is the length of cable the gust acts upon and the system dynamics due to variance in cable length.

Figure 5.12 graphs the motion of the ATV in the *xy*-plane over the period of the simulation for the four system configurations. The motion of the ATV prior to the gust is in the *x* and *z*-directions only. The gust then forces the ATV laterally. The gust subsides and the dynamics of the system eventually restore the motion back to the xz-plane.

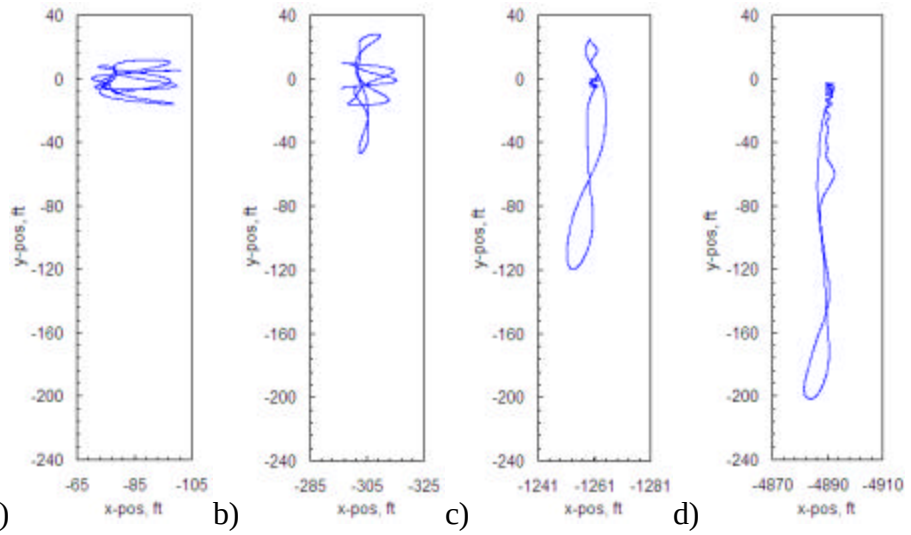

Figure 5.12 ATV motion in the x and y-direction, at a host vehicle cruise altitude of a) 250 ft., b) 500 ft, c) 1000 ft., and d) 2000 ft.

The lateral translation of the ATV due to the gust is greater for the configurations with the longer connecting cable. This happens for two reasons. First, the configurations with longer cables naturally have more cable area for the gust to act upon, thus the system has a larger accumulative applied lateral force. The other reason for the larger lateral translation is that the lateral displacement is directly connected to the vertical displacement. As the ATV is pushed by the side gust, the natural tendency is for the cable to lift the ATV, just as a pendulum's swing increases the altitude of its mass, this can be thought of as the lateral pendulum mode. A given y-displacement is going to have a more drastic effect on the change in altitude for a system with a shorter cable. Therefore, the ATV autopilot will have to respond more quickly to resist the increase in altitude due to the side gust for the shorter cable configuration.

The autopilot can only counter the lateral movement by applying an increased downward force. This is the same mechanism used to control the longitudinal tracking of the ATV. As a result, the lateral correction activates the longitudinal dynamics; that in

combination with the natural behavior of a three-dimensional pendulum results in a coupling of all three coordinate directions. This ellipsoid motion can be seen in figure 5.12. The stronger *xz*-coupling of the short cable configuration produces a larger fore-aft oscillation during correction and tracking. The effect of the coupling on the ability of the system to track the surface waveform is presented in figure 5.13.

Prior to the gust the system is tracking the surface wave form in the *xz*-plane. The 10 knot gust is initiated and ends at 30 and 40 seconds, respectively, this is apparent in the change of the 'Track' wave at the 30 second mark. The difference in the tracking waveform from case to case is due to the difference in the distance the ATV is pushed by the gust. More wave distortion is evident in the cases with the longer connecting cable. The cause is the magnitude of the translation of the ATV in the *y*-direction (figure 5.12 shows the actual *y*-distance traveled for each case). The farther the ATV traverses in the *y*-direction the greater the influence of the neighboring waves.

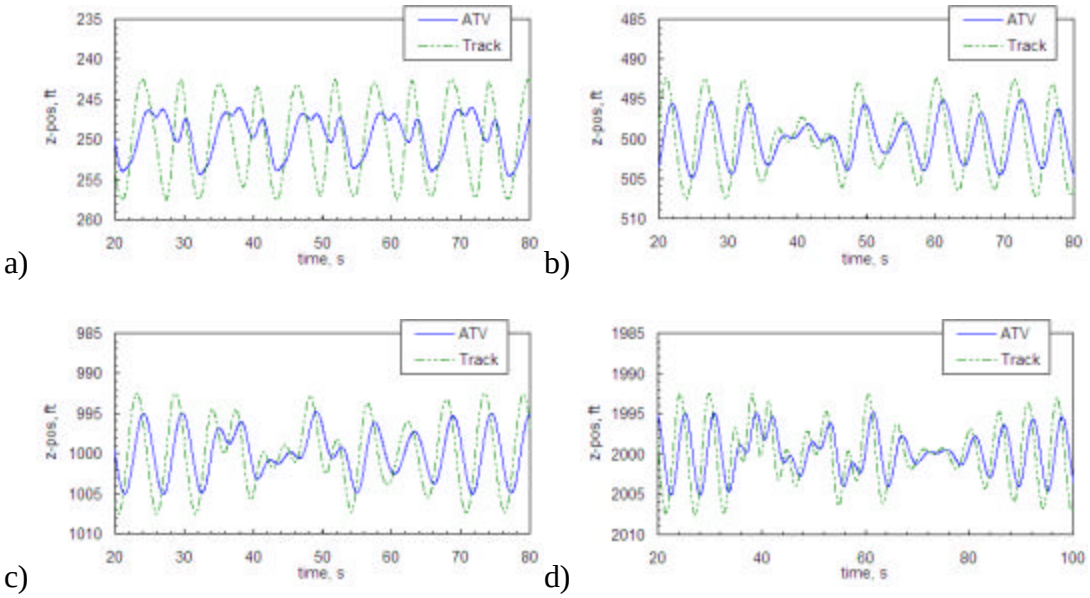

Figure 5.13 Three-dimensional waveform tracking with a 10 knot side gust, host vehicle altitude of a) 250 ft., b) 500 ft., c) 1000 ft., and d) 2000 ft.

When the host vehicle is cruising 250 feet above the desired ATV altitude the side gust causes a *y*-displacement of about 20 feet. Recall that the waveform in the *y*-direction has a wavelength of 150 feet in this simulation. As a result, the lateral translation is not substantial enough to cause any significant change in the height of the lateral wave; therefore, the distortion in the 'Track' waveform is faint.

In general, the shorter cable configuration will have the most difficulty following the waveform while moving in the *y*-direction, as its lateral motion will be more strongly coupled with its vertical and fore-aft motion. However, the lateral ATV translation is arrested by the ATV autopilot and the dynamics of the system before it can be introduced to the complication produced by the neighboring wave. Hence, the system tracks the waveform with the same level of accuracy with or without the 10 knot side gust.

As the connecting cable is lengthened the *y*-direction displacement due to the side gust increases causing the ATV to traverse more of the neighboring wave, and it also increases the time necessary for the system to damp out the lateral effects of the gust. The large *y*-direction displacement requires the ATV to track a varying and increasingly complex waveform than that prior to the gust. Nevertheless, the control system having only one control surface adequately tracks the complicated waveform. The results indicate that the systems track the three-dimensional waveform as accurately as the two-dimensional waveform and thus are not negatively affected by the side gust.

5.4.4 Host Vehicle Oscillation

The final simulation deals with host aircraft oscillations. The host aircraft is equipped with an altitude hold autopilot and will be cruising at a fixed altitude; however

disturbances such as gusts and turbulence will produced temporary deviances of the altitude of the host vehicle, and thusly perturb the entire system. The simulation gives the host vehicle a sinusoidal motion in an effort to exaggerate the longitudinal response of the host aircraft to a disturbance and inspect the ability of the ATV to continue to track the ocean waves.

Of the longitudinal aerodynamic modes, the long period has the largest effect on variation in aircraft altitude. In this system, the long period natural frequency of our host aircraft is just over 30 seconds. Naturally the effect of the atmospheric disturbance on the host vehicle damp out over time; however, in the simulation, the host vehicle continues to oscillate continually (this, in essence, simulates very rough flight conditions). The results of the simulations for various host vehicle cruise altitudes are shown in Figure 5.14. Note that in this figure the *z*-position of the track wave is measured from the host vehicle. Thus, the track wave is a superposition of two waves, the ocean waveform and the host oscillation waveform.

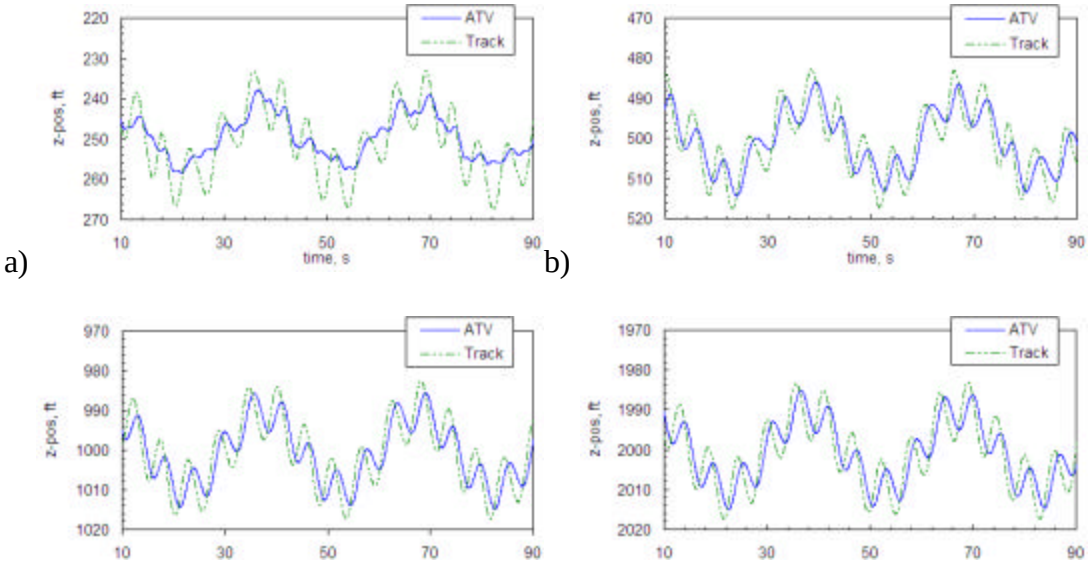

Figure 5.14 Wave tracking during host vehicle oscillation, host vehicle altitude of a) 250 ft., b) 500 ft., c) 1000 ft., and d) 2000 ft.

In the simulations, the various systems attempt to track waveform 2. The results of the simulation show that when the host aircraft is cruising 250 feet above the nominal tracking altitude, Figure 5.14a, the cable and ATV dynamics do not allow a quick enough response to completely track the waveform during oscillation; this is no surprise as this configuration cannot track waveform 2 if the host aircraft is still, figure 5.10. However, the ATV autopilot does successfully counter the oscillation of the host aircraft. As the altitude of the host craft reaches 500 feet and greater the ATV autopilot tracks both the ocean waves and the wave produced by the host aircraft undulation relatively well. Even in the presence of extensive host vehicle disturbances it is possible to configure the aerial tow system such that accurate wave tracking is produced.

CHAPTER 6

CONCLUSIONS

In this paper a methodology is laid out for developing a numerical simulation of the aerial towed system. This includes the mathematical and aerodynamically modeling of the system components such as the host aircraft, connecting cable, and aerial towed vehicle. Of particular interest is the finite element method for modeling the connecting cable. The finite element method models the continuous cable as a series of connected segments from which the equations of motion dictating the dynamics of the cable can be derived. Two models for the cable segments were presented, the lumped mass and thin rod models. Upon modeling the component Lagrange's equation are utilized to develop the two and three-dimensional nonlinear equations of motion for the connecting cable, the cable and ATV system, and the cable, ATV, and host vehicle system. Additional models of the ATV autopilot and ocean surface waveforms allowed for the simulation of the aerial tow system in which the ATV attempts to track the ocean waves. Numerous simulations were under taken to supply validation to the derived equations of motion and subsequently gain insight into the aerial tow system as a means to measure oceanic atmospheric conditions.

A simulation of the cable dynamics in an ideal situation and the comparison of the two and three-dimensional equations of motion supported the validity of the derived

equations of motion. Under ideal conditions the system is conservative. As a result, the simulation should maintain a constant energy through the duration of the simulation. This was indeed the case. Also, the two and three-dimensional systems were set with the same initial conditions while minimizing triviality in the equations of motion, and the simulation of the two systems produced identical results. The results of the two simulations help solidify the quality of the derived equations of motion.

A comparison between the lumped mass and thin rod cable segment model was undertaken. The lumped mass model is quite prevalent in research pertaining to the simulation of the aerial tow system. The thin rod cable segment model was developed by the author as an alternative to the commonly used lumped mass model. Simulations of a system made up of the two models confirmed the benefit of using the thin rod model. The system in which the cable was modeled as a series of thin rods produced the same results as that of the lumped mass system yet did so with much fewer segments. The lumped mass system took 2000 segments to produce the same results as the thin rod system using only 25 segments. This resulted in the thin rod system producing simulation results in a fraction of the time that was required for the lumped mass system. Compared with the lumped mass mode the thin rod segment model is a better physical model of the cable, it produces a more accurate drag prediction, and it results in a more realistic dynamic model.

A simulation of the natural dynamic response of the aerial tow system produced two longitudinal dynamic modes of motion. These modes are corroborated by the research conducted by Nakagawa and Obata[15] and are labeled as the pendulum and bowing modes.

The pendulum mode oscillates the cable and ATV about the cable-host vehicle hitch point. The bowing mode is the first vibration mode of the cable, and is only visible in system in which the connecting cable is curved. The vibration on the curved cable produces an elliptical oscillation of the ATV. Both of the longitudinal modes couple the horizontal and vertical motion of the ATV. This coupled motion becomes the main obstacle for the ATV autopilot during wave tracking due to the fact that the corrective vertical motion naturally induced horizontal motion to varying degrees.

It was found that the degree to which the horizontal and vertical motions of the ATV were coupled depends largely on the length of the cable. As the cable length increases the inertial and aerodynamic forces of the ATV become less significant than the inertial and aerodynamic forces of the connecting cable. Long cable configuration produces a cable profile that is more curved than in the short cable configuration. This curvature reduces fore aft surging produced by the varying cable tension caused by the changing wing incidence angle during wave tracking. As a result, it found that curved cable configurations produced optimal wave tracking.

Adequate wave tracking was produced when there is significant cable to allow the host aircraft to cruise 500 feet or high above the ATV. The simulations suggest that if the ATV is to maintain an altitude of 30 feet above the ocean surface the system can safely record atmospheric measurements for a wide variety of wave conditions. Even in the presence of lateral gusting and oscillation of the host aircraft the autopilot of the ATV can maintain a safe altitude above the water for a wide variety of oceanic conditions.

REFERENCES

[1]Huffman, R. R., Genin J., "The Dynamic Behavior of a Flexible Cable in a Uniform Flow Field," *The Aeronautical Quarterly*, Vol. 22, 1971, pp. 183-195.

[2]Genin, J., Cannon, T. C., "Equilibrium Configuration and Tensions of a Flexible Cable in a Uniform Flowfield," *Journal of Aircraft*, Vol. 4, No. 3, 1967, pp. 200-202.

[3]Genin, J., Citron, J., Huffman, R. R., "Coupling of Longitudinal and Transverse Motions of a Flexible Cable in a Uniform Flow Field," *Journal of the Acoustical Society of America*, Vol. 52, No. 1, 1972, pp. 438-440.

[4]Delmer, T. N., Stephens, T. C., "Numerical Simulation of Towed Cables," *Ocean Engineering*, Vol. 10, No. 2, 1983, pp. 119-132.

[5]Bourmistrov, A. S., Hill, R. D., Riseborough, P., "Nonlinear Control Law for Aerial Towed Target," *Journal of Guidance, Control, and Dynamics*, Vol. 18, No. 6, 1995, pp. 1232-1238.

[6]Cochran, J. E., Innocenti, M., No, T. S., Thukral, A., "Dynamics and Control of Maneuverable Towed Flight Vehicles," *Journal of Guidance, Control, and Dynamics*, Vol. 15, No. 5, 1992, pp. 1245-1252.

[7]Schram, J. W., Reyle, S. P., "A Three-Dimensional Dynamic Analysis of a Towed System," *Journal of Hydrodynamics*, Vol. 2, No. 4, 1968, pp. 213-219.

[8]Jones, S. P., Krausman, J. A., "Nonlinear Dynamic Simulation of a Tethered Aerostat," *Journal of Aircraft*, Vol. 19, No. 8, 1982, pp. 679-686.

[9]Sanders, J. V., "A Three-Dimensional Dynamic Analysis of a Towed System," *Ocean Engineering*, Vol. 9, No. 5, 1982, pp. 483-499.

[10]Choo, Y., Casarella, M. J., "A Survey of Analytical Methods for Dynamic Simulation of Cable-Body Systems," *Journal of Hydronautics*, Vol. 7, No. 4, 1973, pp. 137-142.

[11]Greenwood, D. T., *Principles of Dynamics*, Prentice Hall, New Jersey, 1965, Chaps. 6, 7.

[12]Press, W. H., Teukolsky, S. A., Vetterling, W. T., Flannery, B. P., *Numerical Recipes in Fortran*, 2nd ed., Cambridge University Press, New York, 1992, Chap. 2.

[13]Hoerner, S. F., "Fluid Dynamic Drag," 1965, Chap. 3.

[14]Nelson, R. C., *Flight Stability and Automatic Control*, 2nd ed., McGraw-Hill, New York, 1998, Chap. 3.

[15]Nakagawa, N., Obata, A., "Longitudinal Stability Analysis of Aerial-Towed Systems," *Journal of Aircraft*, Vol. 29, No. 6, 1992, pp. 978-985.

[16]Raymer, D. P., *Aircraft Design: A Conceptual Approach, 3rd Edition*, American Institute of Aeronautics and Astronautics, Inc., Virginia, 1999.

[17]Etkins, B., "Stability of a Towed Body." *AIAA Journal of Aircraft*, Vol. 35, No. 2, Mar.-April. 1998.

[18]Walton, T., Polachek, H., "Calculation of Transient Motion of Submerged Cables." *Mathematics of Computation*, Vol. 14, No. 69, Jan. 1960.

[19]Lawhon, R., D., and Arena, Jr. A. S. "Design considerations for an Aerially Towed Vehicle with Altitude Holding Capability," *AIAA Atmospheric Flight Mechanics Conference 2004*, Providence, Rhode Island, In-Review.

VITA

Johnny Earl Quisenberry Jr.

Candidate for the Degree of

Master of Science

Thesis: DYNAMIC SIMULATION OF LOW ALTITUDE AERIAL TOW SYSTEM

Major Field: Aerospace Engineering

Biographical:

Personal Data: Born in Oklahoma City Oklahoma on July 18, 1979, the son of John E. and Susan L. Quisenberry.

Education: Graduated from Del City High School, Del City Oklahoma, in May 1997; Received Bachelor of Science degree in Aerospace Engineering from Oklahoma State University, Stillwater, Oklahoma, in May 2002; Completed the requirements for the Masters of Science Degree from Oklahoma State University, Stillwater, Oklahoma, July, 2005

Experience: Lab Assistant, OSU Mechanical and Aerospace Engineering, 2002-2004; Engineering Intern, Cessna, Summer of 2001;

Professional Memberships: American Institute of Aeronautics and Astronautics